-

Technische Universität München

Fakultät für Medizin

Nuklearmedizinische Klinik und Poliklinik, Klinikum rechts der Isar

Correlation of molecular imaging of PSMA-ligand uptake with clinicohistopathological parameters and biochemical recurrence prediction in primary prostate cancer patients

Hui Wang

Vollständiger Abdruck der von der Fakultät für Medizin der Technischen Universität München zur Erlangung des akademischen Grades eines

Doctor of Philosophy (Ph.D.)

genehmigten Dissertation

Vorsitzende:	Prof. Dr. Alessandra Moretti
Betreuer:	Prof. Dr. Matthias Eiber
Prüfer der Dissertation:	1. Prof. Dr. Wolfgang Weber
	2. Priv.-Doz. Dr. Thomas Horn

Die Dissertation wurde am 20.04.2021 bei der Technischen Universität München eingereicht und durch die Fakultät für Medizin am 15.06.2021 angenommen.

Table of Contents

Table of Contents I

Abstract IV

List of Acronyms V

1. Introduction 1

1.1. Prostate cancer 1

1.1.1. Epidemiology and etiology 1

1.1.2. Staging 1

1.1.3. Diagnosis 3

1.1.3.1. Screening 4

1.1.3.2. Biopsy 4

1.1.3.3. Imaging 4

1.1.4. Primary treatment 6

1.1.4.1. Treatment planning 6

1.1.4.2. Active surveillance and watchful waiting 6

1.1.4.3. Radical prostatectomy and pelvic lymph node dissection 7

1.1.4.4. Radiation therapy 7

1.1.4.5. Androgen deprivation therapy 8

1.1.4.6. Chemotherapy 9

1.1.4.7. Investigational therapies 9

1.2. Prostate-specific membrane antigen (PSMA) 10

1.2.1. Structure and Expression 10

1.2.2. PSMA-positron emission tomography (PET) imaging 11

1.2.2.1. Primary staging 11

1.2.2.2. Biochemical Recurrence (BCR) 14

1.2.2.3. Advanced Diseases Monitoring 17

1.2.2.4. Prostate cancer molecular imaging standardized evaluation (PROMISE): miTNM classification 18

1.2.3. Radio-guided surgery 21

1.2.4. Correlation between PSMA expression and prognosis 23

1.2.5. Evaluation of PSMA-ligand uptake and histopathological findings 26

2. Objective and planned analysis 28

2.1. Preclinical assessment of PSMA-ligand uptake in prostate cancer 28

2.2. Clinical value of pre-treatment ^{68}Ga-PSMA-11 PET to predict BCR 28

Table of Contents

3. Material 30
3.1. Technical equipment 30
3.2. Consumable supplies 30
3.3. Reagents and chemicals 31
3.4. Buffers and solutions 31
3.5. Antibodies 31
3.6. Kits 32
3.7. Software 32
4. Methods 33
4.1. Preclinical analysis 33
4.1.1. Ex vivo experiment 33
4.1.1.1. Sample preparation 33
4.1.1.2. Autoradiography (ARG) imaging 33
4.1.1.3. Image registration 35
4.1.1.4. Image analysis 35
4.1.2. In vivo experiment 35
4.1.2.1. Patients 36
4.1.2.2. Overview of workflow 36
4.1.2.3. Sample preparation 37
4.1.2.4. ARG imaging 38
4.1.2.5. Histology and immunohistochemistry 38
4.1.2.6. Image registration 39
4.1.2.7. Image analysis 39
4.2. Clinical analysis 41
4.2.1. Patients 41
4.2.2. Imaging protocol 42
4.2.3. Image analysis 43
4.3. Statistical analysis 43
5. Results 45
5.1. Preclinical results 45
5.1.1. Ex vivo PSMA-ligand uptake evaluation 45
5.1.1.1. Patients and clinicopathological findings 45
5.1.1.2. Qualitative analysis 45

5.1.1.3. Quantitative analysis 47
5.1.2. In vivo PSMA-ligand uptake evaluation 49
5.1.2.1. Patients and clinicohistological findings 49
5.1.2.2. Image co-registration of histopathological and autoradiographic data. 52
5.1.2.3. ROI-based analysis 53
5.1.2.4. Grid-based analysis 59
5.1.2.4.1. Sample characteristics: histopathology, immunohistochemistry and ARG signal 59
5.1.2.4.2. PSMA-ligand uptake in relation to Gleason Scores 63
5.1.2.4.3. PSMA-ligand uptake in relation to Gleason Patterns 65
5.1.2.4.4. Correlation of immunohistochemistry and PSMA-ligand uptake 67
5.2. Clinical results 68
5.2.1. Patients 68
5.2.2. ^{68}Ga-PSMA-11 PET findings 70
5.2.3. Correlation of ^{68}Ga-PSMA-11 PET findings with histopathology 71
5.2.4. Predictors of BCR-free survival 73
6. Discussion 84
6.1. Correlation of PSMA-ligand uptake and Histopathology findings 84
6.1.1. Influence of non-pathological parameters on detection of intraprostatic foci by PSMA-ligands imaging 85
6.1.2. Influence of pathological parameters on detection of intraprostatic foci by PSMA-ligands imaging 86
6.2. BCR prediction by ^{68}Ga-PSMA-11 PET findings 91
6.2.1. Value of quantitative parameters from ^{68}Ga-PSMA-11 PET to predict BCR-free survival 91
6.2.2. Value of molecular imaging staging to predict BCR-free survival 92
6.3. Limitations 94
7. Conclusion 96
References 97
List of Figures 109
List of Tables 110
Publications 113
Acknowledgements 114

Abstract

Heterogeneous expression of prostate-specific membrane antigen (PSMA) in immunohistochemistry indicates limitations in the effect of imaging and radionuclide therapy of multifocal disease. Besides, the clinical evaluations of the potential of PSMA-ligand positron emission tomography (PET) to predict disease outcomes are urgently necessary. The goal of the study was to investigate the intraprostatic PSMA-ligand uptake in close correlation with histopathology and assess its association with tumor aggressiveness, and investigate the predictive value of ^{68}Ga-PSMA-11 PET to time to biochemical recurrence (BCR) in primary prostate cancer after radical prostatectomy (RP).

Gleason Pattern 4 and Gleason Pattern 5 correlated with higher uptake of ^{99m}Tc-PSMA-I&S compared with Gleason Pattern 3 and non-neoplastic tissue. Regarding different Gleason Score groups, higher PSMA-ligand uptake was observed in Gleason Score ≥ 8 than Gleason Score < 8. Moreover, multivariate Cox model analysis showed that patients with short BCR-free survival had a high serum PSA level, advanced Gleason Score and a high miT status (miT ≥ 3a vs. miT < 3). In the miT2 subgroup, shorter BCR-free survival was observed in the patients with higher SUV_{max}.

These findings confirm the potential of PSMA-ligand uptake to identify the high-grade disease and imply its use as a noninvasive biomarker in prostate cancer. The high specificity of PSMA-ligand PET for the detection of high-grade prostate cancer and the possibility of BCR prediction was revealed. Thus, PSMA-ligand PET imaging can be used as a noninvasive diagnostic method in prostate cancer patients to stratify tumor aggressiveness.

List of Acronyms

Abbreviation	Description
^{11}C	Carbon-11
^{111}In	Indium-111
^{177}Lu	Lutetium-177
^{18}F	Fluor-18
^{18}F–DCFBC	N-[N-[(S)-1,3-dicarboxypropyl]carbamoyl]-4-[^{18}F]fluorobenzyl-L-cysteine
^{18}F-DCFPyL	2-(3-(1-Carboxy-5-[(6-[^{18}F]fluoro-pyridine-3-carbonyl)-amino]-pentyl)-ureido)-pentanedioic acid
3D-CRT	Three-dimensional conformal radiation therapy
^{68}Ga	Gallium-68
^{99m}Tc	Technetium-99m
ADT	Androgen deprivation therapy
AJCC	American Joint Committee on Cancer
ARG	Autoradiography
AUC	Area under the curve
BCR	Biochemical recurrence
BMI	Body mass index
Bq	Becquerel
BSA	Bovine serum albumin
CeP	Comparative experimental pathology
CHAARTED	Chemohormonal Therapy Versus Androgen Ablation Randomized Trial for Extensive Disease in Prostate Cancer
CI	Confidence interval
CI	Common iliac
CPM	Counts per minute
CRPC	Castration-resistant prostate cancer
CT	Computed tomography
CYP17	Cytochrome P450 17α−hydroxy/17, 20-lyase
DAB	Diaminobenzidine
DDR	DNA damage repair
Diss	Disseminated
Dmi	Diffuse marrow involvement
DNA	Deoxyribonucleic acid
DOTAGA	1,4,7,10-tetraazacyclododececane,1-(glutaric acid)-4,7,10-triacetic acid
DPD	3,3-diphospho-1,2-propanodicarboxylic acid
DRE	Digital rectal examination
EAU	European Association of Urology

List of Acronyms

EBRT	External beam radiation therapy
EI	External iliac
ePLND	Extended pelvic lymph node dissection
ERSPC	European Randomized Study of Screening for Prostate Cancer
FDG	Fluorodeoxyglucose
GCPII	Glutamate carboxypeptidase II
GP	Gleason Pattern
GS	Gleason Score
HBED-CC	*N*,*N*′-bis-[2-hydroxy-5-(carboxyethyl)ben-zyl]ethylenediamine-*N*,*N*′-diacetic acid
HCI	Hydrochloric acid
HE	Hematoxylin and Eosin
HGPIN	High grade prostatic intraepithelial neoplasia
HIFU	High-intensity focused US
HR	Hazard ratio
IGRT	Image guided radiation therapy
IHC	Immunohistochemistry
II	Internal iliac
IMRT	Intensity modulated radiation therapy
iPSA	Initial prostate-specific antigen
IQR	Interquartile range
IRS	Immunoreactive score
ISUP	International Society of Urological Pathology
LA	Left apex
LB	Left base
LBM	lean body mass
LHRH	Luteinizing hormone-releasing hormone
LM	Left mid
mCRPC	Metastatic CRPC
mHSPC	Metastatic hormone-sensitive prostate cancer
mpMRI	Multiparametric MRI
MRI	Magnetic resonance imaging
nPD	Non-progressive disease
OB	Obturator
OCT	Optimal cutting temperature compound
OE	Other extrapelvic
Oligo	Oligometastatic
OP	Other pelvic
OR	Odds ratios
OS	Overall survival
PD	Progressive disease

PET	Positron emission tomography
PIN	Prostatic intraepithelial neoplasia
PLCO	Prostate, Lung, Colorectal, and Ovarian
PLND	Pelvic lymph node dissection
PROMISE	Prostate Cancer Molecular Imaging Standardized Evaluation
PS	Presacral
PSA	Prostate-specific antigen
PSMA	Prostate-specific membrane antigen
pTNM	Pathological tumor-node-metastasis
QL	Quantum level
RA	Right apex
RB	Right base
RECIST	Response Evaluation Criteria in Solid Tumors
RGS	Radio-guided surgery
rhPSMA	Radiohybrid PSMA
RM	Right mid
ROC	Receiver operating characteristic
ROI	Region of interest
RP	Radical prostatectomy
RP	Retroperitoneal
SD	Standard deviation
SD	Supradiaphragmatic
SPECT	Single-photon emission computed tomography
SUL	SUV normalized by lean body mass
SUV	Standardized uptake value
TL	Total lesion
TNM	Tumor, Node, Metastasis
TV	Tumor volume
Uni	Unifocal
US	Ultrasound
VOI	Volume of interest

1. Introduction

1.1. Prostate cancer

1.1.1. Epidemiology and etiology

Prostate cancer is the second most common neoplasia in men worldwide and the most frequently diagnosed among men in western countries. In 2012, an estimated 1.1 million cases were diagnosed worldwide, accounting for 15% of all types of cancers diagnosed in men (J Ferlay et al., 2015; J Ferlay et al., 2013). Due to the growth and aging of the population, the burden of worldwide prostate cancer is expected to grow to approximately 2.3 million new cases and 0.7 million deaths by 2040 (Ferlay J et al., 2020).

Family history, racial background (K Hemminki, 2012) and older age are three non-modifiable risk factors for prostate cancer (MF Leitzmann et al., 2012). There is evidence to suggest that environmental factors such as fried food intake (G Lippi et al., 2015), dairy products (TJ Key, 2014) and alcohol intake (J Zhao et al., 2016) increase the risk of prostate cancer.

During the most recent years, prostate cancer incidence and mortality rates are declining or stabilizing worldwide. These trends may indicate a decline in prostate-specific antigen (PSA) testing (incidence) and improvements in treatment (mortality) (MB Culp et al., 2020).

1.1.2. Staging

Tumor classification and staging systems group the patients with the same clinicopathological conditions. It allows for the recommendations of patients' treatment, the comparison of clinical outcomes worldwide, and the design of multicenter clinical trials.

The Tumor, Node, Metastasis (TNM) system is the most widely used staging system at this time. It provides international standards to describe and categorize cancer staging and progression (Table 1) (JD Brierley et al., 2017). Pathological

staging (pTNM) is based on the assessment of surgical specimens and highly parallels the clinical TNM, except that there is no pT1 category.

Table 1. Clinical TNM classification of prostate cancer (JD Brierley et al., 2017)

T – Primary Tumor (based on digital rectal examination (DRE) only)		
Tx	Primary tumor cannot be assessed	
T0	No evidence of primary tumor	
T1	Clinically inapparent tumor that is not palpable	
	T1a	Tumor incidental histological finding in 5% or less of tissue resected
	T1b	Tumor incidental histological finding in more than 5% of tissue resected
	T1c	Tumor identified by needle biopsy
T2	Tumor that is palpable and confined within the prostate	
	T2a	Tumor involves one half of one lobe or less
	T2b	Tumor involves more than half of one lobe, but not both lobes
	T2c	Tumor involves both lobes
T3	Tumor extends through the prostatic capsule	
	T3a	Extracapsular extension (unilateral or bilateral)
	T3b	Tumor invades seminal vesicle(s)
T4	Tumor is fixed or invades adjacent structures other than seminal vesicles: external sphincter, rectum, levator muscles, and/or pelvic wall	
N – Regional Lymph nodes		
Nx	Regional lymph nodes cannot be assessed	
N0	No regional lymph node metastasis	
N1	Regional lymph node metastasis	
M – Distant Metastasis		
M0	No distant metastasis	
M1	Distant metastasis	
	M1a	Non-regional lymph node(s)
	M1b	Bone(s)
	M1c	Other site(s)

TNM = Tumor, Node, Metastasis.

Moreover, in histopathological processing, the current Gleason Pattern system was developed by Donald Gleason in 1966 (DF Gleason, 1966), which is used for assessing the morphology of cancer cells. The grading system of prostate cancer was continuously developed by Donald Gleason and the Veterans Administration Cooperative Urological Research Group (DF Gleason et al., 1974). The

system designates Gleason Pattern 1 through 5 based on the histological images, adding the primary and secondary patterns end up with Gleason Scores ranging from 2 to 10. Gleason Pattern 1 cells resemble normal prostate tissue cells and Gleason Pattern 5 cells are considered highly aggressive. Over the following 40 years, owing to a large number of clinical studies, the International Society of Urological Pathology (ISUP) modified the Gleason Score system in 2005 and 2014, aiming at further define the clinically highly significant distinction in different groups (Table 2) (JI Epstein et al., 2005; JI Epstein, L Egevad, et al., 2016; JI Epstein, MJ Zelefsky, et al., 2016)

Table 2. Grades of ISUP 2014 (JI Epstein, L Egevad, et al., 2016)

Gleason Score	ISUP grade
2-6	1
7 (3 + 4)	2
7 (4 + 3)	3
8 (4 + 4 or 3 + 5 or 5 + 3)	4
9-10	5

ISUP = International Society of Urological Pathology.

The European Association of Urology (EAU) has further advised a risk group classification based on D'Amico's classification system for prostate cancer, which is broadly used for predicting biochemical recurrence (BCR) following treatments (Table 3) (AV D'Amico et al., 1998; N Mottet et al., 2020).

Table 3. EAU risk groups (N Mottet et al., 2020)

Low-risk	Intermediate-risk	High-risk	
PSA < 10 ng/ml	PSA 10-20 ng/ml	PSA > 20 ng/ml	any PSA
and GS < 7 (ISUP grade 1)	or GS 7 (ISUP grade 2/3)	or GS > 7 (ISUP grade 4/5)	any GS (any ISUP grade)
and cT1-2a	or cT2b	or cT2c	cT3-4 or cN+
Localized			Locally advanced

EAU = European Association of Urology; GS = Gleason Score; ISUP = International Society of Urological Pathology; PSA = prostate-specific antigen.

1.1.3. Diagnosis

1.1.3.1. Screening

The goal of screening for prostate cancer is to identify early-stage diseases that can be treated successfully and reduce the mortality due to prostate cancer. The serum PSA level can be high in prostate cancer, and a cutoff point of 4 ng/ml is used to decide if further testing is required.

However, serum PSA screening is not applied worldwide. Data from the European Randomized Study of Screening for Prostate Cancer (ERSPC) revealed a 21% decrease in mortality after 11 years of follow-up (FH Schröder et al., 2012). In contrast to this, the U.S. Prostate, Lung, Colorectal, and Ovarian (PLCO) Cancer Screening Trial failed to show the evidence of a mortality benefit after 13 years of follow-up (GL Andriole et al., 2012). Thus the screening remains a controversial topic and leads to a lack of consensus (I Heidegger, 2019).

1.1.3.2. Biopsy

Prostate biopsy is recommended after increasing/high level of serum PSA and/or abnormalities found on DRE and/or imaging (N Mottet et al., 2020; SF Shariat et al., 2008). Ultrasound (US)-guided needle biopsy is the most reliable method at present (N Mottet et al., 2020). A meta-analysis revealed no significant differences were proven in prostate cancer detection rate between transrectal and transperineal approaches (J Xue et al., 2017). Thus, both approaches are recommended.

1.1.3.3. Imaging

Although imaging findings cannot be used for cT category as described before, it still plays a vital role in primary, recurrence and metastasis disease detection.

Multiparametric magnetic resonance imaging (mpMRI) is an important tool for the detection and localization of prostate cancer (F Bratan et al., 2013). Le et al. confirmed that the detection rate was associated with index tumor status, tumor size and Gleason Score ($p < 0.001$). They reported 72% sensitivity for prostate cancer of ISUP ≥ 2 or > 1.0 cm in maximal diameter (JD Le et al., 2015). However, the detection rate for prostate cancer of ISUP 1 cancers smaller than 0.5 cc was less than 30% (F Bratan et al., 2013).

Computed tomography (CT) is widely used to detect nodal invasion but still has limitations. Malignant lymph nodes have a short axis of more than 8 mm in the pelvis and more than 10 mm outside the pelvis (N Mottet et al., 2020). However, CT or magnetic resonance imaging (MRI) cannot rule out microscopic lymph node metastases (H Hricak et al., 2007). A meta-analysis reported low pooled sensitivities for CT (42%) and MRI (39%) (AM Hövels et al., 2008). Since the reported sensitivity and specificity for CT are highly dependent on PSA level and risk stratification, it is recommended for high-risk patients with apparent clinical disease (H Hricak et al., 2007).

Malignant tumor cells are further associated with increased cell proliferation and metabolism of cell membranes (IJ de Jong et al., 2002). The radiopharmaceutical ^{11}C-choline can be incorporated into cell membranes in the form of phosphatidyl-choline in proliferating cells, giving it the potential to visualize nodal metastases in prostate cancer (L Van den Bergh et al., 2015). Similar to CT, the PSA level impacts the sensitivity of choline-positron emission tomography (PET). In patients with BCR after radical prostatectomy (RP), PET/CT detection rates ranged from 5% to 24% when the serum PSA level was < 1 ng/ml, but when the PSA was > 5 ng/ml, it rose from 67% to 100% (F Ceci et al., 2014; CR Mitchell et al., 2013; N Mottet et al., 2020; JD Soyka et al., 2012). The current guideline recommends choline-PET imaging to only be used in prostate cancer patients fit enough for curative loco-regional salvage treatment instead of early-stage recurrence (N Mottet et al., 2020).

Another conventional imaging modality is the ^{99m}Tc-bone scan. It has been used for evaluating bone metastases of prostate cancer. The mean detection rate in 23 studies was 2.3% in prostate cancer patients with a PSA level < 10 ng/ml and 5.6% in patients with ISUP ≤ 2 (S Abuzallouf et al., 2004). It has been confirmed that the sensitivity of bone scan is influenced by PSA level, ISUP grade and clinical stage (A Briganti et al., 2010). It is of note that MRI and choline PET/CT can not only detect bone metastases, but also visceral metastases. A meta-analysis reported a higher sensitivity using MRI than choline PET/CT and bone scan for bone metastases detection (G Shen et al., 2014).

Based on the facts above, imaging techniques with high sensitivity, especially for patients with low PSA levels and early-stage disease, are eagerly desired. In 2012, Afshar-Oromieh et al. demonstrated in their initial experience that PET/CT using ^{68}Ga-prostate-specific membrane antigen (PSMA)-11 (also known as *N*,*N*′-bis-[2-hydroxy-5-(carboxyethyl)benzyl]ethylenediamine-*N*,*N*′-diacetic acid [HBED-CC]) could detect prostate carcinoma relapses and metastases (A Afshar-Oromieh et al., 2012). Of 37 patients, 31 (83.8 %) showed at least one lesion suspicious for cancer at a detection rate of 60% at PSA < 2.2 ng/ml and 100% at PSA > 2.2 ng/ml (A Afshar-Oromieh et al., 2013). PET imaging based on PSMA has shown a promising detection rate and will be further discussed in section 1.2.2.

1.1.4. Primary treatment

1.1.4.1. Treatment planning

Therapy options for prostate cancer patients include RP with or without lymphadenectomy, radiation therapy, chemotherapy, androgen deprivation therapy (ADT), etc. The therapy selection depends on the clinicopathological status (PSA value, age, general condition, etc.) and patient preferences, which have placed great importance on medical decision-making (MS Litwin et al., 2017).

1.1.4.2. Active surveillance and watchful waiting

Active surveillance should be considered for low-risk prostate cancer patients to avoid over-treatment. The inclusion criteria for active surveillance lack standardization and the most accepted criteria are a PSA < 10 ng/ml, ISUP grade 1, and a clinical T1c or T2a (S Loeb et al., 2015; FB Thomsen et al., 2014). The active follow-up strategies include yearly DRE, serum PSA test every six months, repeated biopsy and mpMRI (TBL Lam et al., 2019; IG Schoots et al., 2015). It is applied mainly to low-risk patients with a life expectancy of more than ten years. It is agreed that active treatment starts when patient anxiety about surveillance occurs or a confirmatory biopsy is performed (TBL Lam et al., 2019).

Moreover, there is the watchful waiting strategy. It can be applied to patients in all stages and those who have a life expectancy of less than ten years. Watchful

waiting does not aim to cure the disease but aims to treat palliatively to maintain life quality (N Mottet et al., 2020).

1.1.4.3. Radical prostatectomy and pelvic lymph node dissection

For patients with localized prostate cancer, RP is one of the primary choices. During the RP, the entire prostate with its capsule and seminal vesicles will be removed. RP can be performed by open approach and minimally invasive approach with the assistance of laparoscopy or the da Vinci operation system.

Currently, pelvic lymph node dissection (PLND) is recommended in the treatment of intermediate- to high-risk localized prostate cancer patients, especially in whom with higher than 5% risk of lymph node involvement (A Briganti et al., 2012; DC Cheung et al., 2020; N Mottet et al., 2020). Besides, PLND and extended PLND (ePLND) represent the most accurate staging of lymph node metastasis in prostate cancer patients (A Briganti et al., 2009; N Fossati et al., 2017).

Compared to systemic treatment, PSMA-radio-guided surgery (RGS) facilitates targeted molecular surgery. It allows intraoperative detection of PSMA-expressing in small sub-centimeter metastatic lymph nodes and atypically located lesions (T Maurer et al., 2015). RGS will be further discussed in section 1.2.3.

1.1.4.4. Radiation therapy

Radiation therapy is a strategy to eliminate cancer cells using high-energy rays or particles. Radiation therapy is one of the effective treatments for patients with localized prostate cancer and was proven to have similar clinical outcomes compared with RP (FC Hamdy et al., 2016). For locally advanced prostate cancer, the combination of radiation therapy and ADT is superior to ADT or radiation therapy alone (AV D'Amico et al., 2008; P Warde et al., 2011). Besides, it can be used after the RP to further eliminate remaining tumor tissues in the operation field. It can also be applied as a palliative treatment for patients with advanced disease to help control the proliferation of malignant cells and relieve symptoms.

The main types of radiation therapy using high-energy generated outside of the body, known as external beam radiation therapy (EBRT), are Three-dimensional conformal radiation therapy (3D-CRT), Intensity modulated radiation therapy

(IMRT) and proton beam radiation therapy. IMRT is an advanced form of 3D-CRT, and it is the gold standard for EBRT (N Mottet et al., 2020). There are new machines that have scanners built into them, known as image guided radiation therapy (IGRT), which help to deliver the radiation more precisely. Unlike X-rays, protons can pass through tissues with slight damage and release energy after a certain distance. However, there is no evidence that proton beam radiation therapy causes more superior prognosis and fewer side effects than X-rays.

Unlike EBRT, brachytherapy needs an injection of radiopharmaceuticals. This method can be used in patients with massive bone metastasis. In metastatic castration-resistant prostate cancer (mCRPC) patients with bone metastases and no visceral metastases, radium-223 was proven to decrease the risk of death and prolong the time to the first symptomatic skeletal event (C Parker et al., 2013). Besides, ^{177}Lu-PSMA-617 is another promising candidate for mCRPC patients. It has been reported that ^{177}Lu-PSMA-617 radiation therapy has high response rates, low toxic effects, and reduction of pain (MS Hofman, J Violet, et al., 2018; J Violet et al., 2020).

1.1.4.5. Androgen deprivation therapy

When the disease is already in a metastatic stage or patients refuse a curative strategy, ADT can be recommended. The basic of ADT is to reduce levels of androgens and to stop stimulating prostate cancer cells to grow. Two methods can achieve androgen deprivation: suppressing the secretion of androgens and inhibiting the receptors of androgens. The widely accepted castration level is < 50 ng/dl (1.7 nmol/l) (N Mottet et al., 2020).

Bilateral orchiectomy is a simple, cheap surgical procedure and it achieves a castration level quickly after the operation (MG Oefelein et al., 2000). Since it is irreversible, it is not allowed for intermittent treatment (AD Desmond et al., 1988).

Luteinizing hormone-releasing hormone (LHRH) agonists are drugs that suppress testosterone secretion, and the treatment is known as medical castration. The representative LHRH agonists are Leuprolide, Goserelin and Triptorelin. No survival difference between orchiectomy and LHRH agonists has been reported (PB Østergren et al., 2017). LHRH antagonists bind to LHRH receptors leading

to a decrease in testosterone. More than 95% of patients achieved castration level three days after Degarelix treatment (L Klotz et al., 2008). A systematic analysis did not show a significant difference between Degarelix and agonists (A Sciarra et al., 2016). The superiority of LHRH antagonists remains to be proven. Besides, Abiraterone, an inhibitor of cytochrome P450 17α−hydroxy/17, 20-lyase (CYP17), suppresses the synthesis of testosterone in adrenal and inside the cancer cells. Bicalutamide, flutamide and nilutamide are non-steroidal anti-androgens, which connect to androgen receptors keeping the androgens from leading tumor proliferation.

1.1.4.6. Chemotherapy

Chemotherapy is not a standard treatment for early-stage prostate cancer. The indication for chemotherapy often arises when prostate cancer no longer responds to ADT. Some of the chemo drugs frequently used for prostate cancer include Docetaxel, Cabazitaxel, Mitoxantrone, Estramustine, etc. There were two clinic trials (TAX 327 and SWOG 9916), which showed a survival benefit for docetaxel in metastatic hormone-refractory prostate cancer patients (DP Petrylak et al., 2004; IF Tannock et al., 2004).

Moreover, the recent phase III Chemohormonal Therapy Versus Androgen Ablation Randomized Trial for Extensive Disease in Prostate Cancer (CHAARTED) trial revealed that the overall survival (OS) of metastatic hormone-sensitive prostate cancer (mHSPC) patients with ADT plus docetaxel was 10.4 months longer than ADT alone (57.6 vs. 47.2 months; HR 0.72; 95% CI, 0.59 to 0.89; $p = 0.0018$) (CE Kyriakopoulos et al., 2018). Chemotherapy is recommended to be used in the combination treatment.

1.1.4.7. Investigational therapies

In patients with localized prostate cancer, several potential therapeutic options have emerged. High-intensity focused US (HIFU), cryotherapeutic ablation of the prostate (cryotherapy) and focal photodynamic therapy are well established, and sufficient clinical data are available. Other therapy methods such as radiofrequency ablation and electroporation are still in the early application phases (HG

van der Poel et al., 2018). These modalities all aim to boost oncology outcomes and provide equivalent safety.

1.2. Prostate-specific membrane antigen (PSMA)

1.2.1. Structure and Expression

PSMA also known as glutamate carboxypeptidase II (GCPII) (Figure 1) (JC Evans et al., 2016) is a type II integral membrane glycoprotein with folate hydrolase, carboxypeptidase and internalization activities produced by prostatic epithelium (A Cimadamore et al., 2018; DA Silver et al., 1997). It is weakly expressed in healthy prostate tissue but is strongly overexpressed in PSMA positive prostate cancer cells (DA Silver et al., 1997). Besides, PSMA expression increases progressively in high-grade prostate tumor cells and metastatic lesions (S Mannweiler et al., 2009; S Minner et al., 2011). Only 5%-10% of primary prostate cancer lesions are PSMA negative (N Woythal et al., 2018). It is also expressed in the neovasculature of numerous solid malignancies (renal cell, bladder transitional cell, and colon) (DA Silver et al., 1997). Weak to moderate PSMA expression levels were found in endometrium glands, testis, bladder, kidney tubules, pancreas islets, heart, ganglion cells in the gastrointestinal tract and brain (P Mhawech-Fauceglia et al., 2007). Besides, Mhawech-Fauceglia et al. defined the sensitivity and specificity of PSMA in distinguishing prostate cancer from any other type of malignancy as 65.9% and 94.5%, respectively. So PSMA is still considered to be rather sensitive and highly specific for prostate cancer despite its expression by subsets of various types of tissues (P Mhawech-Fauceglia et al., 2007).

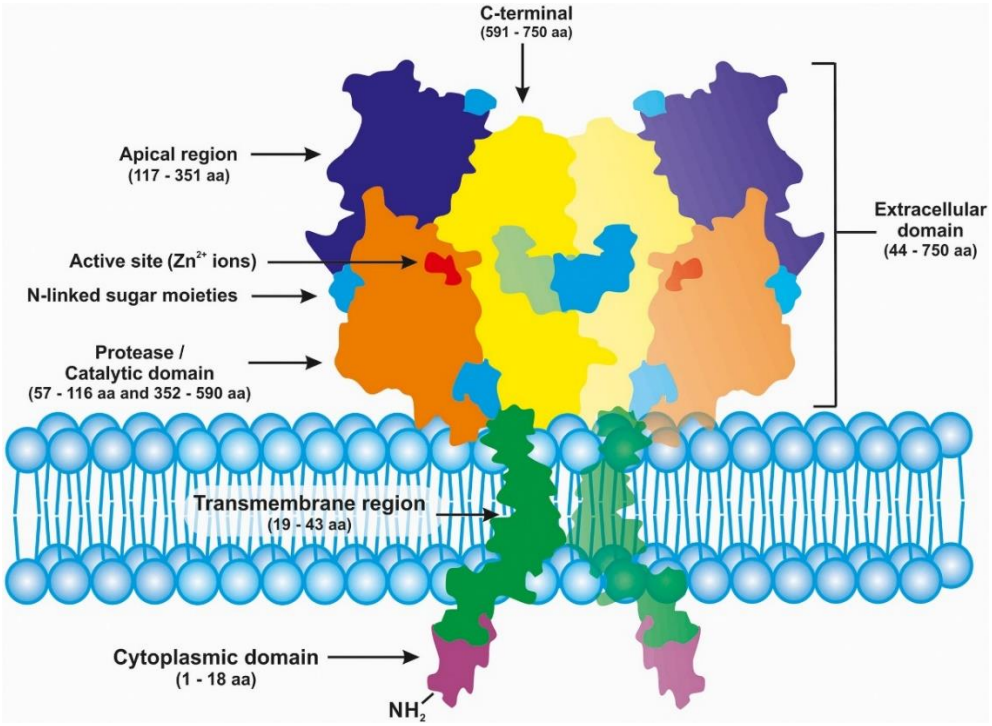

Figure 1. Schematic representation of PSMA/GCPII transmembrane protein (homodimer) (JC Evans et al., 2016).

1.2.2. PSMA-positron emission tomography (PET) imaging

The use of PET probes targeting PSMA has gained increasing interest for both imaging and therapy of prostate cancer during the last few years, not only because of its specificity for prostate tissues, but also because it proves excellent contrast-to-noise ratio and improves the detectability of lesions (T Maurer, JE Gschwend, et al., 2016; SM Schwarzenboeck et al., 2017). PSMA ligand PET-CT/MRI is mainly used in the following clinical indications: primary staging, BCR detecting and advanced disease monitoring.

1.2.2.1. Primary staging

Low-risk prostate cancer is very unlikely to spread as metastatic disease. However, in intermediate-risk to high-risk prostate cancer patients, accurate staging (Diagnosis of the local extent and extraprostatic metastasis is crucial to further treatment choices, such as RP with standard nodal dissection or extended dissection, ePLND, radiotherapeutic treatment and consideration of multimodal therapy) benefits the disease management.

1.Introduction

There is growing evidence on the performance of PSMA-ligand PET/CT in initial staging. A systematic review including 12 studies and comprising a total of 322 patients who underwent ^{68}Ga-PSMA-11 PET scanning for primary stage reported high variation in methodology and outcomes such as sensitivity (median sensitivity on per-lesion analysis 33-92%, and on per-patient analysis 66-91%) and specificity (median specificity on per-lesion 82-100%, and on per-patient 67-99%). The ability of ^{68}Ga-PSMA-11 PET to detect malignant lesions is evident across studies. Most studies demonstrate increased detection rates with respect to conventional imaging modalities (bone scan and CT) (J Corfield et al., 2018). A retrospective review has identified the ability of ^{68}Ga-PSMA-11 PET to detect metastatic prostate cancer, especially in high-risk groups. In 1,253 patients (high-risk disease in 47.6%), metastatic disease was identified by PSMA PET in 12.12% of the cohort. Lymph node metastases were suspected in 107 men, with 47.7% outside the boundaries of an ePLND. Skeletal metastases were identified in 59 men (4.7%). In men with intermediate-risk prostate cancer, metastases were identified in 5.2%, compared to 19.9% with high-risk disease (JW Yaxley et al., 2019).

Regarding intraprostatic tumor localization by ^{68}Ga-PSMA-11 PET/CT, imaging findings were confirmed histopathologically (WP Fendler et al., 2016; K Rahbar et al., 2016; N Woythal et al., 2018; C Zamboglou et al., 2017). These studies demonstrated that compared with PSMA histopathology-confirmed negative segments, the standardized uptake value (SUV) of PSMA ligand in lesions is significantly higher (SUV_{max}: 11.0 ± 7.8 vs. 2.7 ± 0.9, 11.8 ± 7.6 vs. 4.9 ± 2.9, 14.06 ± 15.56 vs. 2.43 ± 0.63, respectively, $p < 0.001$, respectively) (WP Fendler et al., 2016; K Rahbar et al., 2016; N Woythal et al., 2018). Results from a study of ^{68}Ga-PSMA-11 and multiparametric MRI using slice by slice comparison with histopathology on seven preoperative intermediate (three patients)-/high (four patients)-risk patients (340 segments) indicated that ^{68}Ga-PSMA-11 PET/CT significantly outperformed multiparametric MRI and a combination of both methods performed even better (75% and 87% for ^{68}Ga-PSMA-11 PET/CT, 70% and 82% for multiparametric MRI, and 55% and 99% for combination) (C Zamboglou et al., 2017).

An assessment of PSMA PET/CT shows an increased detection rate due to the addition of metabolic information. A recent prospective proPSMA trial demonstrated that PSMA PET/CT had a 27% greater accuracy than that of conventional imaging (92% [88-95] vs. 65% [60-69]; $p < 0.001$) (MS Hofman et al., 2020). Moreover, A retrospective study including 130 patients with primary intermediate- to high-risk prostate cancer proved ^{68}Ga-PSMA-11 PET/CT to be superior to standard routine imaging on a patient and a template basis (template-based pelvic histopathology as a reference, $p = 0.002$ and < 0.001, respectively). On template-based analysis, sensitivity, specificity, and accuracy for ^{68}Ga-PSMA PET/CT were 68.3%, 99.1%, and 95.2%, while for morphological imaging were 27.3%, 97.1%, and 87.6% (T Maurer, JE Gschwend, et al., 2016). Similar data from another study reported high sensitivity and specificity (94%, 99%, respectively) (S Hijazi et al., 2015). As a result of PSMA-negative tumors or micrometastases in single lymph node under detectable level, patients with malignant lymph nodes were missed by PSMA-ligand PET (T Maurer, M Eiber, et al., 2016).

Furthermore, for bony lesions of prostate cancer delectation, several studies showed clear superiority of PSMA-ligand PET over standard routine imaging (CT, MRI, and bone scanning) (JC Janssen et al., 2018; T Pyka et al., 2016). One study that including 75 patients and 410 bone regions indicated that ^{68}Ga-PSMA-11 PET outperformed planar ^{99m}Tc bone scintigraphy to detect affected bone regions. Sensitivities and specificities in patient-based analysis were 98.7-100% and 88.2-100% for PET, and 86.7-89.3% and 60.8-96.1% ($p < 0.001$) for ^{99m}Tc bone scintigraphy. In the region-based analysis, sensitivities and specificities were 98.8-99% and 98.9-100% for PET, and 82.4-86.6%, 91.6-97.9% ($p < 0.001$) for ^{99m}Tc bone scintigraphy, respectively (T Pyka et al., 2016). Another study including 54 prostate cancer patients who received ^{68}Ga-PSMA-11 PET/CT and ^{99m}Tc-3,3-diphospho-1,2-propanodicarboxylic acid (DPD)-single-photon emission computed tomography (SPECT)/CT within 80 days showed similar results, ^{68}Ga-PSMA-11 PET outperformed ^{99m}Tc-DPD-SPECT in detecting bone metastases in prostate cancer patients. Sensitivities and specificities in the region-based analysis were 97.7% and 100% for ^{68}Ga-PSMA-11 PET/CT, 69.4% and 98.3% for ^{99m}Tc-DPD-SPECT/CT, respectively, $p < 0.05$, respectively) (JC Janssen et al., 2018).

One prospective study evaluated changes in primary staging before and after PSMA-ligand PET/CT in 108 intermediate- and high-risk patients. Compared to conventional imaging, PSMA-ligand PET/CT upstaged an additional seven patients (6.4%) from M0 to M1, 16 from N0M0 to N1M0 (14.7%), and downstaged 3 (2.8%) from M1 to M0 disease, management changes occurred in 21% of patients (G Hruby et al., 2018). Thus, PSMA-ligand PET/CT or MRI could enable a more accurate staging of the local tumor, lymph node involvement, bone, and organ metastases, superseding the current stage and possibly improving treatment planning and prognosis. However, published data on ex vivo experiment, intraprostatic distribution, and primary staging with PSMA-ligands are still minimal, and further researches are needed to draw robust conclusions (T Maurer, M Eiber, et al., 2016).

1.2.2.2. Biochemical Recurrence (BCR)

Approximately 30% to 40% of prostate cancer patients will fail primary treatment, with a rising PSA level usually indicating recurrent disease (SM Schwarzenboeck et al., 2017). Once the BCR has been detected, it is mandatory to locate the lesions because of the great importance to further disease management. However, localization of lesions is a major challenge. Some studies indicated that salvage radiotherapy was the most effective in patients with BCR after RP at serum PSA < 0.5 ng/ml (CR King, 2012; D Pfister et al., 2014). Thus, the timing for the radiotherapy in these patients is an essential factor that affects the prognosis, which cannot be readily determined by monitoring PSA.

In patients with BCR after RP, only 11-14% of them had a positive CT (MJ Beresford et al., 2010). The pooled specificity of choline-based PET imaging was proven higher than bone scan with fewer false-positive lesions (0.99 (95% CI: 0.93-1.00) vs. 0.82 (95% CI: 0.78-0.85)) (G Shen et al., 2014). However, the PSA level and kinetics dramatically impact the sensitivity of choline PET (C Brogsitter et al., 2013; P Castellucci et al., 2014; G Treglia et al., 2014).

Afshar-Oromieh et al. further studied in a larger cohort with 319 patients with recurrent prostate cancer and a median serum PSA value of 4.59 ng/ml (mean: 161 ng/ml; range: 0.01-41395). They indicated detection rates of 47% for serum PSA values ≤ 0.2 ng/ml, 50% for serum PSA values from 0.21-0.5 ng/ml, 58% for

serum PSA values from 0.51-1 ng/ml, 71.8% for serum PSA values from 1.1-2 ng/ml, 85.9% for serum PSA values from 2.1-5 ng/ml, 92.3% for serum PSA values from 5.1-10 ng/ml, 86.2% for serum PSA values from 10.1-20 ng/ml, 100% for serum PSA values >20 ng/ml (A Afshar-Oromieh et al., 2015). Results from our group were in line with these findings, and we also demonstrated the relatively high detection rate of BCR with low PSA levels using ^{68}Ga-PSMA-11 PET (M Eiber et al., 2015; I Rauscher et al., 2018).

Moreover, data from several research groups that studied ^{18}F-labeled PSMA-ligands indicated similar and promising results. In a prospective study of 68 patients with BCR after RP underwent N-[N-[(S)-1,3-dicarboxypropyl]carbamoyl]-4-[^{18}F]fluorobenzyl-L-cysteine (^{18}F–DCFBC) PET/CT, the detection rate of ^{18}F–DCFBC PET also positively correlated with serum PSA levels, which were 15%, 46%, 83%, and 77% for PSA values < 0.5, 0.5 to < 1.0, 1.0 to < 2.0, and ≥ 2.0 ng/ml, respectively. Disease treatment was changed in 51.2% of patients due to the positive findings in the ^{18}F–DCFBC PET (E Mena et al., 2018). Results from another study including 248 patients using 2-(3-(1-Carboxy-5-[(6-[^{18}F]fluoro-pyridine-3-carbonyl)-amino]-pentyl)-ureido)-pentanedioic acid (^{18}F-DCFPyL) demonstrated similar results. The detection rate increased with higher serum PSA values: 59% with PSA level < 0.5 ng/ml, 69% with PSA level from 0.5 to < 1.0 ng/ml, 85% with PSA level from 1.0 to < 2.0 ng/ml, 95% with PSA from 2.0 to < 5.0 ng/ml, and 96% with PSA level ≥ 5.0 ng/ml (M Wondergem et al., 2019). Radiohybrid PSMA (rhPSMA)-ligands (Figure 2) are a new class theragnostic PSMA-targeting tracer, which has notably low bladder retention one-hour post-injection. Our group has shown the clinical data of the cohort with 261 patients (median PSA level: 0.961 ng/ml). The detection efficacy of ^{18}F-rhPSMA-7 PET/CT positively correlated with serum PSA levels, which were 32%, 71%, 86%, 86%, and 95% for PSA levels < 0.2, 0.2 to < 0.5, 0.5 to < 1, 1.0 to < 2.0, and ≥ 2.0 ng/ml, respectively (M Eiber et al., 2020).

Figure 3 shows a review of the comparison of the detection rates with different PSMA-ligands. However, we need to consider these results with caution considering follow-up imaging was incomplete in the whole cohort and the lack of sys-

tematic histological confirmation in the majority of the patients. There is no recommendation of a single radiopharmaceutical in the current guideline. Still, the term “PSMA-ligand PET” refers to several different tracers because there are no conclusive data about their comparison (N Mottet et al., 2020). Further clinical studies with standardized follow-up protocols and histological validation are needed to compare the outcomes of these tracers.

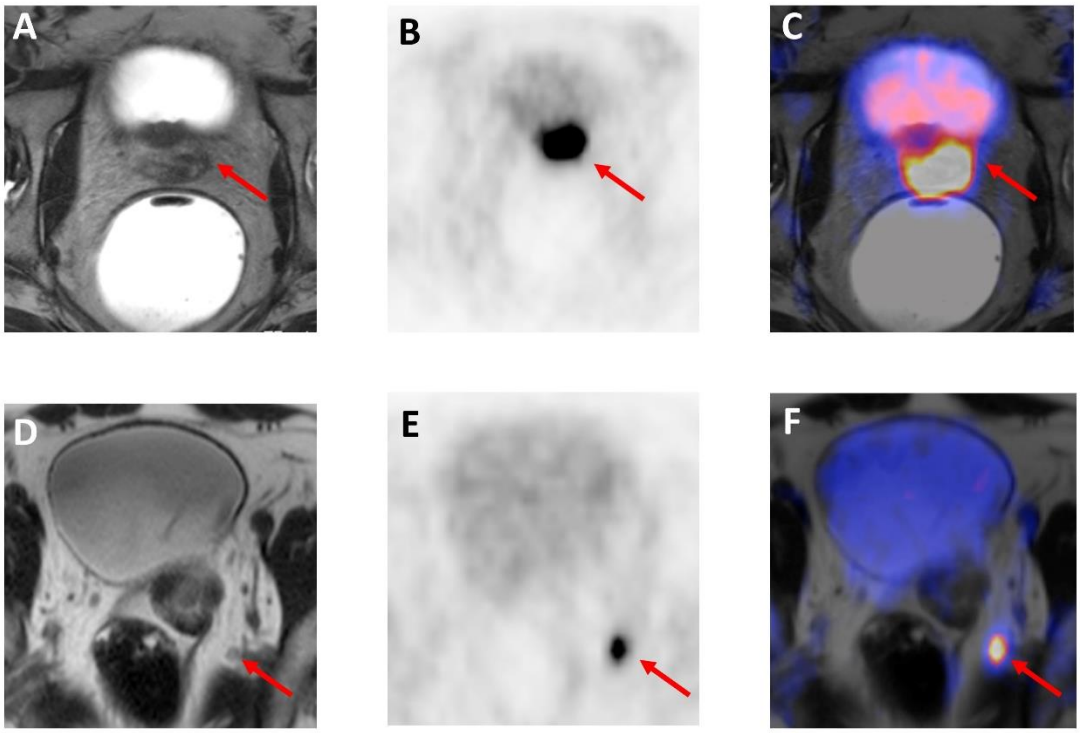

Figure 2. ^{18}F-rhPSMA7–PET/MRI of a 66-year-old patient with primary prostate cancer (serum initial PSA (iPSA): 8.74 ng/ml and Gleason Score 8 at radical prostatectomy).

A. MRI-T2 sequence shows a lesion (23 mm) in the peripheral zone in the prostate. B. PET and C. fused PET-MRI images demonstrate intense PSMA expression in the lesion. D. A small lymph node (5 mm) adjacent to the left internal iliac artery is depicted in the T2 sequence of MRI. E. PET and F. fused PET-MRI images demonstrate intense PSMA expression in the correlated lymph node. Pathological diagnosis confirmed the specimen of lymphadenectomy metastasis.

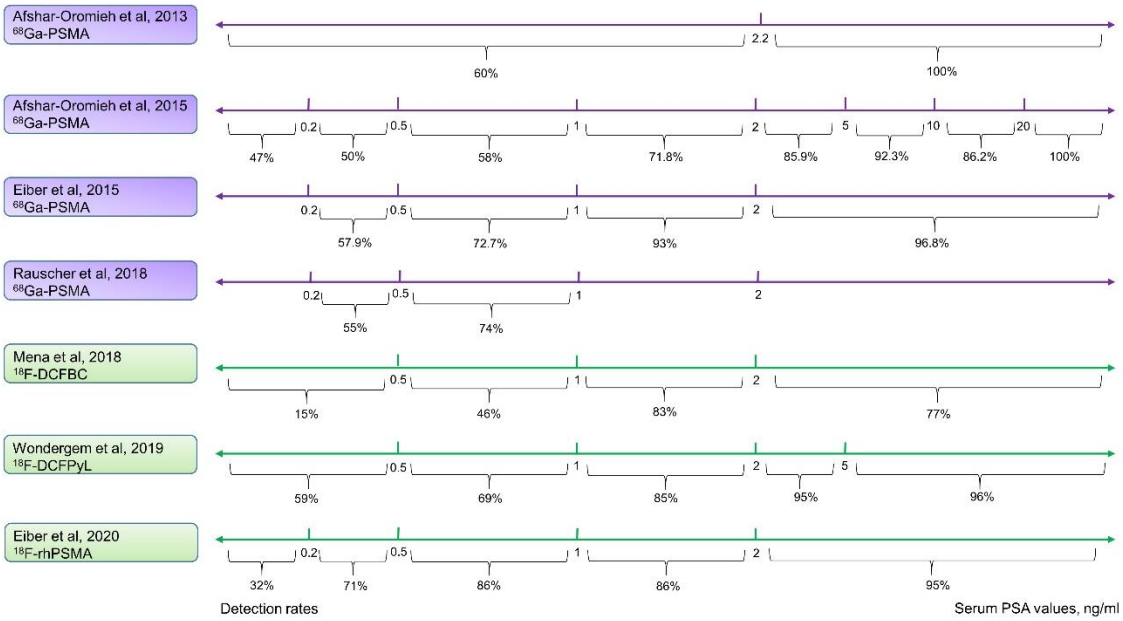

Figure 3. Comparison of detection rates of ^{68}Ga and ^{18}F labeled PSMA-ligands.

Purple lines indicate the ^{68}Ga-PSMA-11, and green lines show ^{18}F-PSMA-ligands. The ^{68}Ga-PSMA-11 PET has a modest high detection rate even in low serum PSA levels. ^{18}F-DCFPyL has a higher detection rate in all the deferent PSA levels than ^{18}F-DCFBC, and they are comparable with ^{68}Ga-PSMA-11. ^{18}F-rhPSMA performs the best among these ^{18}F labeled ligands and similar to ^{68}Ga-PSMA-11.

1.2.2.3. Advanced Diseases Monitoring

For prostate cancer patients who experience relapsed or advanced disease, ADT represents the backbone of treatment (F Ceci et al., 2016; A Davies et al., 2019). However, 10-20% of patients will develop castration-resistant prostate cancer (CRPC) in the first five years from the initiation of ADT (SIR Alpajaro et al., 2019). Once the mCRPC is detected, OS ranges from 2 to 3 years (F Ceci et al., 2016; A Davies et al., 2019).

The assessment of serum PSA values is routinely used to monitor the disease. Of note, the reflection of serum PSA conveys information about both disease burden and disease biology. A patient with mCRPC may have a low PSA level because of a tropical disease burden or because his tumor is less reliant on androgen receptor signaling. Besides, visceral metastases may develop without rising PSA (C Pezaro et al., 2014). Thus, increasing PSA values is associated with disease progression, and decreasing PSA values is not always related to therapy

response (F Ceci et al., 2016). PSA alone is not reliable enough for monitoring (H Payne et al., 2011).

Some preliminary studies demonstrated the possibility of choline PET/CT in disease monitoring of mCRPC patients (U De Giorgi et al., 2014; U De Giorgi et al., 2015). However, another prospective study reported no significant correlation between image findings from ^{11}C-choline-PET/CT and therapy response assessment of Response Evaluation Criteria in Solid Tumors (RECIST 1.1) and clinically routine criteria (progressive disease (PD) and non-progressive disease (nPD)) (SM Schwarzenböck et al., 2016). In summary, the routine application of choline PET/CT in disease monitoring of mCRPC patients seems to be limited.

Beyond choline, new tracers have been invented for monitoring disease. Although they demonstrated promising results, e.g., ^{68}Ga-PSMA-11 PET/CT (N Plouznikoff et al., 2019), these procedures' efficacy as indicators in mCRPC patients has not yet been recommended by the guideline (N Mottet et al., 2020).

1.2.2.4. Prostate cancer molecular imaging standardized evaluation (PROMISE): miTNM classification

Most recently, a unified language-imaging TNM system (miTNM, version 1.0) was proposed for imaging reporting and guiding standardized image interpretation. An overview of miTNM, anatomic regions, and disease patterns are given in Table 4 to Table 8 and Figure 4 (M Eiber et al., 2018).

Table 4. miTNM Classification for PSMA-ligand PET/CT or PET/MRI (M Eiber et al., 2018).

Class	Description
Local tumor (T)	
miT0	No local tumor
miT2	Organ-confined tumor; report intraprostatic tumor location on sextant basis (Table 5)
u	Unifocality
m	Multifocality
miT3	Non-organ-confined tumor; report intraprostatic tumor location on sextant basis (Table 5)
a	Extracapsular extension
b	Tumor invading seminal vesicles

miT4	Tumor invading adjacent structures other than seminal vesicles, such as external sphincter, rectum, bladder, levator muscles, or pelvic wall
miTr	Presence of local recurrence after radical prostatectomy
Regional nodes (N)	
miN0	No positive regional lymph nodes
miN1a	Single lymph node region harboring lymph node metastases; report location by standardized template (Table 6 and Table 7)
miN1b	Multiple (≥2) lymph node regions harboring lymph node metastases; report locations by standardized template (Table 6 and Table 7)
Distant metastases (M)	
miM0	No distant metastasis
miM1	Distant metastasis
a	Extrapelvic lymph nodes; additionally report location by standardized miM1a template (Table 6 and Table 7)
b	Bones; additionally report pattern (Table 8) and involved bones if unifocal or oligometastatic
c	Other sites; additionally report involved organ

CT = computed tomography; MRI: magnetic resonance imaging; PET = positron emission tomography; PSMA = prostate-specific membrane antigen.

Table 5. Sextant Segmentation of Prostate Gland (M Eiber et al., 2018).

Segment	miT2-4 template
LB	Left base
RB	Right base
LM	Left mid
RM	Right mid
LA	Left apex
RA	Right apex

Table 6. Lymph Node Regions (M Eiber et al., 2018).

Region	Template	Report left/right
miN1a/b		
II	Internal iliac	Yes
EI	External iliac	Yes
CI	Common iliac	Yes

OB	Obturator	Yes
PS	Presacral (presciatic)	No
OP	Other pelvic (specify)	No
miM1a		
RP	Retroperitoneal	No
SD	Supradiaphragmatic	Yes or no
OE	Other extrapelvic (specify)	Yes or no

Table 7. Description of anatomical delineation of pelvic lymph node territories (M Eiber et al., 2018).

miNa/b template	Anatomical boundaries
Internal iliac (II)	bifurcation internal/external iliac arteries, pelvic floor, bladder wall, obturator nerve
External iliac (EI)	bifurcation internal/external iliac arteries, circumflex iliac vein and endopelvic fascia, psoas muscle and genitofemoral nerve and medial border external iliac artery
Common iliac (CI)	aortic bifurcation, bifurcation internal/external iliac arteries, psoas muscle and genitofemoral nerve and medial border common iliac artery
Obturator (OB)	bifurcation internal/external iliac arteries, pelvic floor, obturator nerve, and medial border external iliac artery
Presacral (PS, aka: presciatic)	Triangle between medial borders of common iliac arteries and line connecting internal/external iliac arteries' bifurcations; dorsal border: promontory and proximal sacrum (S1–S2)

Table 8. Pattern of Bone Involvement (M Eiber et al., 2018).

Abbreviation	Pattern of bone involvement
Uni	Unifocal
Oligo	Oligometastatic (n ≤ 3)
Diss	Disseminated
Dmi	Diffuse marrow involvement

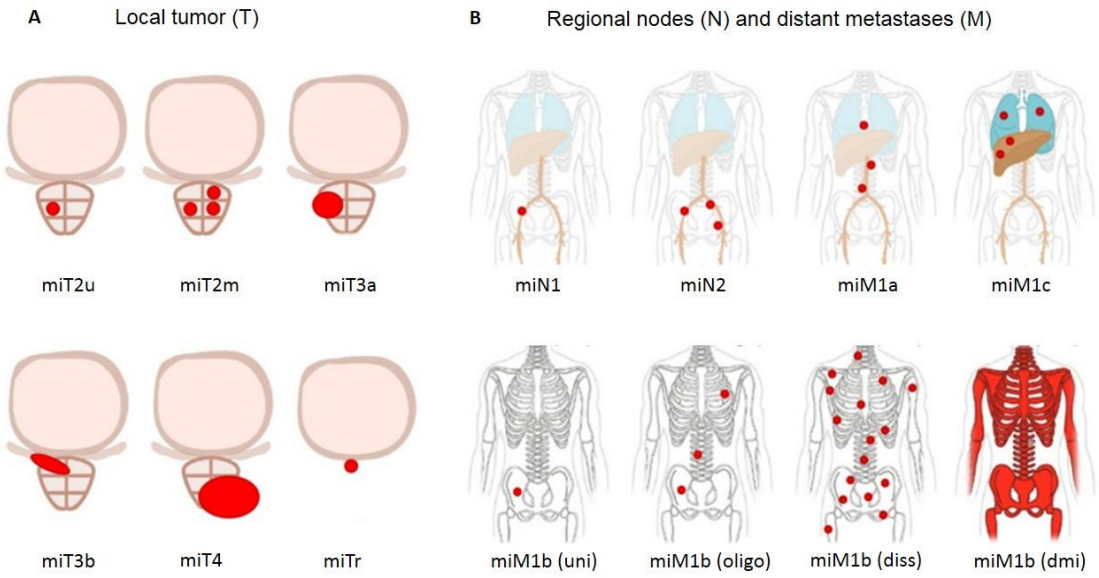

Figure 4. miTNM classification for reporting by PSMA-ligand PET/CT/MRI.

(A) local tumor sketch map and lymph node, visceral and (B) bone metastases. Tumor involvement is delineated in red (M Eiber et al., 2018).

1.2.3. Radio-guided surgery

As described in section 1.2.2.2., many prostate cancer patients have a BCR even after primary treatment with RP and/or radiation therapy. In early BCR, prostate cancer recurrence within the lymph nodes is commonly present in addition to local recurrence. Salvage lymph node resection is increasingly used in this scenario. However, metastatic lymph nodes can be atypically located and/or morphologically small, hampering its accurate identification both before potential surgery as well as during resection (T Maurer et al., 2018).

PSMA-radioguided surgery allows the detection of PSMA positive prostate cancer cells and metastatic lymph nodes (T Maurer et al., 2015). Radioguided surgery employs γ-emission from ^{111}In or ^{99m}Tc-labelled PSMA-ligands for intraoperative measurements and acoustic feedback by a gamma probe (Figure 5.) (T Maurer, M Eiber, et al., 2016).

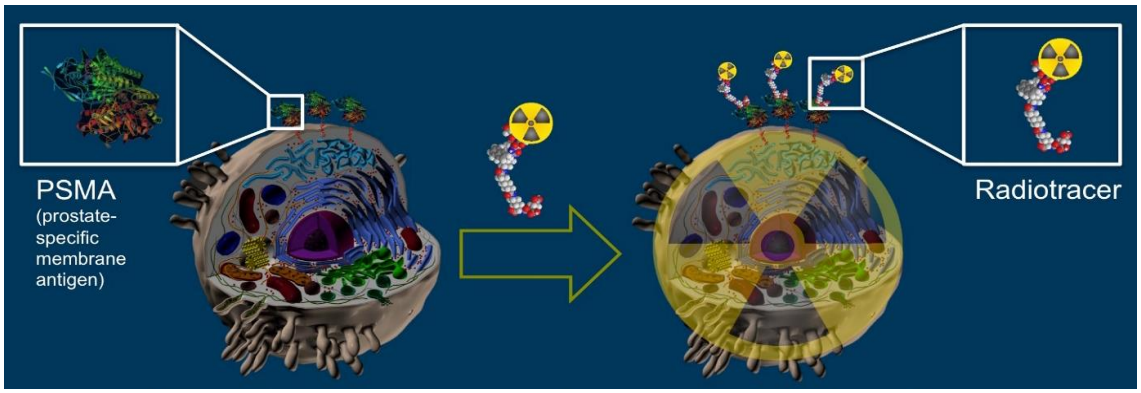

Figure 5. PSMA positive prostate cancer cells can be targeted using radiotracers.

This figure was modified from Maurer et al. (T Maurer et al., 2018).

Mauer et al. has reported a method for direct detection of metastatic prostate cancer lesions via PSMA targeted radioactivity which has been primarily used for early BCR. In the proof-of-concept report, one patient with primary prostate cancer and evidence of lymph nodes metastases and four patients with evidence of recurrent disease to regional lymph nodes on preoperative ^{68}Ga-PSMA-11 PET imaging were included. A 1,4,7,10-tetraazacyclododececane,1-(glutaric acid)-4,7,10-triacetic acid (DOTAGA)-conjugated peptide-based ligand targeting PSMA (PSMA-I&T; investigation and therapy) was used (M Weineisen et al., 2015). All patients received an intravenous injection of the ^{111}In-PSMA-I&T 24 h before surgeries. In this feasibility study, ^{111}In-PSMA-I&T-RGS facilitated intraoperative resection of subcentimeter metastatic lymph nodes. The minimal size of the resected metastatic lesion was 2 mm. Histological analysis confirmed that all suspicious lesions with positive measurement in RGS were metastatic (T Maurer et al., 2015).

Although ^{111}In-PSMA-I&T showed promising results, it has several disadvantages like high radiation burden, limited availability of ^{111}In and high costs (P Benz et al., 1991; A Bunschoten et al., 2016). In contrast, ^{99m}Tc is the most widely applied and available radioisotope. It emits γ-photons of 141 keV and has a half-life of 6h. Due to the medium energy γ-radiation, the radiation burden is relatively low (A Bunschoten et al., 2016).

In 2016 ^{99m}Tc-PSMA-I&S (imaging and surgery) was developed, which is a ^{99m}Tc-labeled probe for PSMA-targeted RGS with high stability in vivo and elevates lesion-to-background contrast at the time of surgery (S Robu et al., 2017). Maurer et al. reported a retrospective analysis including 31 patients with BCR after primary RP and then underwent ^{99m}Tc-PSMA-RGS. All the patients were intravenously injected ^{99m}Tc-PSMA-I&S the day before surgeries. In 132 surgical specimens, 58 (43.9%) contained metastatic lesions confirmed pathologically. Forty-six samples were correctly identified intraoperative using gamma probe measurements. No specimen was false positive, while 12 were false negative. They concluded this novel approach had a sensitivity of 83.6% (95% confidence interval [CI]: 70.9-91.5%), a specificity of 100%, a positive predictive value of 100%, a negative predictive value of 89.2% (78.0-95.0%), and an accuracy of 93.0% (85.8-96.7%) (T Maurer et al., 2018).

Moreover, the same group carried out an expanded study including 121 patients with recurrent prostate cancer who underwent PSMA RGS (^{111}In-PSMA-I&T and ^{99m}Tc-PSMA-I&S) to describe the outcome. Nearly all the prostate lesions were removed and 66% of patients achieved a complete biochemical response, which is higher than other studies (N Fossati et al., 2019; N Suardi et al., 2015). A 64% of treatment-free survival in the 1st year after RGS was reported. The side effects were considered to be dependent on the location of recurrent lesions (T Horn et al., 2019).

Clinically, patients benefit from RGS due to accurate resection of suspicious metastatic lymph nodes, besides, it also provides an excellent research opportunity.

1.2.4. Correlation between PSMA expression and prognosis

Currently used risk stratification systems have limited prognostic value in prostate cancer. To date, PSA is the most widely used biomarker for prostate cancer detection and prognosis prediction. However, it also has limitations and inconsistency (DA Chistiakov et al., 2018). Consequently, there is a clear need for more accurate and reliable biomarkers for prostate cancer.

1.Introduction

Numerous studies correlated the PSMA expression (immunohistochemical staining) with Gleason Score and/or Gleason Pattern, and results focus on different aspects. Early studies associated PSMA expression with prostate cancer malignancy, and a positive correlation between PSMA expression and Gleason Score was observed (RS Israeli et al., 1994; M Kawakami et al., 1997; C Marchal et al., 2004; DA Silver et al., 1997; SD Sweat et al., 1998). One recent study including 79 prostate biopsies and 28 prostatectomies using three subgroups (group1: Gleason Score 6; group2: Gleason Score 7; group3: Gleason Score 8-10) indicated that PSMA expression was positively correlated with Gleason Score (biopsies and prostatectomy samples, $p < 0.001$ and $= 0.007$, respectively). They did not observe the differentiated expression of PSMA between Grade Group 2 (Gleason Score 7a) and Grade Group 3 (Gleason Score 7b). Regarding Gleason Pattern, relatively lower expression of PSMA was observed in Gleason Pattern 3 compared with Gleason Pattern 4 and Gleason Pattern 5 ($p < 0.001$) (S Bravaccini et al., 2018).

As a potential biomarker, PSMA could be able to predict disease outcomes. Increasing evidence shows that the PSMA expression of the primary tumor is associated with a worse prognosis (MC Hupe et al., 2018; S Minner et al., 2011; A Paschalis et al., 2019; S Perner et al., 2007; JS Ross et al., 2003). For example, one study with 450 patients (S Perner et al., 2007) and another study with 1700 samples (S Minner et al., 2011) demonstrated that PSMA expression was independently associated with PSA recurrence post-operation (Figure 6 and Figure 7). Paschalis et al. found tumors with deoxyribonucleic acid (DNA) damage repair (DDR) correlated with higher PSMA expression ($p = 0.016$), which could be a further explanation of the association between PSMA expression and survival (A Paschalis et al., 2019). Besides, PSMA expression can be heterogeneous even within the same primary tumor (S Mannweiler et al., 2009), and around 5-10% of primary prostate cancer are PSMA negative on Immunohistochemistry (IHC) (S Minner et al., 2011). Despite these, PSMA is still a promising biomarker for molecular therapy, imaging approaches, and prognosis prediction.

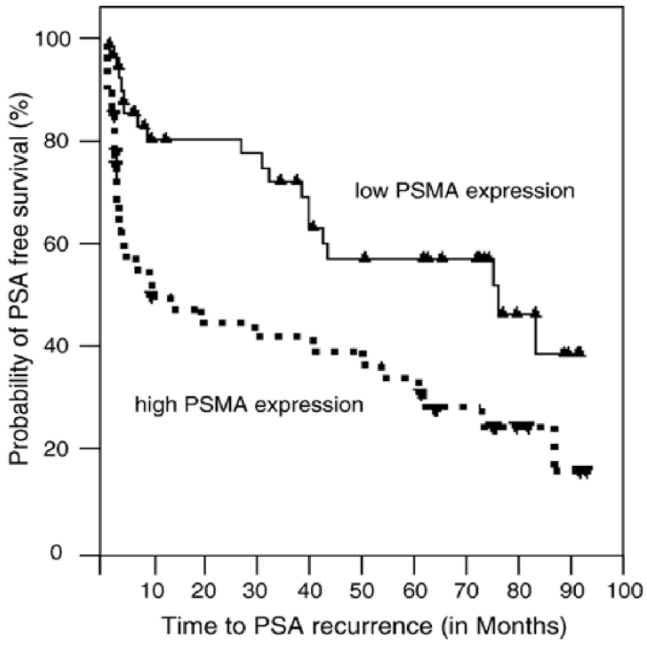

Figure 6. Kaplan-Meier curves of PSMA expression in prostate cancer patients.

Patients with high PSMA expression tumors had a significantly high PSA recurrence rate (log-rank, $p = 0.003$) compared with low PSMA expression tumor patients. PSA failure in this study was defined as a serum PSA value greater than 0.4 ng/ml during follow-up. This figure was modified from Perner et al. (S Perner et al., 2007).

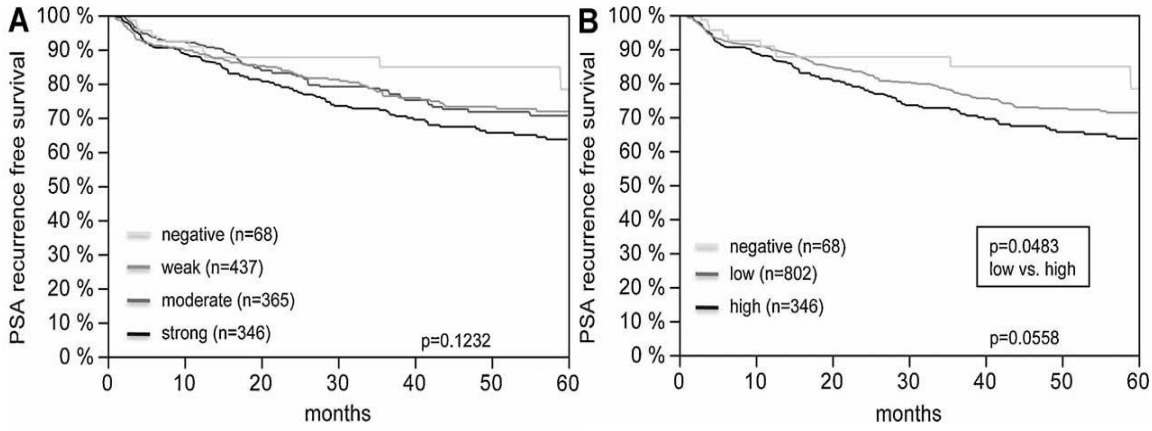

Figure 7. PSMA expression and recurrence (postoperative PSA of 0.1 ng/ml and rising) free survival in prostate cancer patients.

A: comparison of 4 groups with different levels of PSMA staining in IHC. B: analysis in the same cohort after combing the weak and the moderate group as “low.” This figure was modified from Minner et al. (S Minner et al., 2011).

1.2.5. Evaluation of PSMA-ligand uptake and histopathological findings

^{68}Ga-PSMA-11 and other PSMA-ligands bind the enzymatic pocket of PSMA based on the glutamate-urea-lysine moiety but different linkers and chelators (KL Chatalic et al., 2016). The J591 PSMA antibody binds a site located in the apical region of the extracellular domain of PSMA, which is distant from the enzymatic pocket (MI Davis et al., 2005; JR Mesters et al., 2006; PM Smith-Jones et al., 2000). It is hypothesized that different tumor uptake of ^{68}Ga-PSMA-11 correlates with PSMA expression and thereby with the prognosis of prostate cancer patients.

In order to register images of PSAM-ligand PET and histopathology, manual re-assembly using imaging process software is the most common method. One study analyzed 112 segments from six patients using a mapping method (O Bettendorf et al., 2007; O Eminaga et al., 2010) for the topographic analysis (Figure 8). They demonstrated that the correlation of ^{68}Ga-PSMA-11 PET and histological results. Moreover, they showed the median SUV_{max} of lesions that were histologically confirmed was significantly higher than that of normal tissue (11.0 ± 7.8 vs. 2.7 ± 0.9, $p < 0.001$) (K Rahbar et al., 2016). Another study from Rowe et al. enrolled 13 patients, and the imaging process software was also used to assemble the images from histology sections to ^{18}F-DCFBC PET manually. They proved by per-segment analysis that ^{18}F-DCFBC PET had significantly higher specificity than MRI (0.96 and 0.89, respectively), especially for detecting high-grade (Gleason Score 8 and 9) and greater than 1 ml in size lesions. Besides, ^{18}F-DCFBC uptake in tumors was positively correlated with Gleason Score and was significantly higher than in benign prostatic hypertrophy (median SUV_{max}: 3.5 vs. 2.2; $p = 0.004$) (SP Rowe et al., 2015).

Although these studies have shown promising results, the method of assembling the images from histology sections to PET CT/MRI has limitations: 1) the resolution of PET images is relatively low, and the precise image registration is complicated; 2) pathologists routinely cut the prostate specimens perpendicular to the long axis of urethra. PET images need to be rotated to find a proper orientation.

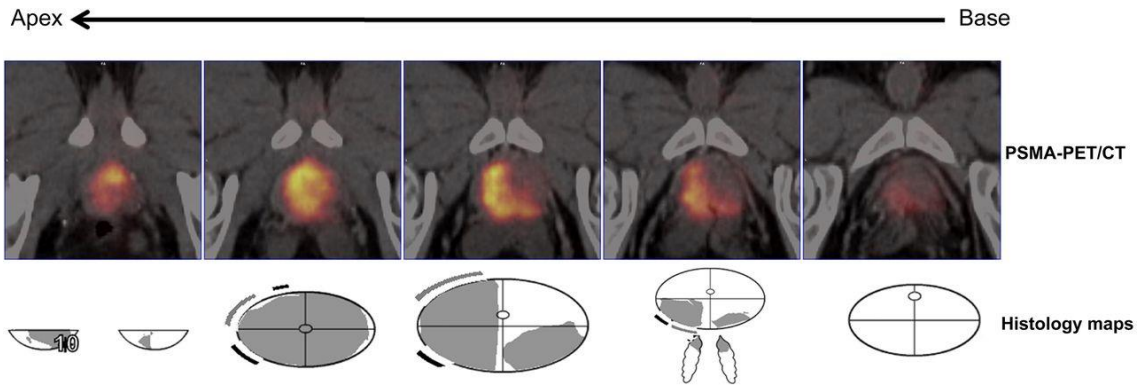

Figure 8. An example map of reangulated slices from one patient.

The upper line lists the ^{68}Ga-PSMA-11 PET imaging, and the lower line shows the concordant histological maps. This figure was modified from Rahbar et al. (K Rahbar et al., 2016).

2. Objective and planned analysis

PSMA expression in prostate cancer has gained increasing attention in the past decade since PSMA-ligands have been widely used for PET/CT or PET/MRI and therapeutic applications (C Zamboglou et al., 2016). PSMA-expression assessment using IHC is well established. Due to the different binding mechanisms, the bio-distribution of antibodies and peptides are potentially different. Quantitative analysis of the association between PSMA-ligands uptake and histopathology remains to be determined. Moreover, the predictive value of PSMA-ligands uptake and PET imaging in primary prostate cancer patients is still unclear. The current project aimed to assess the biodistribution of ^{99m}Tc-PSMA-I&S within prostate cancer lesions using high-resolution autoradiography (ARG) and explore the correlation between PSMA-ligand uptake in clinical PET-imaging and histopathological findings (Gleason Pattern, Gleason Score, PSMA expression, etc.).

2.1. Preclinical assessment of PSMA-ligand uptake in prostate cancer

In the preclinical research, we aimed to exploit a detailed comparison of ^{99m}Tc-PSMA-I&S uptake by performing high-resolution ARG and histopathology using the same tissue. The intriguing aspect of this approach is that the signal of radioactivity arises from the exact same tissue, which is further processed for histopathology sections. Compared with the registration of PET and histopathology images, the misalignment caused by manual image rotation and processing was avoided. We could then investigate the tracer uptake on the microscopic level, especially in different Gleason Scores and Gleason Patterns of prostate cancer cells.

2.2. Clinical value of pre-treatment ^{68}Ga-PSMA-11 PET to predict BCR

Second, we aimed to investigate the value of ^{68}Ga-PSMA-11 PET to predict time to BCR in primary prostate cancer patients after RP. In a retrospective analysis,

the PROMISE miTNM classification system and relevant clinicopathological parameters were evaluated. We intended to discover their potential for predicting prognosis and establish a prognosis prediction system including mainly information from PSMA-ligand PET imaging.

3. Material

3.1. Technical equipment

Table 9. Technical equipment

Device	Company
Aperio AT2 scanner	Leica Biosystems, Nussloch, Germany
Aperio CS scanner	Leica Biosystems, Nussloch, Germany
Crystal Probe CXS-SG603	Crystal Photonics, Berlin, Germany
CRC-15R Dose Calibrator	Capintec, Inc, Florham Park, USA
Freezer (4 °C)	Robert Bosch, Gerlingen, Germany
Freezer (-20 °C)	Liebherr-International, Bulle, Switzerland
Freezer (-80 °C)	UniEquip, Planegg, Germany
Gamma counter 2480 Wizard	PerkinElmer, Waltham, USA
Microscope Axiovert 10	Carl Zeiss, Oberkochen, Germany
Molecular Dynamics Storage Phosphor Screen	GE Healthcare, Chicago, United States
Imaging plate scanner CR35 Bio	Elysia-raytest, Straubenhardt, Germany
Pipette	Eppendorf, Hamburg, Germany
Pipetus	Hirschmann, Eberstadt, Germany
Precision Balance	Sartorius, Göttingen, Germany
Temperature control ETS-D4 fuzzy	IKA, Staufen, Germany
Thermomixer comfort	Eppendorf, Hamburg, Germany
X-Ray cassette	Rego X-ray GmbH, Augsburg, Germany

3.2. Consumable supplies

Table 10. Consumable supplies

Consumable	Company
50 ml/15 ml tube	Greiner Bio-One, Kremsmünster, Austria
96 well cell culture plate	Greiner Bio-One, Kremsmünster, Austria
Aspiration Pipette (2 ml)	Sarstedt, Nümbrecht, Germany
Gloves nitrile	Sempermed, Wien, Austria

Grace Bio-Labs Press-To-Seal silicone isolator	Sigma-Aldrich, Missouri, United States
PAP pen	Sigma-Aldrich, Missouri, United States
Phosphor imaging plate	Fujifilm, Tokyo, Japan
Pipette tips (10 µl, 200 µl, 1000 µl)	Sarstedt, Nümbrecht, Germany
Serological Pipettes (5 ml, 10 ml, 25 ml)	Greiner Bio-One, Kremsmünster, Austria
SuperFrost Ultra Plus Adhesion Slides	Thermo Fisher Scientific, Massachusetts, United States

3.3. Reagents and chemicals

Table 11. Reagents and chemicals

Reagent	Company
DPBS	Gibco, Thermo Fisher Scientific, Waltham, USA
Ethanol	Merck, Darmstadt, Germany
Hydrochloric acid (HCl) 30%	Merck, Darmstadt, Germany
$MgCl_2$	Sigma-Aldrich, Taufkirchen, Germany
Tris	Sigma-Aldrich, Taufkirchen, Germany

3.4. Buffers and solutions

Table 12. Buffers and solutions

Buffer/solution	Composition	Application
PSMA buffer	170 mM Tris-HCl buffer, PH 7.4 containing 10 g/l bovine serum albumin (BSA), 5 mM $MgCl_2$	Ex vivo incubation

3.5. Antibodies

Table 13. Antibodies used for IHC

Antibody	Clone	Dilution	Company
PSMA	3E6	1:50	Dako, California, USA

3.6. Kits

Table 14. Kits

Reagent	Produced by
Precursor PSMA-I&S synthesis	Chair for Pharmaceutical Radiochemistry Technische Universität München Walther Meissner Strasse 3, 85748 München, Germany

3.7. Software

Table 15. Software

Adobe Photoshop version CS5
AIDA Image analyzer software version 4.21
EndNote version X9
GraphPad Prism version 8.0
Leica Aperio ImageScope version 12.4.0.7018
Microsoft Office (Word, Excel, PowerPoint) 2013
SPSS version 20.0
Siemens Syngo.via

4. Methods

4.1. Preclinical analysis

4.1.1. Ex vivo experiment

4.1.1.1. Sample preparation

One 10 µm cryosection from each prostate was collected from the tissue for intraoperative frozen section diagnosis. A continuous slide of each fresh cryosection was provided for hematoxylin and eosin (HE) staining, and HE slides were then scanned with a Leica AT2 scanner (Table 9) into our e-slide database.

Fresh cryosections were stored in a dry ice box and delivered to our Nuclear medicine department. Sections were kept at -80 °C for at least seven days to decay the remaining ^{99m}Tc.

Ice-cold PSMA buffer (Table 12) was used to re-hydrate sections and remove the optimal cutting temperature (OCT) compound. After the section was dried carefully, a hydrophobic barrier outlining the tissue was drawn using a PAP pen. After it dried out, approximately 1 ml ^{99m}Tc-PSMA-I&S for patients was dropped on the tissue. ^{99m}Tc-PSMA-I&S was prepared as previously described (S Robu et al., 2017). The section was then incubated at room temperature for 1.5 hours. During the incubation, a slide box with wet paper towels added for humidity control was used. Radioligand solution was removed and followed by three 5 min washes with PSMA buffer (Table 12). After it dried under the fume hood, the samples were ready for ARG.

4.1.1.2. Autoradiography (ARG) imaging

Standards preparation

We prepared standards to normalize the exposure time in each experiment and to generate calibration curves between the density of ARG signal and units of radioactivity.

Firstly, the shape modified Grace Bio-Labs Press-To-Seal silicone isolator was fixed on a microscope slide. Then 10 1:2 dilutions of ^{99m}Tc-PSMA-I&S solution using DPBS were prepared. Then 5 µl of each dilution were added into Gamma counter sample containers for counts per minute (CPM) measurement. The same samples were measured by a CRC-15R dose calibrator for absolute values (Becquerel [Bq]). Afterward, 5 µl of each dilution were spotted into the small holes within the silicone. After they dried on the surface of a thermomixer, standards preparation was accomplished, and they can be placed into the cassette with the tissues for ARG.

ARG

For determining the activity accumulation of ^{99m}Tc-PSMA-I&S on the microscopic level, the prepared samples were placed in a light-proof box together with standards. Photos of samples and standards were taken before the measurement as references for image registration. A plastic film was covered on the top of samples to protect the phosphor imaging plate from contamination. Afterward, radioactive tissue samples were exposed for 6 h in a dark enclosure to prevent exposing to ambient light (Figure 9). Activities of samples were measured by phosphor imaging plates and scanned by the imaging plate scanner, and then images were analyzed using AIDA Image analyzer software (Table 15).

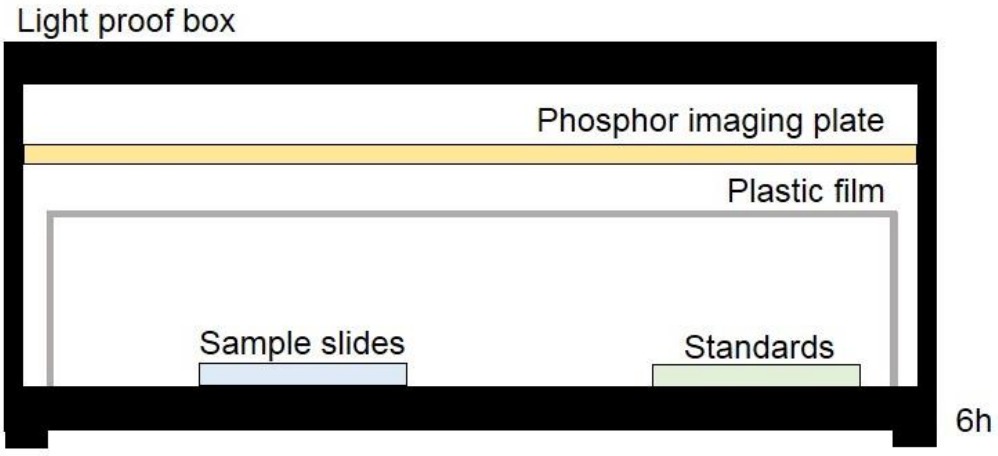

Figure 9. Schematic diagram of ARG for ex vivo analysis.

4.1.1.3. Image registration

Digitalized HE slides and autoradiographic data were registered using Adobe Photoshop (Version CS5, Table 15). A combination of visual landmarks such as tumor edges, holes from vessels, and ink marks was used to register image datasets. Registration errors of each image set were almost free from subsequent registration, because these two sections were cut continuously.

A 1×1 mm^2 matrix was applied to each HE digital image. An experienced pathologist indicated benign and malignant regions using Leica Aperio ImageScope (Table 15) and annotated the percentage of malignant cells in each grid. Then the same matrix was applied to the autoradiographic data. The quantum level (QL) value in each grid was analyzed using AIDA Image analyzer.

4.1.1.4. Image analysis

Relative activity in each grid based on the tumor-to-normal ratio was calculated. In each section, we calculated the mean QL of grids that contain non-tumor cells (QL_{mean}), and then the relative activities of the grids that contain tumor cells were calculated using the formula:

$$\text{Relative Activity}_{\text{grid}} = \frac{\text{QL}_{\text{grids with tumor}}}{\text{QL}_{\text{mean}}} \qquad \text{Eq.1}$$

The absolute activities of autoradiographic data were calibrated using standards with a known activity concentration. The absolute activity of each grid was calculated using the following formula:

$$\text{Absolute Activity}_{\text{grid}} = \frac{(a\times \text{QL}_{\text{standard}}+b)\times \text{Area}_{\text{grid}}}{\text{Area}_{\text{standard}}} \qquad \text{Eq.2}$$

where $QL_{standard}$ is the QL of each standard, $a\times QL_{standard}+b$ is the formula generated from calibration curves, $Area_{grid}$ is the area of the grid, $Area_{standard}$ is the area of standards.

4.1.2. In vivo experiment

4.1.2.1. Patients

Between November 2018 and January 2020, 17 consecutive primary prostate cancer patients with PSMA-ligand PET confirmed PSMA positive metastatic pelvic lymph nodes were scheduled for RGS. All investigations were conducted following the Helsinki Declaration and national regulations. The Ethics Committee of the Technical University Munich approved the retrospective analysis of the clinical data.

4.1.2.2. Overview of workflow

In the first step, a feasible workflow was established considering the clinical use of RGS in primary prostate cancer. As this was an exploratory investigation, care was taken that the usual clinical workflow and treatment of the patient was unaffected. Only patients in whom PSMA RGS in primary prostate cancer was performed for a clinical indication were potential candidates for this analysis.

We have successfully established a workflow that allows the correlation of ^{99m}Tc-PSMA-I&S labeled prostatectomy specimens ARG with histology and PSMA IHC staining on the same tissue material without interfering with the clinical diagnostics. Figure 10 shows the workflow we developed for this project.

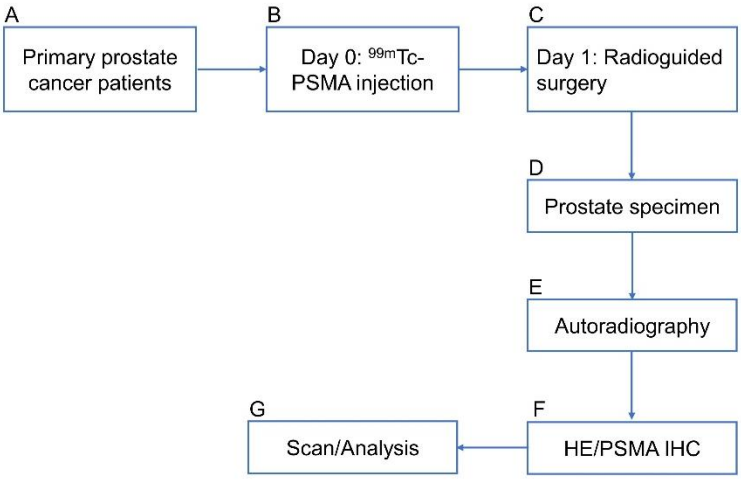

Figure 10. The workflow of preclinical study.

A: Primary prostate cancer patients with PSMA-ligand PET confirmed PSMA positive pelvic lymph nodes metastasis underwent RGS. B: ^{99m}Tc-PSMA-I&S was injected intravenously one day before RGS. C: RGS was performed one day after

the injection. D: Prostate specimens were resected and routinely delivered to pathology for further processing. E: The prostate specimen was processed according to the diagnostic standard. Every second slice was fixed in formalin and performed ARG measurement. F: After overnight exposure, the slices were reintroduced into routine diagnostics. HE staining and PSMA IHC staining sections were accomplished. G: All slides were digitized with an Aperio CS slide scanner or Aperio AT2 slide scanner. The slides were annotated using Aperio ImageScope and then overlaid with the ARG images using Adobe Photoshop for further analysis.

4.1.2.3. Sample preparation

The prostate specimens were cut perpendicular to the long axis of the urethra into 6-10 slides according to the diagnostic standard. Every second slice was put into a handmade plastic bag. Then, the bag was filled with formalin and sealed properly (Figure 11).

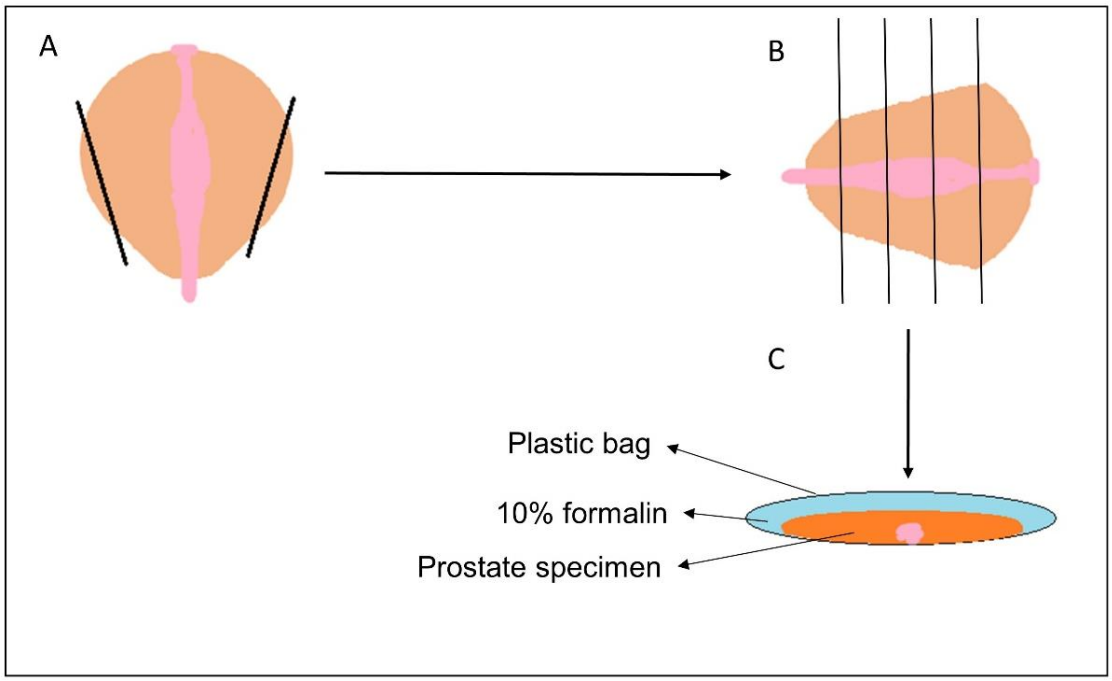

Figure 11. Sample preparation of in vivo PSMA-ligand uptake analysis.

A: The prostate specimen from RP (black lines indicate the resected parts for cryosections). B: The prostate specimen was cut from base to apex and perpendicular to the long axis of the urethra. C: Every 2nd slice of the specimen was fixed in a sealed plastic bag filled with 10% neutral-buffered formalin for ARG.

4.1.2.4. ARG imaging

Standards preparation and ARG procedure were the same as 4.1.1.2. However, the incubation time was 24h instead of 6h (Figure 12).

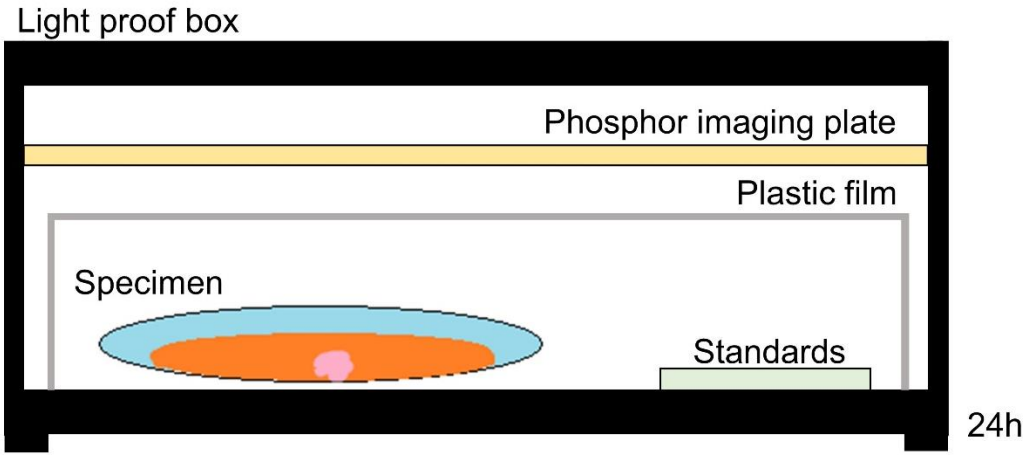

Figure 12. Schematic diagram of ARG for in vivo PSMA-ligand uptake analysis.

4.1.2.5. Histology and immunohistochemistry

HE and Immunohistochemical staining were performed in collaboration with Dr.med.vet. Katja Steiger (Institute of Pathology, comparative experimental pathology [CeP], Klinikum rechts der Isar). Postoperative prostate specimens were fixed in 10% neutral-buffered formalin solution for at least 72 h, and then samples were dehydrated and embedded in paraffin. Serial sections of 2 µm were cut using a rotary microtome for HE and IHC staining.

Regarding HE staining, the procedure was: Xylene (5 min), Xylene (5 min), Isopropanol (5 min), Isopropanol (5 min), Ethanol 96% (2 min), Ethanol 96% (2 min), Ethanol 70% (2 min), Ethanol 70% (2 min), Aqua dest (25 s), HTX-Mayer (8 min), Tap water (10 min), Eosin alcoholic 1% (4 min), Ethanol 96% (30 s), Isopropanol (25 s), Isopropanol (25 s), Xylene (1.5 min), Xylene (1.5 min). Sections were scanned with a Leica CS system to our e-slide database.

IHC was performed automatically using the Ventana BenchMark XT (Roche, Basel, Switzerland) and diaminobenzidine (DAB) was applied for visualization using

the ultra View Univeral DAB Detection KIT (Roche, Basel, Switzerland). PSMA antibody was described in

Table 13. Slides were scanned with a Leica AT2 system to our e-slide database and were analyzed with Imagescope.

4.1.2.6. Image registration

The image registration approach was the same as in section 4.1.1.3. Of note, autoradiographic data was generated from postoperative prostatic specimens in sealed plastic bags. However, the digital HE and IHC data were produced from the surface of each tissue. Registration errors of digital pathological data and autoradiographic data were observed because of the different sources of samples.

4.1.2.7. Image analysis

Region of interest (ROI)-based analysis

In the ROI-based analysis, we defined an ROI as an area containing cancer cells, and there is at least a 5 mm distance with only normal prostate tissue between two ROIs. ROIs were generated manually using Imagescope. The same ROIs were drawn in the corresponding position in ARG data. QL value in each ROI was analyzed using AIDA Image analyzer.

Grid-based analysis

In the grid-based analysis, the size of the matrix for postoperative prostate specimen HE slides was 3×3 mm^2. A trained pathologist annotated each grid based on the percentage of different cell types: Epithelial (cancer cell [Gleason pattern 3, 4 and 5], normal tissue, prostatic intraepithelial neoplasia [PIN]), Stroma, Inflammation, seminal vesicle, and open area. The same matrix was then applied in the corresponding position in ARG data. QL value in each grid was analyzed using AIDA Image analyzer.

The absolute activity of each grid was assessed using calibration curves generated from standards (Eq.2).

SUV_{ARG} was calculated using the following formula:

$$\mathrm{SUV_{ARG}} = \frac{\mathrm{A_{spec}/W_{spec}}}{\mathrm{A_{inj}/BW_t}} \quad \text{Eq.3}$$

where A_{spec} is the specimen activity decay corrected to the injection time point. W_{spec} is the grid's weight. A_{inj} is the injected activity, and BWt is the weight of the patient. The grid's weight was calculated using the following formula:

$$\mathrm{W_{spec}} = 3 \times 3 \times \frac{\mathrm{L_{pros}}}{\mathrm{No.tiss}} \times \rho_{\mathrm{pros}} \quad \text{Eq.4}$$

where L_{pros} is the length of the prostate from apex to base, ρ_{pros} is the density of prostates. The number of 0.98 g/ml was used in the formula (G Torlakovic et al., 2005). $No._{tiss}$ is the number of slices of the prostate specimen.

SUV normalized by lean body mass $(SUL)_{ARG}$ was calculated using the following formula:

$$\mathrm{SUL_{ARG}} = \frac{\mathrm{A_{spec}/W_{spec}}}{\mathrm{A_{inj}/LBM}} \quad \text{Eq.5}$$

$$\mathrm{LBM\ (male)} = \frac{9.27 \times 10^3 \times \mathrm{BW_t}}{6.68 \times 10^3 + 216 \times \mathrm{BMI}}$$

(S Janmahasatian et al., 2005) Eq.6

Where LBM is lean body mass, BMI is body mass index.

$$\mathrm{BMI} = \frac{\mathrm{BW_t}}{\mathrm{Height^2}} \quad \text{Eq.7}$$

Histopathological analysis

The immunohistochemical analysis was performed by one experienced investigator, and all question sections were rescored by another experienced pathologist. Results were calculated based on the 4-point immunoreactive score (IRS) classification (Table 16), considering not only visualized grade of staining intensity, but also a fraction of cells in each intensity category (percentage of positive staining cells). Heterogeneity was defined by different staining patterns existing in at least 5% of the studied region (DA Ferraro et al., 2020).

Table 16. Four-point IRS Classification (KS McCarty, Jr. et al., 1985; N Woythal et al., 2018)

Intensity of staining (membrane)	Percentage of positive cells	IRS	IRS Classification
0 = no color reaction	0 = no positive cells	0-1 = negative	0 = negative
1 = mild reaction	1 = < 10% positive cells	2-3 = mild	1 = mild
2 = moderate reaction	2 = 10%-50% positive cells	4-8 = moderate	2 = moderate
3 = intense reaction	3 = 51%-80% positive cells	9-12 = strongly positive	3 = strong
	4 = > 80%positive cells		

IRS = immunoreactive score.

4.2. Clinical analysis

4.2.1. Patients

A retrospective study was carried out on patients with D'Amico intermediate- to high-risk primary prostate cancer treated with RP and underwent ^{68}Ga-PSMA-11 PET imaging maximum three months before the surgery between January 2013 and August 2017. Exclusion criteria were neoadjuvant therapy, PSA persistence after RP, and incomplete follow-up. Figure 13. shows the flowchart of inclusion and exclusion criteria.

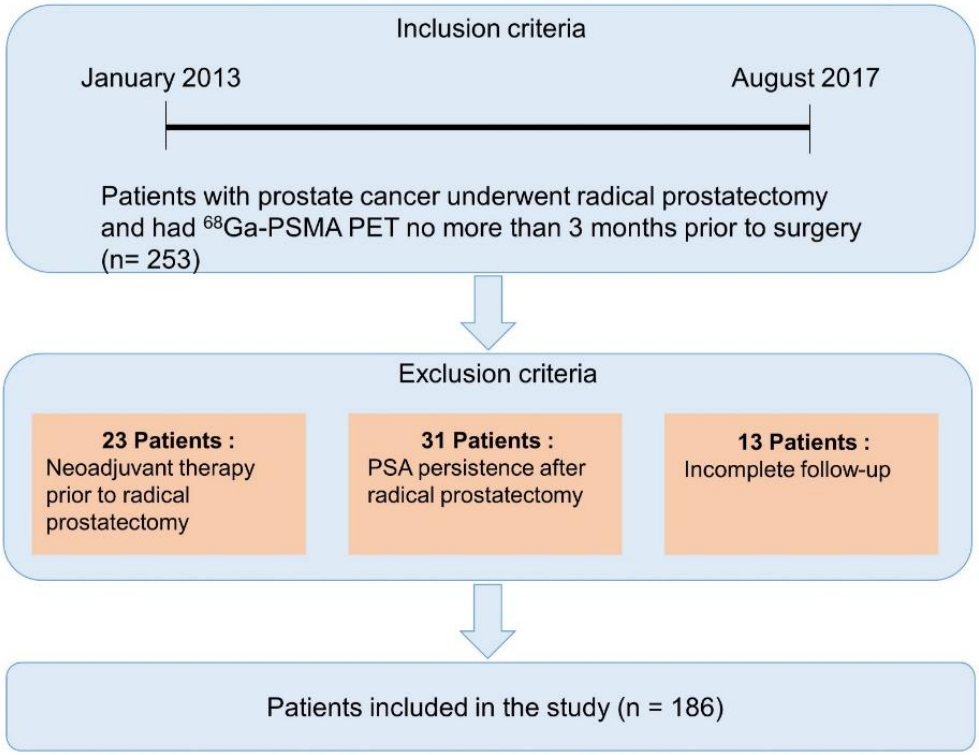

Figure 13. Flowchart of inclusion and exclusion steps, narrowing down initially 253 patients to the final 186 eligible patients.

Clinicopathological information, including age, iPSA, ^{68}Ga-PSMA-11 PET parameters, prostatectomy Gleason Score, and pathological characteristics, were collected. BCR was defined as a PSA level increase above 0.2 ng/ml. The endpoint in this study was the assessment of BCR. BCR was calculated from the date of surgery to the date of BCR or the most recent follow-up. All patients gave written informed consent for evaluation and publication of their data. The retrospective study has been approved by the Ethics Committee of the Technical University Munich.

4.2.2. Imaging protocol

The synthesis of ^{68}Ga-PSMA-11 was described previously (R Martin et al., 2014). Patients fasted before ^{68}Ga-PSMA-11 PET scan for at least six hours. After intravenously injecting a median of 139 MBq of ^{68}Ga-PSMA-11 (IQR: 112-156), PET acquisition was started at a median of 54 min (IQR: 49-65) after the tracer injection. Nighty-three patients underwent ^{68}Ga-PSMA-11 PET/CT on a Biograph

mCT flow scanner (Siemens Medical Solutions, Erlangen, Germany), and 93 patients underwent ^{68}Ga-PSMA-11 PET/MRI on a Biograph mMR scanner (Siemens Medical Solutions, Erlangen, Germany). Details on PET/CT and PET/MR acquisition were described previously (M Eiber et al., 2020; M Souvatzoglou et al., 2013).

4.2.3. Image analysis

One trained nuclear medicine Ph.D. student blinded to the postoperative histopathological results analyzed all ^{68}Ga-PSMA-11 PET/CT and ^{68}Ga-PSMA-11 PET/MR datasets. All questioned lesions were reannotated by two experienced board-certified nuclear medicine physicians. For calculation of the SUV, tumor volume (TV), and total lesion (TL) of prostatic lesions, any focal or diffuse tracer uptake above the surrounding background and not associated with physiological uptake was drawn as circular regions in trans-axial slices and automatically adapted to a three-dimensional volume of interest (VOI) using Syngovia (Table 15) at 40% isocontour. Typical pitfalls in PSMA-ligand PET including low to moderate PSMA-ligand uptake associated with osteoblastic changes (i.e., with fractures or degenerative changes) or the low uptake associated with celiac and other ganglia were taken into account (MS Hofman, RJ Hicks, et al., 2018). All lesions suspicious for prostate cancer and lymph node metastases were noted and grouped according to miTNM classification (M Eiber et al., 2018).

Moreover, we established a molecular staging (miTNM staging) system (version 1.0), which could benefit the prognosis prediction of prostate cancer patients. A cutoff of SUV_{max} 5.4 from Hoffmann et al.'s study was applied for IA and IB stage separation. They revealed a SUV_{max} 5.4 from ^{68}Ga-PSMA-11 PET /CT as an optimal cut-off to distinguish between GS ≤ 7a and GS ≥ 7b with a sensitivity and specificity of 84% and 100% (MA Hoffmann et al., 2017).

4.3. Statistical analysis

Descriptive statistics were used to display continuous variables as the median and interquartile range (IQR) with 25th and 75th percentiles (Q1-Q3), mean ± standard deviation (SD), as well as percentages.

4.Methods

Data normal distribution was analyzed using the histography with the normal curves and the Kolmogorov-Smirnov test. The equality of variances was assessed by Levene's test.

Correlations were done using bivariate Spearman's test, and results were presented with the coefficient (r) and *p* value. Independent-samples T-test was used to compare the means of two independent groups of samples which were normally distributed and had equal variances. ANOVA was used to compare the means of more than three groups. When equal variances were assumed, the Bonferroni test was used for Post Hoc comparison. When equal variances were not assumed, the Games-Howell test was used for pairwise comparison. The linear mixed model method was used for detecting the correlation between PSMA-ligand uptake and different tissue types. The efficacy to predict prostate cancer using SUV_{ARG} and SUL_{ARG} was evaluated by the receiver operating characteristic (ROC) curve and the area under the curve (AUC).

The association between positive pathological results and ^{68}Ga-PSMA-11 PET findings was investigated univariately and multivariately using Logistic regression, and the corresponding odds ratio (OR) and 95% CI were calculated. Post-operative BCR-free survival was estimated using the Kaplan-Meier method and compared between groups using the log-rank test. Moreover, univariable and multivariable Cox regression analysis were performed to determine the ability of the clinicopathological factors to predict BRC after RP, and the corresponding hazard ratio (HR) and 95%CI were calculated. Only parameters showing a significant association on univariable analysis were included in the multivariable model. A multivariable analysis was performed when more than one risk factor was identified at the univariable analysis. Baseline factors included iPSA, age, Gleason Score, miTNM stage, pathological stage, surgical margin, and findings including TV, TL, $SUV_{mean,}$ and SUV_{max} from ^{68}Ga-PSMA-11 PET.

A *p* value of 0.05 was used as the cut-off for statistical significance. All tests were two-tailed. Statistical evaluation was performed using SPSS.

5. Results

5.1. Preclinical results

5.1.1. Ex vivo PSMA-ligand uptake evaluation

5.1.1.1. Patients and clinicopathological findings

Samples from 8 prostate cancer specimens were collected for ex vivo experiments. The mean age was 65 ± 8.2 years. Regarding Gleason Scores, four of them were Gleason 7b, one of them was Gleason 8, and the last three were Gleason 9.

5.1.1.2. Qualitative analysis

Figure 14 shows autoradiographic images, histological images, the overlapped images, and tumor density heat maps. The ARG images (Figure 14A) were acquired after 1.5 hours of incubation and 6 hours of exposure and shown in heat maps from blue (lowest uptake) to red (highest uptake).

Generally, tumor sections were heterogeneous in HE. Although the annotated areas with green lines contained tumor cells, normal epithelia and stoma was observed (Figure 14B). In the overlapped images of histology and ARG (Figure 14C), the distribution of ^{99m}Tc-PSMA-I&S uptake and corresponding tumor areas were clearly shown. High level ^{99m}Tc-PSMA-I&S ligand uptake was associated with regions of tumor cells. Conversely, regions with stroma and normal prostate glands were associated with low ^{99m}Tc-PSMA-I&S ligand uptake. Tumor density heat maps based on 1*1mm^2 grids were shown in Figure 14D from green (lowest density) to red (highest density). There was a clear correlation of high ^{99m}Tc-PSMA-I&S uptake with regions of high tumor density.

Figure 15 shows a scatter plot of the activities (QL) of each grid from eight sections. The positive correlation between tumor density and tracer uptake was clearly shown in all samples.

5.Results

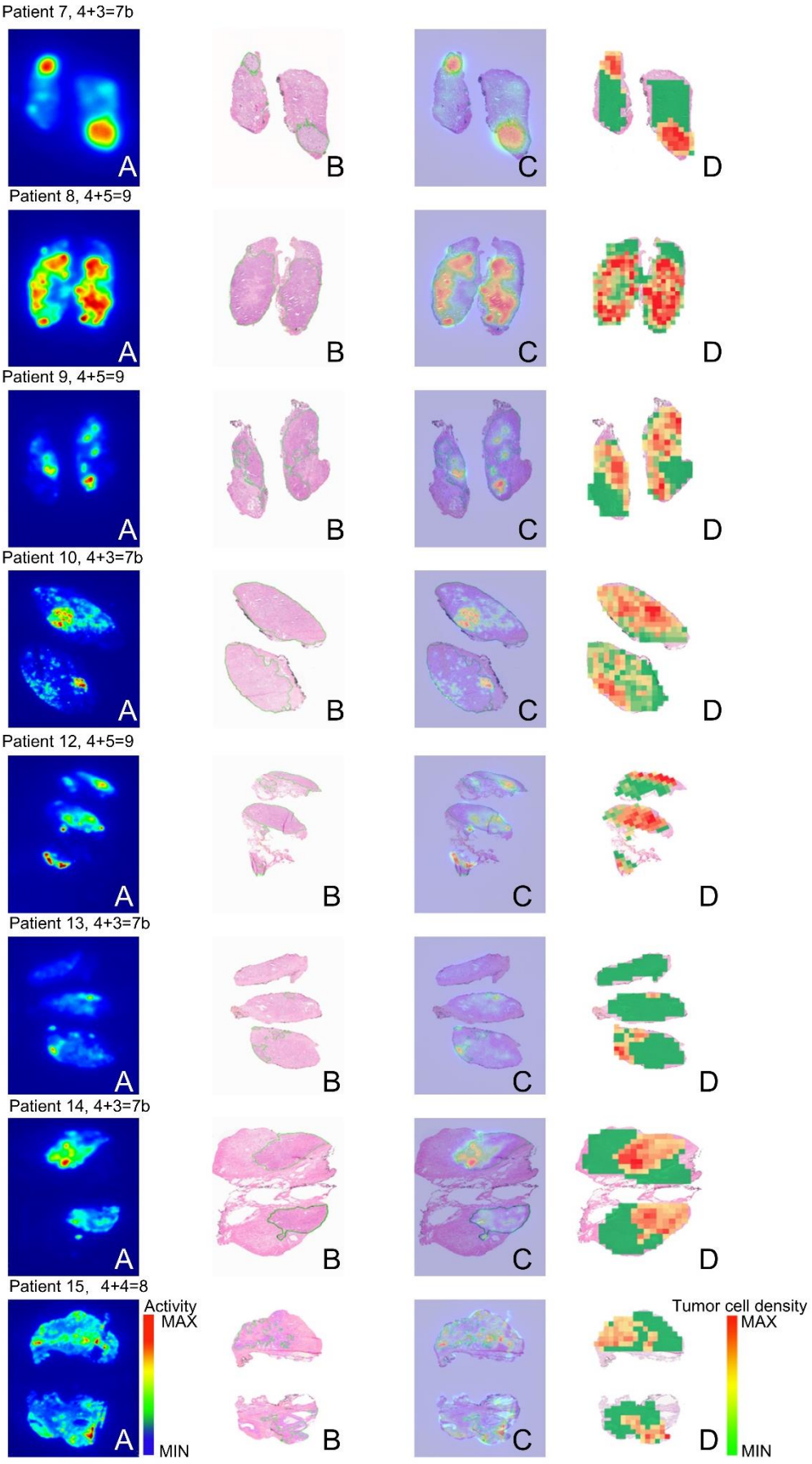
Patient 7, 4+3=7b
A
B
C
D
Patient 8, 4+5=9
A
B
C
D
Patient 9, 4+5=9
A
B
C
D
Patient 10, 4+3=7b
A
B
C
D
Patient 12, 4+5=9
A
B
C
D
Patient 13, 4+3=7b
A
B
C
D
Patient 14, 4+3=7b
A
B
C
D
Patient 15, 4+4=8
Activity
MAX
MIN
A
B
C
Tumor cell density
MAX
MIN
D

Figure 14. Representative images from eight specimens.

A. ARG images. B. histology (HE staining) images. Ares annotated with green lines are areas containing tumor cells. C. Overlapped images. D. Tumor density heat maps.

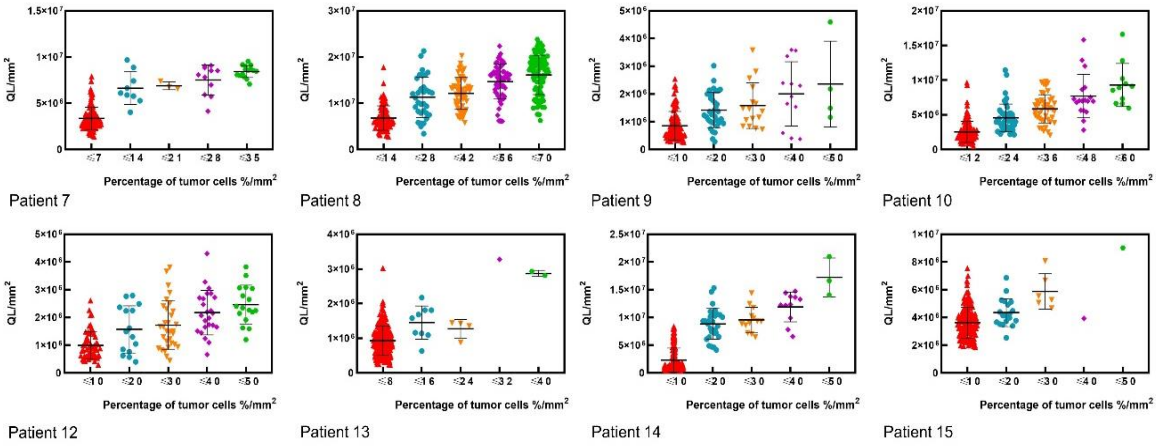

Figure 15. Scatter plot of QLs in eight sections.

5.1.1.3. Quantitative analysis

A total of 1787 grids were included in the analysis. Relative activity in each grid was calculated using the tumor-to-normal ratio (Eq.1). Absolut activity in each grid was calculated using calibration curves (Eq.2). The dataset was split into deciles, each group containing the same number of densities. Less than the 10% of tumor density was analyzed as group 1, then higher than 10% but lower than 20% as group 2, etc. Table 17 shows the activity in each tumor density group.

Table 17. Relative and absolute activities in tumor density groups.

Tumor cell density	No. of grids	Relative activity	CPM/grid	Bq/grid
Normal tissue	745	1	17971 ± 18024	603 ± 537
< 10%	245	1.8 ± 1.4	26854 ± 21253	922 ± 604
≥ 10%	239	2.8 ± 2.1	31625 ±26185	1130 ± 795
≥ 20%	150	3.2 ± 2.1	40911 ± 34292	1349 ± 890
≥ 30%	143	3.0 ± 1.7	46010 ± 36886	1416 ± 914
≥ 40%	89	4.0 ± 2.8	54499 ±41583	1730 ± 1067
≥ 50%	75	3.4 ± 1.9	93244 ± 46281	2542 ± 1101
≥ 60%	54	3.0 ± 0.9	110244 ± 37769	2874 ± 913

≥ 70%	47	3.3 ± 0.7	136074 ± 27658	3500 ± 728
Total	1787			

CPM = counts per minuets.

Data were presented as mean ± SD.

Relative activity analysis

The dataset was divided into deciles in order to display the distribution of raw data. Then, data were divided into three groups: grids with only normal tissue and grids with less than 40% of tumor cells, and grids with more than 40% of tumor cells. Significantly higher relative activity was observed in high density tumors (≥ 40%) than in normal prostate tissue and low density tumors (< 40%) ($p < 0.001$, Figure 16B). The tracer uptake in prostate cancer was significantly higher than in normal prostate tissue ($p < 0.001$, Figure 16B).

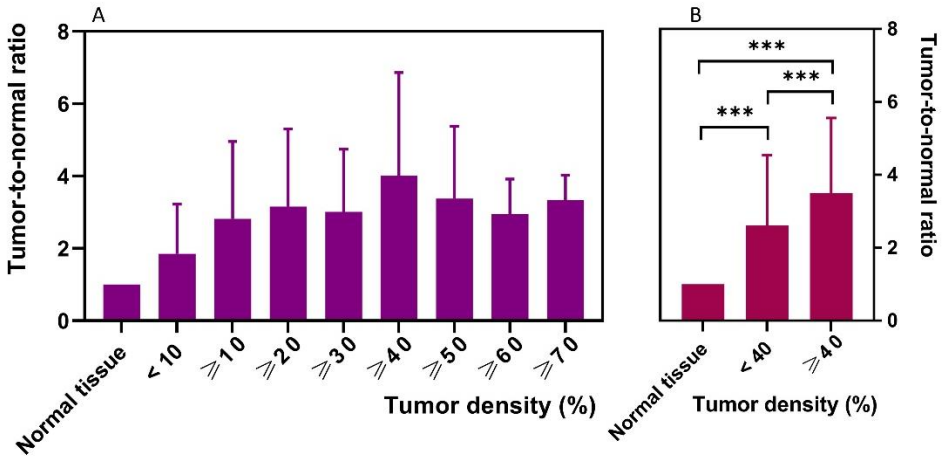

Figure 16. Relative activities in different tumor density groups.

A. Mean ± SD of tumor-to-normal ratio in normal tissue and groups split into deciles. B. Mean ± SD of tumor-to-normal ratio in normal tissue, grids with less than 40% of tumor cells and grids with more than 40% of tumor cells. ***: $p < 0.001$.

Absolute activity analysis

Using both units (Bq/grid and CPM/grid), significantly higher uptake was observed in high density tumors (≥ 40%) than in normal prostate tissue and low density tumors (< 40%) ($p < 0.001$). Similar to the relative activity analysis, the

tracer uptake in prostate cancer was significantly higher than in normal prostate tissue ($p < 0.001$, Figure 17).

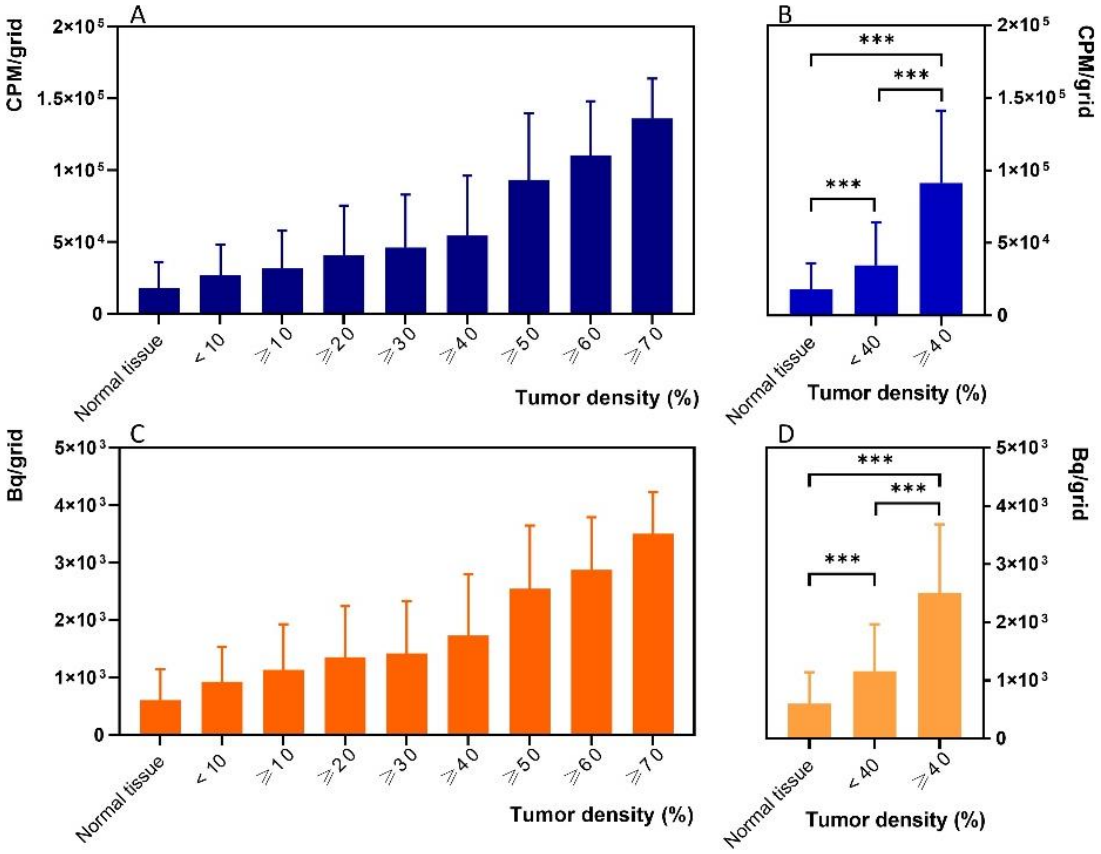

Figure 17. Absolute activities in different tumor density groups.

A. Mean ± SD of CPM/grid in normal tissue and groups split into deciles. B. Mean ± SD of CPM/grid in normal tissue, grids with less than 40% of tumor cells, and grids with more than 40% of tumor cells. C. Mean ± SD of Bq/grid in normal tissue and groups split into deciles. D. Mean ± SD of Bq/grid in normal tissue, grids with less than 40% of tumor cells, and grids with more than 40% of tumor cells. ***: $p < 0.001$.

5.1.2. In vivo PSMA-ligand uptake evaluation

5.1.2.1. Patients and clinicohistological findings

A total of 17 patients with a mean age of 67.4 ± 8.4 years were included in the study. The average serum PSA level was 17.1 ± 12.1 ng/ml, and the average injected dose of ^{99m}Tc-PSMA-I&S before the operation was 648 ± 128 MBq. The postoperative Gleason Score was 7a in one (5.9%), 7b in six (35.3%), 8 in two

(11.8%), 9 in seven (41.2%). Clinicopathological information of each patient was summarized in Table 18.

Table 18. Patient Characteristics

Characteristic																	
Patient ID	3	4	5	6	7	8	9	10	11	12	13	15	16	17	18	19	20
Age (y)	66	80	51	70	72	69	67	66	70	55	78	53	72	79	66	63	69
iPSA (ng/ml)	8.74	35	26.7	30	17.8	9.17	5.93	5.2	12.9	12.31	15.7	6.96	7.5	20.5	2.82	44	30.6
Pathological stage	pT3b pN1	pT3b pN1	pT2c pN1	/[a]	pT3b pN1	pT3b pN1	pT3b pN1	pT3b pN0	pT3a pN1	pT3b pN1	pT3a pN1	pT4 pN1	pT3b pN1	pT2c pN0	pT2c pN1	pT3b pN1	pT2c pN1
Gleason Score	8	7b	7b	/	7b	9	9	7b	7b	9	7b	8	9	7a	9	9	9
Preoperative PSMA PET	F^{18}-rhPSMA7	F^{18}-PSMAS1	/	F^{18}-rhPSMA7	F^{18}-rhPSMA7	/	G^{68}-PSMA	F^{18}-rhPSMA7	/	F^{18}-rhPSMA7	F^{18}-rhPSMA7	F^{18}-rhPSMA7	F^{18}-rhPSMA7	G^{68}-PSMA	/	G^{68}-PSMA	/
No of specimens	3	5	1	1	1	1	1	2	1	2	2	2	3	4	1	3	4
No of grids for analysis	385	689	82	196	48	102	34	243	94	125	245	235	401	727	151	285	617
Injected dose (MBq)	699	702	663	745	768	648	379	531	678	827	417	531	788	656	735	728	531
Time between injection to operation (min)	1036	1152	1082	1314	1163	1120	1343	1133	1136	1095	1359	1073	1139	1228	1117	1023	1170
Time between operation to ARG (min)	184	231	244	171	265	125	231	188	148	140	191	197	166	282	222	147	272

ARG = autoradiography; iPSA = initial prostate-specific antigen; PET = positron emission tomography; PMSA = prostate-specific membrane antigen; rhPSMA = radiohybrid PSMA

a: The pathological finding of Patient 6 after the operation was high grade prostatic intraepithelial neoplasia (HGPIN).

5.1.2.2. Image co-registration of histopathological and autoradiographic data

Figure 18 shows the representative examples of autoradiographic images, histological images, the overlapped images, and IHC staining images. ARG was performed an average of 200 ± 48.5 min after the operation. The ARG images (Figure 18A) were acquired after 24 hours of exposure and were shown in heat maps from blue (lowest uptake) to red (highest uptake). In the histological images, tumor areas were circled with yellow lines (Figure 18B), and the correlated IHC images were prepared for the PSMA expression analysis (Figure 18C). In the overlapped images of histology and ARG (Figure 18D), the ^{99m}Tc-PSMA-I&S uptake and corresponding tumor areas were clearly shown. High ^{99m}Tc-PSMA-I&S uptake was associated with the tumor cell region. Conversely, regions with stroma and normal prostate tissues were associated with low ^{99m}Tc-PSMA-I&S uptake. Moreover, some areas without tracer uptake and the PSMA negative tumor cells in IHC images were observed.

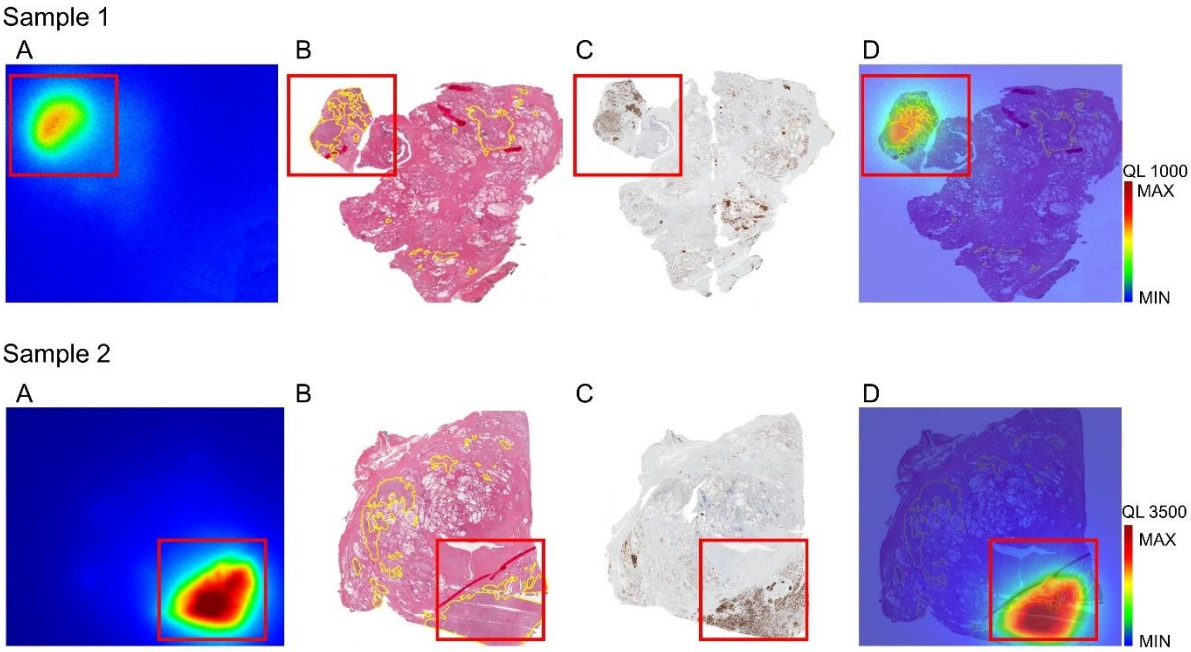

Figure 18. Representative sections of image registration.

A. ARG images. B. histology (HE staining) images. Ares annotated with yellow lines represent tumor areas. C. PSMA IHC staining images. D. Overlapped images.

5.1.2.3. ROI-based analysis

PSMA expression patterns

A total of 59 ROIs were included in the analysis. Examples of PSMA expression patterns were shown in Figure 19, and the examples of heterogeneity were shown in Figure 20.

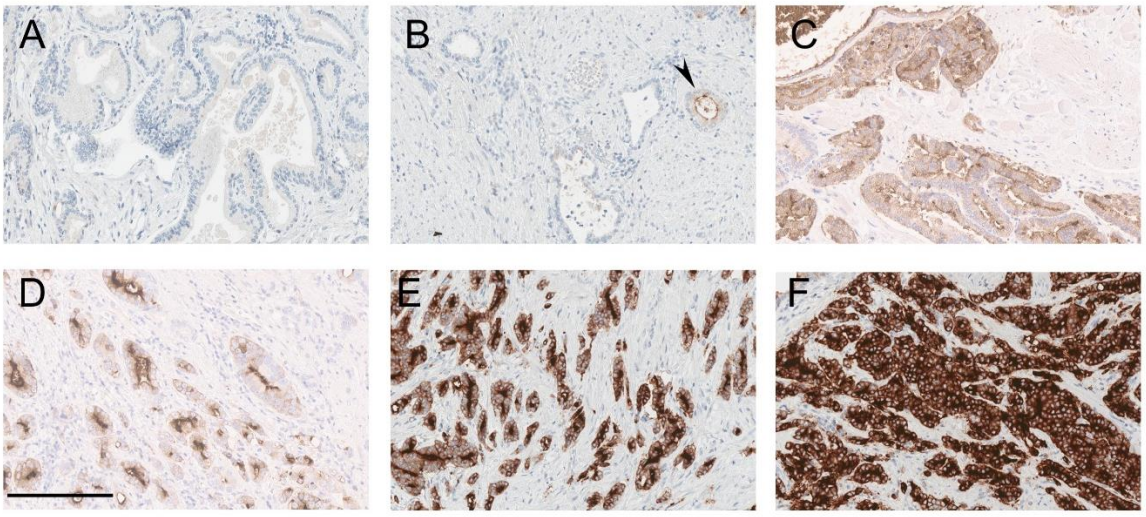

Figure 19. Overview of the different PSMA staining patterns.

A. Complete negativity of PSMA expression. B. Low expression of cytoplasmic and membranous PSMA (black arrow). C. Moderate cytoplasmic and membranous PSMA. D. Low cytoplasmic and strong membranous staining. E. Moderate cytoplasmic and strong membranous staining. F. Diffuse strong cytoplasmic and membranous expression. Scale bar 200 µm.

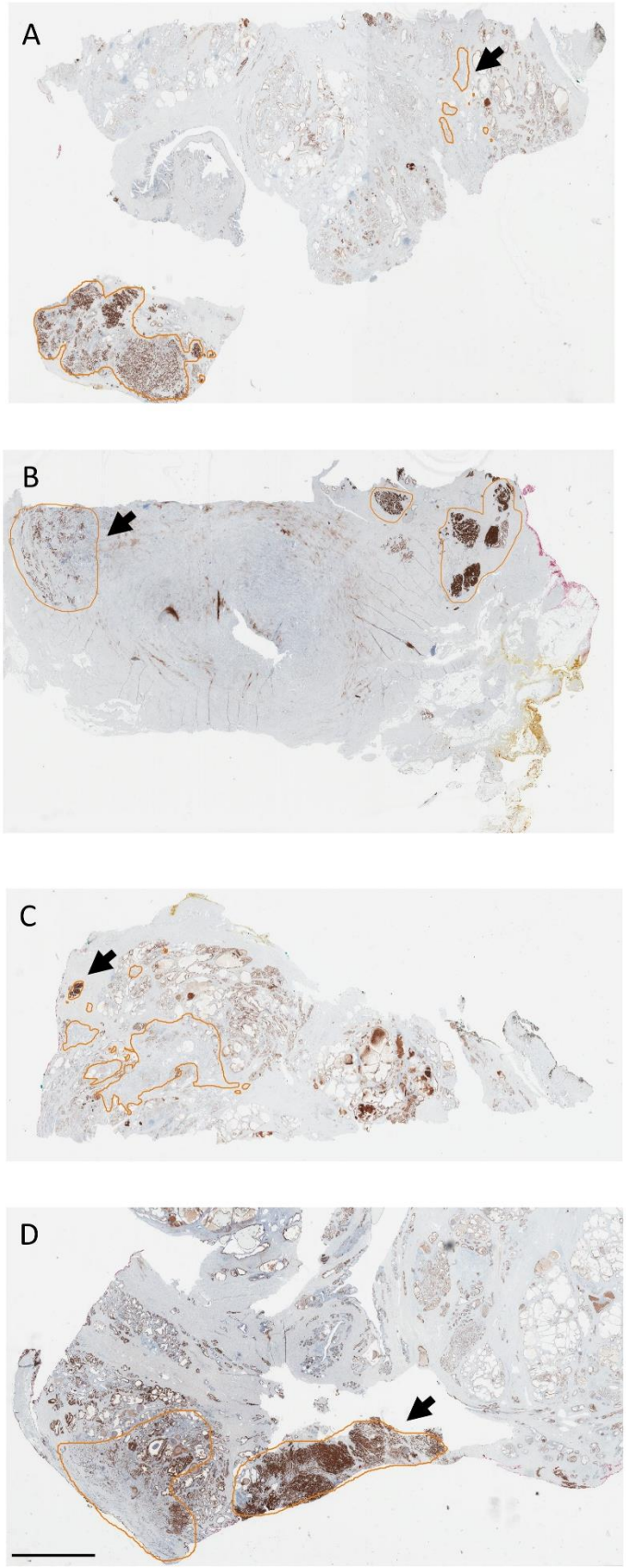

Figure 20. Overview of the different PSMA heterogeneity patterns.

A. In one slice, the circled carcinoma (orange line) consists of diffuse positive expression of PSMA and the circled areas with a black arrow consist of completely negative parts. B. The circled areas show diffuse positive expression of PSMA and the arrowhead depicts low to mediate expression of PSMA. C. In roughly 90% of the marked carcinoma shows completely negative areas and the arrow points a part with diffuse positivity. D. In the circled carcinoma consists of approximately 40% negative areas, whereas 80% of areas with an arrow show diffuse positivity and 20% moderate expression. Scale bar 5 mm.

PSMA expression and Gleason Score

Thirty (51%) ROIs fully expressed PSMA, 25 (42%) showed negative areas and four (7%) were PSMA negative in the whole area. In 10 ROIs with a PSMA negative area larger than 50%, four were Gleason score 6, five were Gleason score 7a, and one was Gleason score 8. In the rest 49 ROIs with a negative area less than 50%, 6.1% had a Gleason score 6, 16.3% had a Gleason score 7a, 16.3% had a Gleason score 7b, 42.9% had a Gleason score 8, and 18.4% had a Gleason score 9 (Figure 21A and B). The primary tumor exhibited a heterogeneous in 26 ROIs (53.1%). PSMA-expressing tumor area positively correlated with Gleason Score ($r = 0.388$, $p = 0.002$, Figure 21C). The intensity of PSMA expression for membrane and cytoplasm positively correlated with Gleason Score ($r = 0.592$, $p < 0.001$; $r = 0.576$, $p < 0.001$, respectively; Figure 21D). Besides, the intensity of PSAM expression in the membrane positively correlated with the intensity of PSMA expression in the cytoplasm ($r = 0.782$, $p < 0.001$). IRS in different Gleason Scores was displayed in Figure 21E, and a positive correlation was observed ($r = 0.607$, $p < 0.001$).

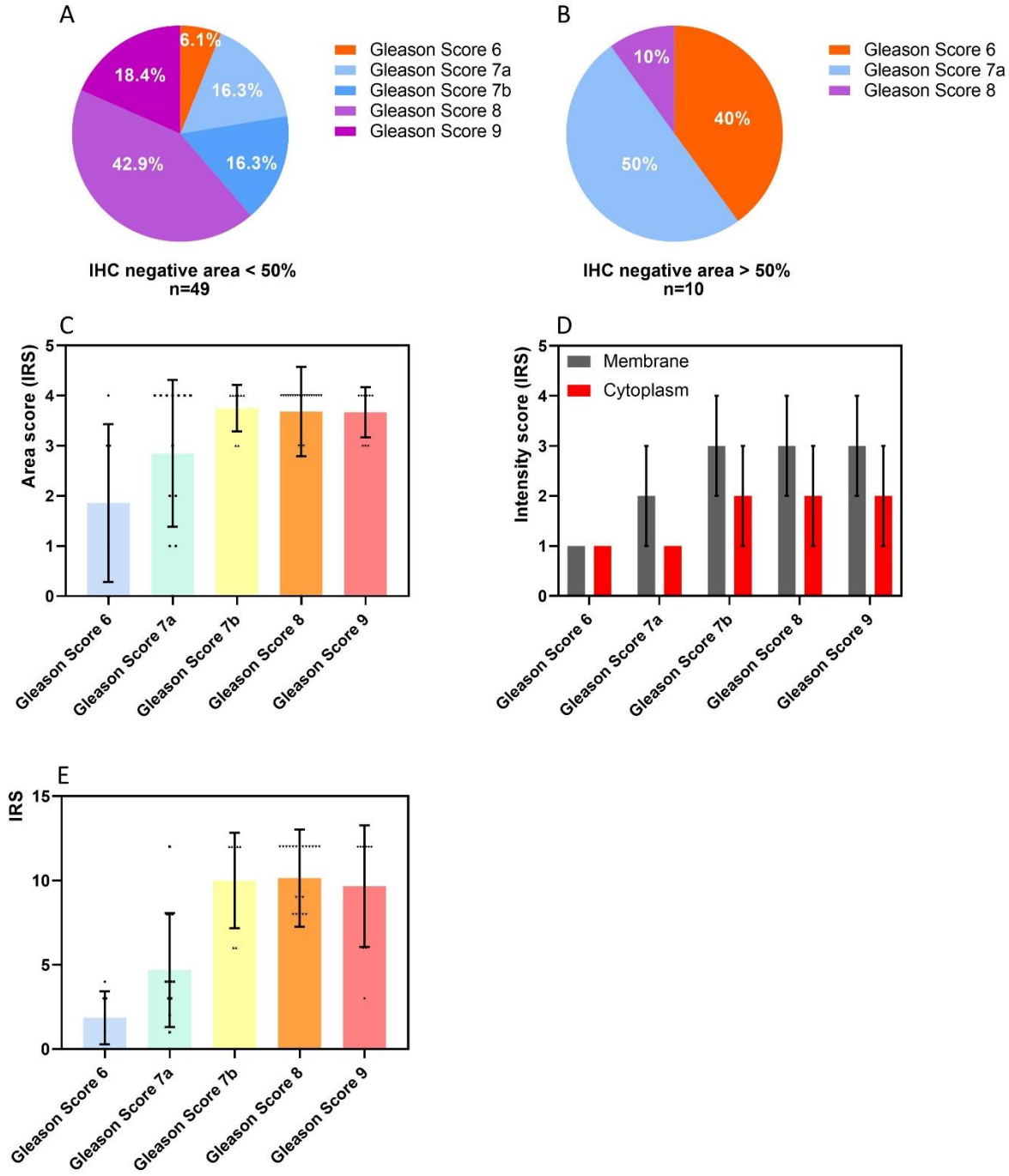

Figure 21. Correlation of histology and IHC.

A. The percentage of different Gleason Scores in ROIs with immunohistochemical PSMA negative parts less than 50%. B. The percentage of different Gleason Scores in ROIs with immunohistochemical PSMA negative parts more than 50%. C. The scores of stained areas in different Gleason Scores. D. The scores of intensities of membrane and cytoplasm in different Gleason Scores. E. The IRS in different Gleason Scores.

PSMA expression and PSMA-ligand uptake

Of all 59 ROIs, 32 (65.3%) were observed in ARG images. In ARG positive ROIs, Gleason Score ≥ 8 was predominantly observed (72%) (Figure 22A). In 27 ARG negative ROIs, 26% was Gleason Score 6, 37% was Gleason Score 7a, 7% was Gleason Score 7b and 30% was Gleason Score 8 (Figure 22B). The average IRS of ARG positive ROIs was 10 ± 3, and it was significantly higher than the IRS (5 ± 4) in ARG negative ROIs ($p < 0.001$, Figure 22C). Moreover, the average area of ARG positive ROIs was 179846378 ± 195127004 (Range: 1176526-853872717) μm^2, which was significantly larger than the area of ARG negative ROIs (7654639 ± 14641578, range: 45921-58860293, $p < 0.001$, Figure 22D). Furthermore, in ARG negative ROIs, four of 27 were PSMA negative, 15 were PSMA weak expression (score of intensity < 2) and the rest eight were PSMA moderate to strong expression (score of intensity ≥ 2). The average area of PSMA negative ROIs was 4975505 ± 7147544 mm^2 (n = 4), and of PSMA weak expression ROIs was 9759672 ± 17972130 mm^2 (n = 15), and of PSMA moderate to strong expression ROIs was 5047270 ± 10343937 mm^2 (n = 8).

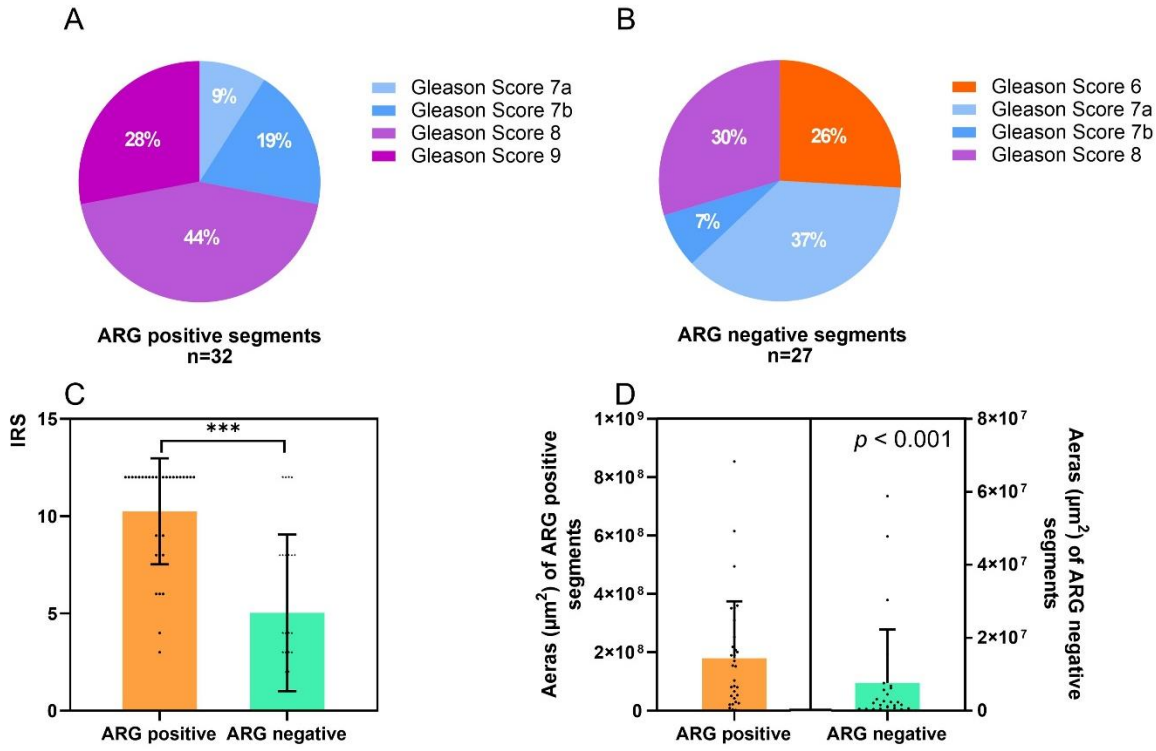

Figure 22. Comparison between ARG positive and negative ROIs.

A. The percentages of Gleason Scores in ARG positive ROIs. B. The percentages of Gleason Scores in ARG negative ROIs. C. Scatter plot and bar charts of mean and SD were used to display IRS in ARG positive and negative groups. A significant difference was observed. D. Scatter plot and bar charts of mean and SD of areas in ARG positive and negative groups. The detectable areas in ARG were significantly larger than the non-detectable areas ($p < 0.001$). ***: $p < 0.001$.

5.1.2.4. Grid-based analysis

5.1.2.4.1. Sample characteristics: histopathology, immunohistochemistry and ARG signal

A total of 4660 grids were included in the grid-based analysis. The percentage of different cell types was annotated in each grid, and it was summarized in Table 19. The distribution of the raw dataset was shown in Figure 23.

Table 19. Sample characteristics

Cell type	Median (IQR) [%]	Mean ± SD[%]	No of grids containing specific cell type
Gleason Pattern 3	0 (0-0)	0.35 ± 1.89	336
Gleason Pattern 4	0 (0-0)	3.98 ± 10.31	1120
Gleason Pattern 5	0 (0-0)	0.72 ± 4.43	299
Normal epithelia	1.13 (0-5)	3.42 ± 5.41	2507
Seminal vesicle	0 (0-0)	0.15 ± 1.34	96
PIN	0 (0-0)	0.09 ± 0.96	81
Inflammation cells	0 (0-0)	0.41 ± 3.25	557
Stroma	70 (50-85)	65.13 ± 24.43	4635
Open area	16.13 (10-35)	25.75 ± 23.57	4433
Total		4660	

IQR = interquartile range; PIN = prostatic intraepithelial neoplasia; SD = standard deviation.

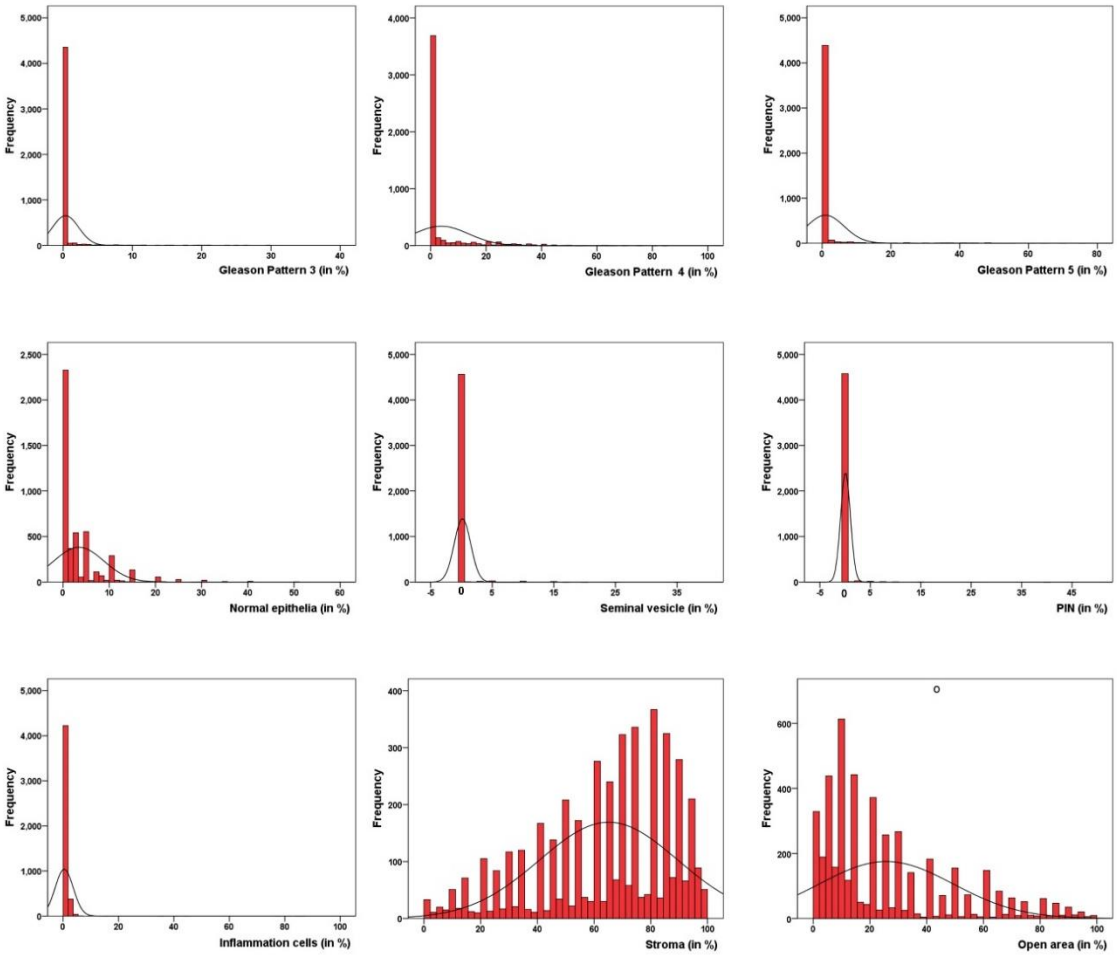

Figure 23. Distribution of the percentage of different cell types with the normal curves.

The tracer uptake in tumor and non-tumor grids were analyzed. There were 1177 grids (25.3%) containing prostate tumor cells. The tracer uptake of each grid was analyzed using four different units (Figure 24A). The mean Bq/mm^2 of prostate cancer was 734.2 ± 530.6 (n = 1177) and 228.7 ± 239.6 for non-tumor prostate tissue (n = 3483, $p < 0.001$). The mean CPM/mm^2 of prostate cancer was 43526.9 ± 45383.2 (n = 1177) and 12301.4 ± 21329.2 for non-tumor prostate tissue (n = 3483, $p < 0.001$). The mean SUV_{ARG} of prostate cancer was 15.6 ± 11.7 (n = 1177) and 5.0 ± 5.4 for non-tumor prostate tissue (n = 3483, $p < 0.001$). The mean SUL_{ARG} of prostate cancer was 11.9 ± 9.1 (n = 1177) and 3.8 ± 4.3 for non-tumor prostate tissue (n = 3483, $p < 0.001$). An analysis of the area under the ROC curve for SUL_{ARG} and SUV_{ARG} (Figure 24B) in correlation with the histological results revealed an AUC of 0.851 (95% CI, 0.838-0.863; $p < 0.001$) of SUL_{ARG} and 0.848 (95% CI, 0.835-0.860; $p < 0.001$) of SUV_{ARG}. Using an SUL_{ARG} cutoff of 4.6, sensitivity and specificity of 78.2% and 76.6% were achieved. Using an SUV_{ARG} cutoff of 6.2, sensitivity and specificity of 77.7% and 76.8% were achieved.

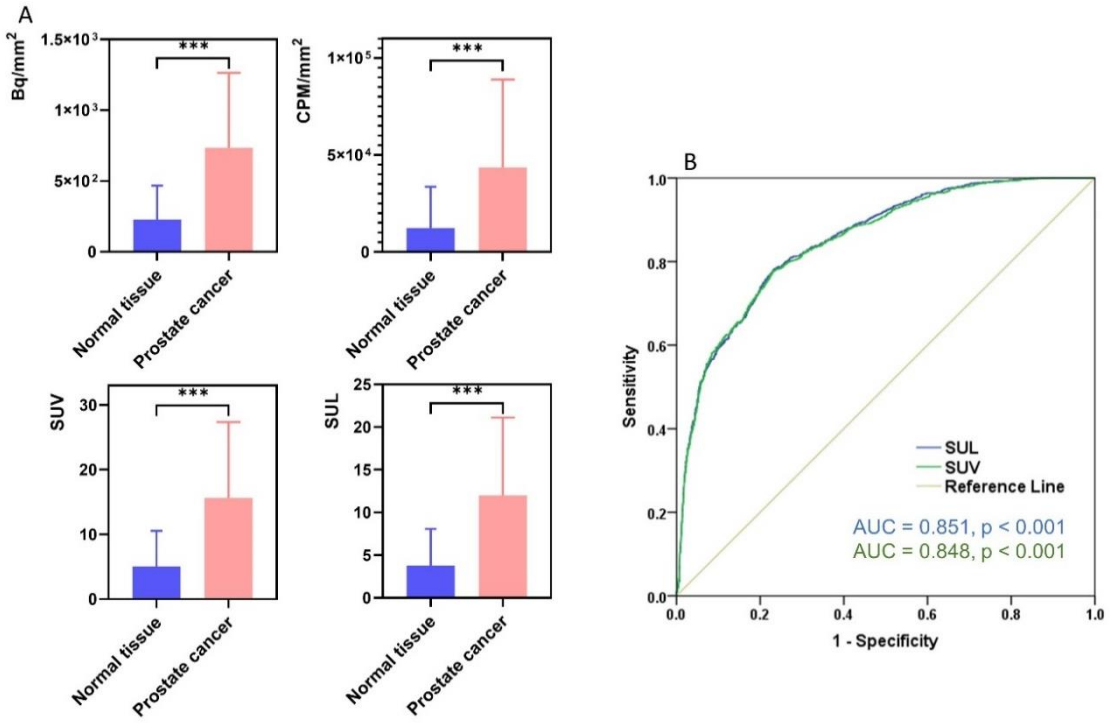

Figure 24. PSMA-ligand uptake in tumor and non-tumor grids.

A. Comparison of tracer uptake in grids with normal prostate tissue and prostate cancer. Datasets with four units: Bq/mm^2, CPM/mm^2, SUV_{ARG}, and SUL_{ARG} were displayed. ***: $p < 0.001$. B. ROC curves of SUL_{ARG} and SUV_{ARG}.

PSMA expression in different Gleason Patterns was evaluated. The majority of Gleason Pattern 3 had a score of percentage of positive cells less than two. Only 6% of Gleason Pattern 5 had a score of percentage of positive cells less than 2 (Figure 25A). The average score of the intensity of normal prostate tissue was 0.25 ± 0.49, 1.15 ± 0.79 in Gleason Pattern 3, 2.41 ± 0.76 in Gleason Pattern 4, and 2.56 ± 0.71 in Gleason Pattern 5 (Figure 25B). The mean IRS for normal prostate tissue was 0.3 ± 0.63, 3.43 ± 3.25 for Gleason Pattern 3, 8.96 ± 3.59 for Gleason Pattern 4, and 9.53 ± 3.43 for Gleason Pattern 5 (Figure 25C). Significant differences were observed in all pairwise comparisons.

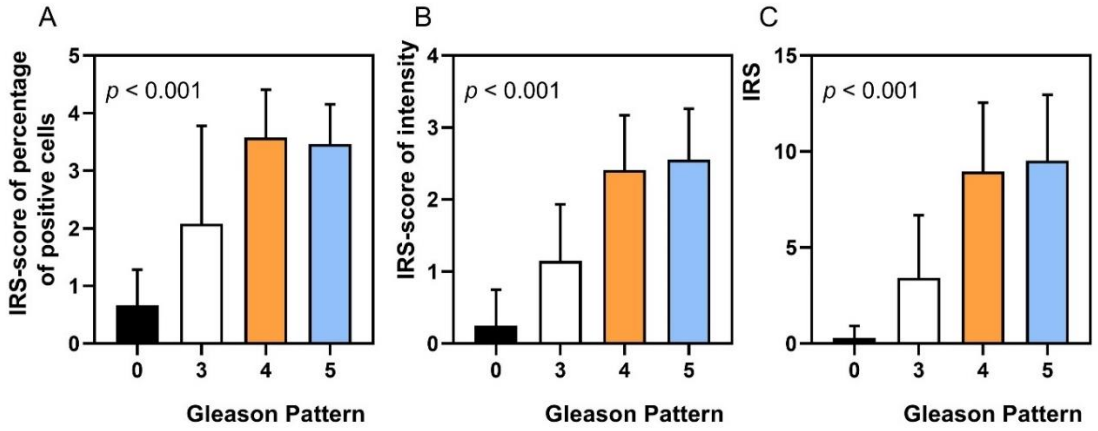

Figure 25. Bar charts of IRS-related parameters in normal prostate tissue and Gleason Patterns.

A. Scores of percentage of positive cells in different groups. Pairwise comparison: normal prostate tissue vs. Gleason Pattern 3: $p < 0.001$; normal prostate tissue vs. Gleason Pattern 4: $p < 0.001$; normal prostate tissue vs. Gleason Pattern 5: $p < 0.001$; Gleason Pattern 3 vs. Gleason Pattern 4: $p < 0.001$; Gleason Pattern 3 vs. Gleason Pattern 5: $p < 0.001$; Gleason Pattern 4 vs. Gleason Pattern 5: $p = 0.006$. B. Scores of intensity in different groups. Pairwise comparison: normal prostate tissue vs. Gleason Pattern 3: $p < 0.001$; normal prostate tissue vs. Gleason Pattern 4: $p < 0.001$; normal prostate tissue vs. Gleason Pattern 5: $p < 0.001$; Gleason Pattern 3 vs. Gleason Pattern 4: $p < 0.001$; Gleason Pattern 3 vs. Gleason Pattern 5: $p < 0.001$; Gleason Pattern 4 vs. Gleason Pattern 5: $p = 0.02$. C. IRS in different groups. Pairwise comparison: normal prostate tissue vs. Gleason Pattern 3: $p < 0.001$; normal prostate tissue vs. Gleason Pattern 4: $p < 0.001$; normal prostate tissue vs. Gleason Pattern 5: $p < 0.001$; Gleason Pattern 3 vs. Gleason Pattern 4: $p < 0.001$; Gleason Pattern 3 vs. Gleason Pattern 5: $p < 0.001$; Gleason Pattern 4 vs. Gleason Pattern 5: $p = 0.005$.

5.1.2.4.2. PSMA-ligand uptake in relation to Gleason Scores

Activities using four units were calculated and summarized in Table 20. Bar graphs (Figure 26A) illustrated the mean activities in normal prostate tissue and different Gleason Scores from 6 to 10 in the grid-based analysis. Significantly higher PSMA-ligand uptake was observed in the aggressive tumor (Gleason Score ≥ 8) compared to the normal prostate tissue and Gleason Score < 8 ($p < 0.001$, Figure 26B). The tracer uptake of Gleason Score < 8 tissues was significantly higher than normal prostate ($p < 0.001$, Figure 26B).

Table 20. Respective activities using four units in different Gleason Scores.

	Normal tissue	Gleason Score 6	Gleason Score 7a	Gleason Score 7b	Gleason Score 8	Gleason Score 9/10
No of grids	3483	54	92	176	556	299
Bq/mm2						
Median (IQR)	166 (76.7-277)	253 (226.4-276.1)	246 (173.5-459)	336.2 (175.6-676)	778 (391-1143)	836 (544-1275)
Mean ± SD	228.6 ± 239.7	272.8 ± 128.6	340.3 ± 252.6	457.2 ± 351.8	797 ± 476	983 ± 627
CPM/mm2						
Median (IQR)	7899 (4740-12306)	11426 (9775-12360)	10922 (7589-20213)	14076 (10309-27640)	41168 (22373-59219)	46041 (29355-79577)
Mean ± SD	12291 ± 21327	11359 ± 4957	18650 ± 21755	22413 ± 22599	42846 ± 24555	70753 ± 71868
SUV						
Median (IQR)	4 (2-6)	4.8 (4.3-5.3)	5.26 (4-10.4)	9.1 (4.79-15.02)	16.1 (8.38-23.55)	15.28 (9.73-26.86)
Mean ± SD	5.03 ± 5.51	5.4 ± 2.5	7.98 ± 6	11.52 ± 8.87	16.79 ± 9.6	20.14 ± 15.52
SUL						
Median (IQR)	3 (1-4.13)	3.5 (3.2-3.9)	4.14 (3-8)	6.25 (3.57-11.04)	12.18 (6.36-18)	12.12 (7.69-20.96)
Mean ± SD	3.8 ± 4.3	4 ± 1.9	6.04 ± 4.63	8.56 ± 6.71	12.76 ± 7.37	15.84 ± 12.14

Bq = becquerel; CPM = counts per minute; IQR = interquartile range; SD = standard deviation; SUL = SUV normalized by lean body mass; SUV = standardized uptake value.

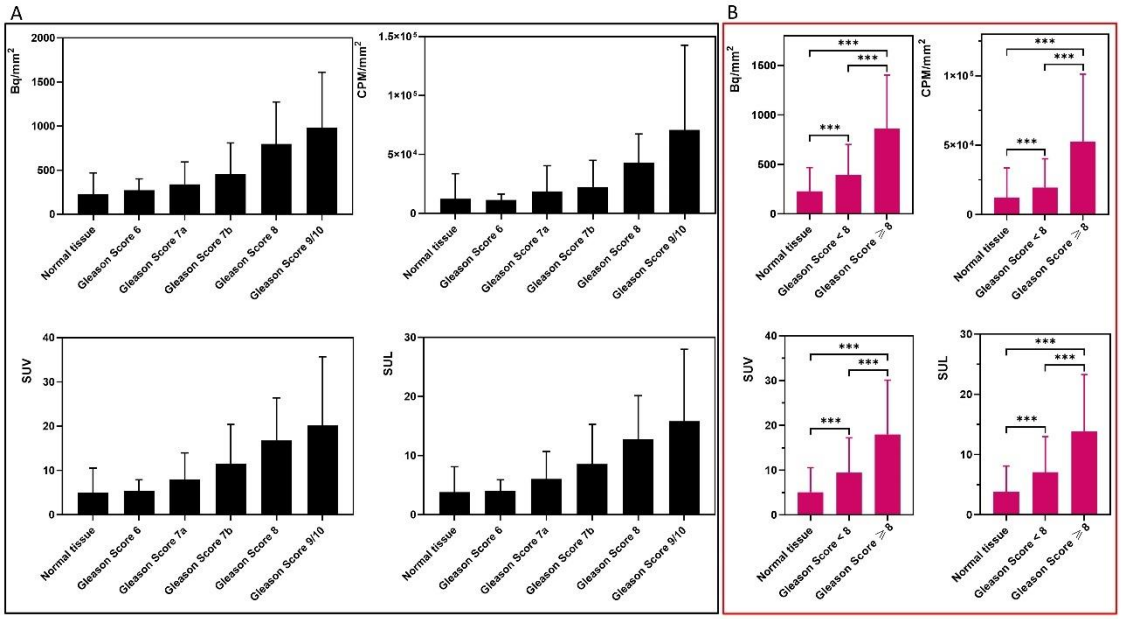

Figure 26. PSMA-ligand uptake in different Gleason Scores and groups.

A. Mean activities in normal prostate tissue and different Gleason Scores with four units. B. The average tracer uptake in normal prostate tissue, Gleason Score < 8 and ≥ 8. ***: $p < 0.001$.

5.1.2.4.3. PSMA-ligand uptake in relation to Gleason Patterns

The correlation of PSMA ligand uptake and Gleason Pattern was inspected. Pathological annotation of grids was summarized in Table 19. Using the unit of Bq/mm^2, Gleason Pattern 4, Gleason Pattern 5, seminal vesicle, PIN and stroma significantly correlated with tracer uptake ($p < 0.001$, $p < 0.001$, $p = 0.035$, $p = 0.029$, $p = 0.01$, respectively). The same results were observed using CPM/mm^2, except seminal vesicle, but including normal epithelial. After standardized to SUV_{ARG}, the significant association between tracer uptake and Gleason Pattern 4, Gleason Pattern 5, PIN, and stroma ($p < 0.001$, $p = 0.013$, $p = 0.035$, $p = 0.002$, respectively) were observed. Similar findings were observed with the unit SUL_{ARG}. The estimated increase of PSMA-ligand uptake following the increase (one percent) of corresponding variables were listed as Estimate value in Table 21.

Table 21. The correlation of PSMA ligand uptake and Gleason Pattern.

Unit	Variable	Estimate value	*p* value*	95% CI	
				Lower Bound	Upper Bound
Bq/mm^2	GP 3	-7.2	**0.006**	-12.35	-2.04
	GP 4	20.15	**0.000**	19.12	21.16
	GP 5	10.95	**0.000**	8.66	13.23
	Normal tissue	-0.39	0.679	-2.24	1.46
	Seminal vesicle	7.79	**0.035**	0.55	15.04
	PIN	11.14	**0.029**	1.12	21.16
	Inflammation cells	-2.16	0.153	-5.14	0.80
	Stroma	0.55	**0.010**	0.13	0.97
CPM/mm^2	GP 3	-782.76	**0.001**	-1238.91	-326.61
	GP 4	1185.36	**0.000**	1094.79	1275.93
	GP 5	419.82	**0.000**	217.44	622.20
	Normal tissue	-169.96	**0.042**	-333.93	-5.99
	Seminal vesicle	-84.12	0.797	-725.09	556.83
	PIN	928.17	**0.040**	41.8	1814.49
	Inflammation cells	-214.59	0.110	-477.73	48.55
	Stroma	56.96	**0.003**	19.75	94.16
SUV	GP 3	-0.10	0.093	-0.22	0.02
	GP 4	0.43	**0.000**	0.41	0.46
	GP 5	0.07	**0.013**	0.01	0.12
	Normal tissue	-0.01	0.611	-0.05	0.03
	Seminal Vesicle	0.15	0.078	-0.02	0.31
	PIN	0.24	**0.035**	0.02	0.47
	Inflammation cells	-0.05	0.177	-0.11	0.02
	Stroma	0.02	**0.002**	0.01	0.02
SUL	GP 3	-0.09	0.059	-0.18	0.003
	GP 4	0.33	**0.000**	0.32	0.35
	GP 5	0.07	**0.001**	0.03	0.11
	Normal tissue	-0.01	0.528	-0.04	0.02
	Seminal vesicle	0.10	0.108	-0.02	0.23
	PIN	0.19	**0.030**	0.02	0.37
	Inflammation cells	-0.04	0.170	-0.09	0.02
	Stroma	0.01	**0.001**	0.004	0.02

Bq = becquerel; CI = confidence interval; CPM = counts per minute; GP = Gleason Pattern; PIN = prostatic intraepithelial neoplasia; PSMA = prostate-specific membrane antigen; SUL = SUV normalized by lean body mass; SUV = standardized uptake value.

*Significant associations are given in bold.

5.1.2.4.4. Correlation of immunohistochemistry and PSMA-ligand uptake

A total of 4646 grids were included in the analysis. Fourteen grids (10 in Patient 4 and four in Patient 16) were excluded because of artifacts during the IHC sample preparation procedure. The grids were divided into the following groups according to the IRS of PSMA expression: ≤ 50% stained cells vs. > 50% stained cells, IRS < 2 vs. IRS ≥ 2. The average PSMA-ligand uptake (displayed with four units: Bq/mm^2, CPM/mm^2, SUV_{ARG}, and SUL_{ARG}) in different groups were shown in Figure 27, and the values were listed in Table 22. High tracer uptake was observed in the high IRS (IRS ≥ 2) and the large staining area (> 50% stained cells).

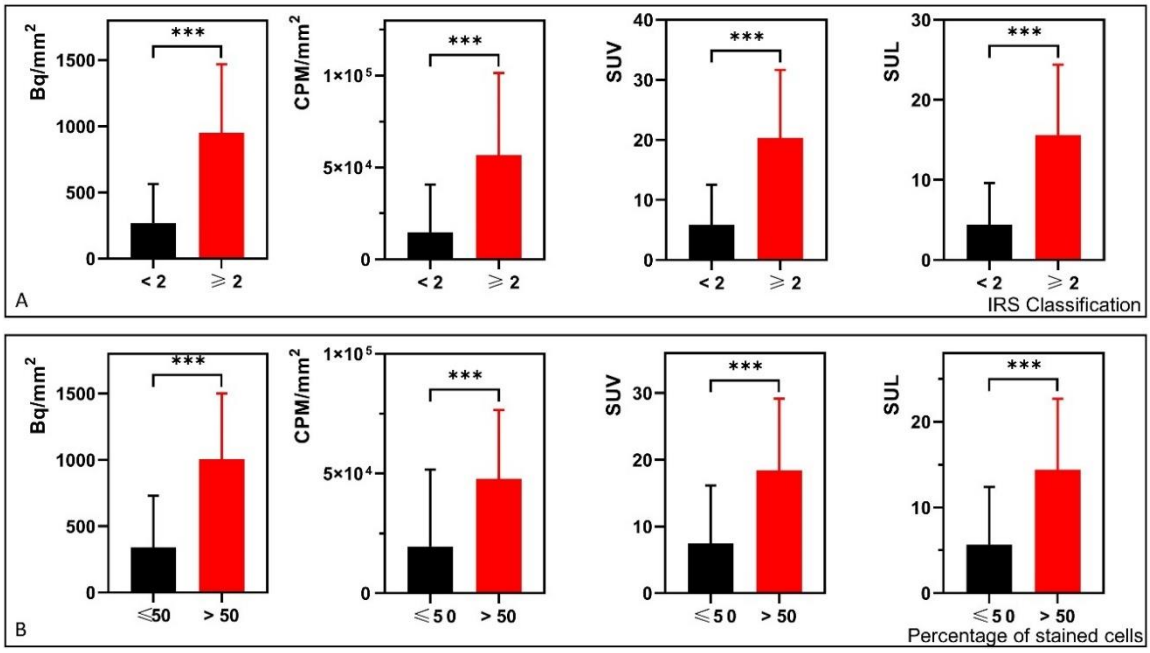

Figure 27. Bar charts of PSMA-ligand uptake in different groups.

A. Mean Bq/mm^2 in ARG was 268.2 ± 294.6 for IRS < 2 (n = 4050) and 949.6 ± 519.7 for IRS ≥ 2 (n = 596; ***: $p < 0.001$). Mean CPM/mm^2 in ARG was 14754.4 ± 26078.2 for IRS < 2 (n = 4050) and 56830.7 ± 44636.6 for IRS ≥ 2 (n = 596; ***: $p < 0.001$). Mean SUV_{ARG} was 5.8 ± 6.6 for IRS < 2 (n = 4050) and 20.3 ± 11.3 for IRS ≥ 2 (n = 596; ***: $p < 0.001$). Mean SUL_{ARG} was 4.4 ± 5.2 for IRS < 2 (n = 4050) and 15.6 ± 8.8 for IRS ≥ 2 (n = 596; ***: $p < 0.001$). B. Mean

Bq/mm^2 in ARG was 341 ± 388.2 for ≤ 50% stained cells (n = 4544) and 1005.4 ± 496.7 for > 50% stained cells (n = 102; ***: $p < 0.001$). Mean CPM/mm^2 in ARG was 19533.4 ± 32150.5 for ≤ 50% stained cells (n = 4544) and 47761 ± 28812.7 for > 50% stained cells (n = 102; ***: $p < 0.001$). Mean SUV_{ARG} was 7.5 ± 8.6 for ≤ 50% stained cells (n = 4544) and 18.4 ± 10.7 for > 50% stained cells (n = 102; ***: $p < 0.001$). Mean SUL_{ARG} was 5.7 ± 6.7 for ≤ 50% stained cells (n = 4544) and 14.4 ± 8.3 for > 50% stained cells (n = 102; ***: $p < 0.001$).

Table 22. PSMA expression vs. PSMA ligand uptake.

Unit	Parameter	Mean ± SD	*p* value
Bq/mm2	IRS < 2	268.2 ± 294.6	< 0.001***
	IRS ≥ 2	949.6 ± 519.7	
	≤ 50% stained cells	341 ± 388.2	< 0.001***
	> 50% stained cells	1005.4 ± 496.7	
CPM/mm2	IRS < 2	14754.4 ± 26078.2	< 0.001***
	IRS ≥ 2	56830.7 ± 44636.6	
	≤ 50% stained cells	19533.4 ± 32150.5	< 0.001***
	> 50% stained cells	47761 ± 28812.7	
SUV	IRS < 2	5.8 ± 6.6	< 0.001***
	IRS ≥ 2	20.3 ± 11.3	
	≤ 50% stained cells	7.5 ± 8.6	< 0.001***
	> 50% stained cells	18.4 ± 10.7	
SUL	IRS < 2	4.4 ± 5.2	< 0.001***
	IRS ≥ 2	15.6 ± 8.8	
	≤ 50% stained cells	5.7 ± 6.7	< 0.001***
	> 50% stained cells	14.4 ± 8.3	

Bq = becquerel; CPM = counts per minute; IRS = immunoreactive score; PSMA = prostate-specific membrane antigen; SD = standard deviation; SUL = SUV normalized by lean body mass; SUV = standardized uptake value.

***: $p < 0.001$.

5.2. Clinical results

5.2.1. Patients

A total of 186 patients were finally included in this retrospective study. In brief, the median age was 68 years, and the median serum iPSA was 9.7 ng/ml (IQR 6.5-15.1). The number of patients classified within the D'Amico high-risk group was 126 (68.1%). The median time between ^{68}Ga-PSMA-11 PET examination and radical prostatectomy was 26 days (IQR 13-46). On histopathology, a total of 133 (71.5%) patients had a Gleason Score < 8, and 53 (28.5%) of the patients had a Gleason Score 8 or 9. Lymph node metastasis was detected in 32 (17.2%) patients, and 49.5% (n = 92) had pT2. Twenty-eight of 186 patients (15.6%) had positive surgical margins (R1). At a median follow-up after RP of 38 months (IQR: 22-53), BCR was observed in 58 (31.2%) patients during the follow-up period.

Table 23 lists characteristics of patients and clinicopathological findings.

Table 23. Patient characteristics.

Characteristic	Patients, N = 186
Age (yr), median (IQR), n = 186	68 (61-72)
iPSA (ng/ml), median (IQR), n = 184[a]	9.7 (6.5-15.1)
Administered ^{68}Ga-PSMA-11 activity (MBq), median (IQR), n = 185[b]	139 (112-156)
Time PET to RP (day), median (IQR), n = 186	26 (13-46)
D'Amico risk groups, no. (%), n = 185[c]	
Intermediate risk	59 (31.9%)
High risk	126 (68.1%)
Gleason score in surgical specimen, no. (%), n = 186	
6	11 (5.9%)
7a	63 (33.9%)
7b	59 (31.7%)
8	28 (15.1%)
9	25 (13.4%)
Pathological stage, no. (%), n = 186	
pT status	
2a	11 (5.9%)
2b	10 (5.4%)
2c	71 (38.2%)
3a	49 (26.3%)
3b	44 (23.7%)
4	1 (0.5%)
pN status	

0	154 (82.8%)
1	32 (17.2%)
Surgical margin, no. (%), n = 180[d]	
Negative	152 (84.4%)
Positive	28 (15.6%)

iPSA = initial prostate-specific antigen; IQR = interquartile range; PET = positron emission tomography; PSA = prostate-specific antigen; RP = radical prostatectomy.

a: iPSA of two patients were unavailable; b: the injected dose of ^{68}Ga-PSMA-11 from one patient was unavailable; c: the Gleason score of biopsy sample from one patient was unavailable; d: the status of surgical margin from six patients were unavailable.

5.2.2. ^{68}Ga-PSMA-11 PET findings

On ^{68}Ga-PSMA-11 PET findings, 67.2% (n = 125) were classified into miT2, 90.3% (n = 168) were classified into miN0 and 96.2% (n = 179) were classified into miM0. ^{68}Ga-PSMA-11 PET parameters (SUV_{max}, SUV_{mean}, TV, TL) of prostatic lesions were analyzed in 183 patients because three patients were reported negative PSMA prostate cancer. The median numbers of SUV_{max}, SUV_{mean}, TV, TL were 10.6 (IQR 6.4-18.9), 6.2 (IQR 3.2-11.0), 3.9 (IQR 1.7-10.5), and 24.7 (IQR 15.9-44.4), respectively. Table 24 lists information from ^{68}Ga-PSMA-11 PET.

The sensitivity and specificity of ^{68}Ga-PSMA-11 PET detecting lymph nodes metastasis in pelvic were 41% and 96.8%, respectively (13/32, 95% CI: 24%-59% and 149/154, 95% CI: 92%-98%, respectively).

Table 24. ^{68}Ga-PSMA-11 PET findings.

No. of patients	186
PROMISE (miTNM) classification, no. (%), n = 186	
miT status from PSMA PET	
2u	73 (39.2%)
2m	52 (28%)
3a	27 (14.5%)
3b	24 (12.9%)
4	10 (5.4%)
miN status from PSMA PET	

0	168 (90.3%)
1a	7 (3.8%)
1b	11 (5.9%)
miM status from PSMA PET	
0	179 (96.2%)
1a	3 (1.6%)
1b	4 (2.2%)
PSMA PET parameters of prostatic lesions, median (IQR), n = 183[a]	
SUV_{max}	10.6 (6.4-18.9)
SUV_{mean}	6.2 (3.2-11.0)
TV	3.9 (1.7-10.5)
TL	24.7 (15.9-44.4)

IQR = interquartile range; PET = positron emission tomography; PROMISE = prostate cancer molecular imaging standardized evaluation; PSMA = prostate-specific membrane antigen; SUV = standardized uptake value; TL = total lesion; TV = tumor volume.

a: three patients had PSMA negative prostate cancer.

5.2.3. Correlation of ^{68}Ga-PSMA-11 PET findings with histopathology

In the univariate analysis (Table 25), a significant association was detected between a positive surgical margin and the following parameters: high miT status (miT ≥ 3a, OR: 3.38, $p = 0.004$), miN1 status (OR: 7.526, $p < 0.001$), SUV_{max} (OR: 1.026, $p = 0.039$) and TL (OR: 1.007, $p = 0.021$). In the multivariate analysis (Table 26), miN1 (OR: 5.428, $p = 0.004$) significantly associated with a positive surgical margin.

Table 25. Univariate analysis for the association of ^{68}Ga-PSMA-11 PET findings with surgical margin status.

	No. of evaluable patients	Odds ratio	95% CI	p value*
PROMISE (miTNM) classification, no., n = 186				
miT status				
2	125	Reference		
≥ 3a	61	3.380	1.477-7.732	**0.004**
miN status				
No LN metastasis	168	Reference		
With LN metastasis	18	7.526	2.659-21.305	**<0.001**

SUV_{mean} of prostatic lesions	183	1.035	0.996-1.076	0.076
SUV_{max} of prostatic lesions	183	1.026	1.001-1.052	**0.039**
TV of prostatic lesions	183	0.992	0.941-1.046	0.775
TL of prostatic lesions	183	1.007	1.001-1.014	**0.021**

CI = confidence interval; LN = lymph node; PET = positron emission tomography; PROMISE = prostate cancer molecular imaging standardized evaluation; PSMA = prostate-specific membrane antigen; SUV = standardized uptake value; TL = total lesion; TV = tumor volume.

*Significant associations are given in bold.

Table 26. Multivariate analysis for the association of ^{68}Ga-PSMA-11 PET findings with surgical margin status.

	No. of evaluable patients	Odds ratio	95% CI	*p* value*
PROMISE (miTNM) classification, no., n = 186				
miT status				
2	125	Reference		
≥ 3a	61	2.065	0.802-5.315	0.133
miN status				
No LN metastasis	168	Reference		
With LN metastasis	18	5.428	1.708-17.249	**0.004**
SUV_{max} of prostatic lesions	183	1.015	0.988-1.044	0.282
TL of prostatic lesions	183	1.004	0.998-1.011	0.166

CI = confidence interval; LN = lymph node; PET = positron emission tomography; PROMISE = prostate cancer molecular imaging standardized evaluation; PSMA = prostate-specific membrane antigen; SUV = standardized uptake value; TL = total lesion; TV = tumor volume.

*Significant associations are given in bold.

Moreover, a significant association was found between miT ≥ 3a and Gleason Score ≥ 8 (OR: 2.696, *p* = 0.003) (Table 27).

Table 27. Univariate analysis for the association of ^{68}Ga-PSMA-11 PET findings with Gleason Score.

	No. of evaluable patients	Odds ratio	95% CI	*p* value*
PROMISE (miTNM) classification, no., n = 186				
miT status				
2	125	Reference		
≥ 3a	61	2.696	1.39-5.23	**0.003**
miN status				
No LN metastasis	168	Reference		
With LN metastasis	18	2.187	0.812-5.887	0.122
SUV_{mean} of prostatic lesions	183	1.020	0.986-1.056	0.248
SUV_{max} of prostatic lesions from	183	1.017	0.995-1.040	0.138
TV of prostatic lesions	183	0.981	0.941-1.022	0.353
TL of prostatic lesions	183	1.006	1-1.012	0.056

CI = confidence interval; LN = lymph node; PET = positron emission tomography; PROMISE = prostate cancer molecular imaging standardized evaluation; PSMA = prostate-specific membrane antigen; SUV = standardized uptake value; TL = total lesion; TV = tumor volume.

*Significant associations are given in bold.

5.2.4. Predictors of BCR-free survival

Kaplan-Meier curves of BCR free-survival with different clinicopathological parameters and imaging findings were shown in Figure 28-Figure 33.

Patients in miT2 status showed superior BCR free survival rates compared with patients in miT3 and higher status (log-rank, $p < 0.001$) (Figure 28A). The higher BCR free survival rates were observed in patients without pelvic lymph node metastasis than patients with pelvic lymph node metastasis detected in ^{68}Ga-PSMA-11 PET (miN0, log-rank, $p = 0.005$) (Figure 28B).

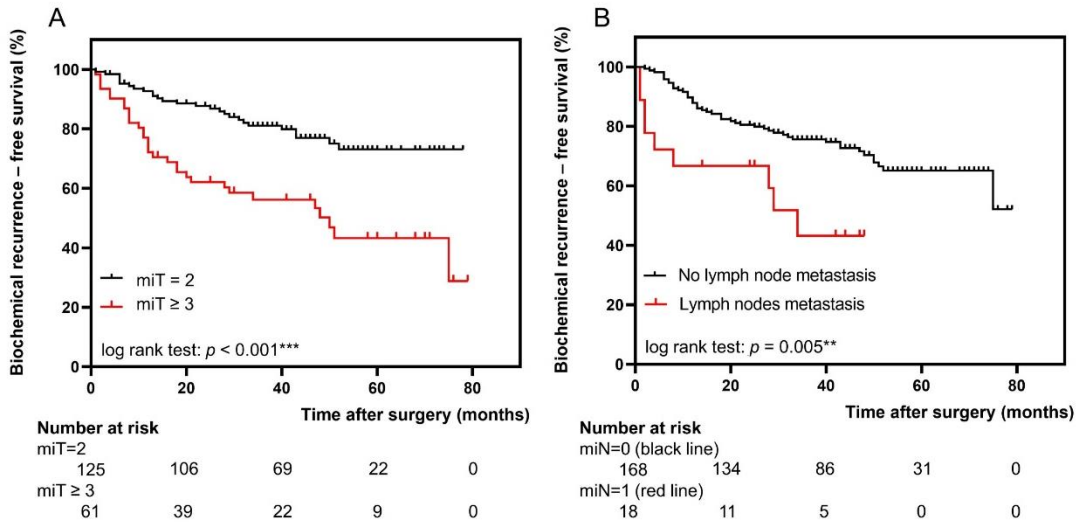

Figure 28. Longer biochemical recurrence-free survival was associated with (A) miT = 2 and (B) miN = 0.

Patients with pT ≥ 3 showed worse BCR free survival rates compared with pT2 patients (log-rank, $p < 0.001$) (Figure 29A). The higher BCR free survival rates were observed in patients without pelvic lymph node metastasis in pathology findings (pN0) (Figure 29B) (log-rank, $p < 0.001$). Herein, less aggressive tumor type (GS < 8) (Figure 29C) and negative surgical margin (Figure 29D) were associated with long BCR free survival (log-rank, $p < 0.001$, respectively).

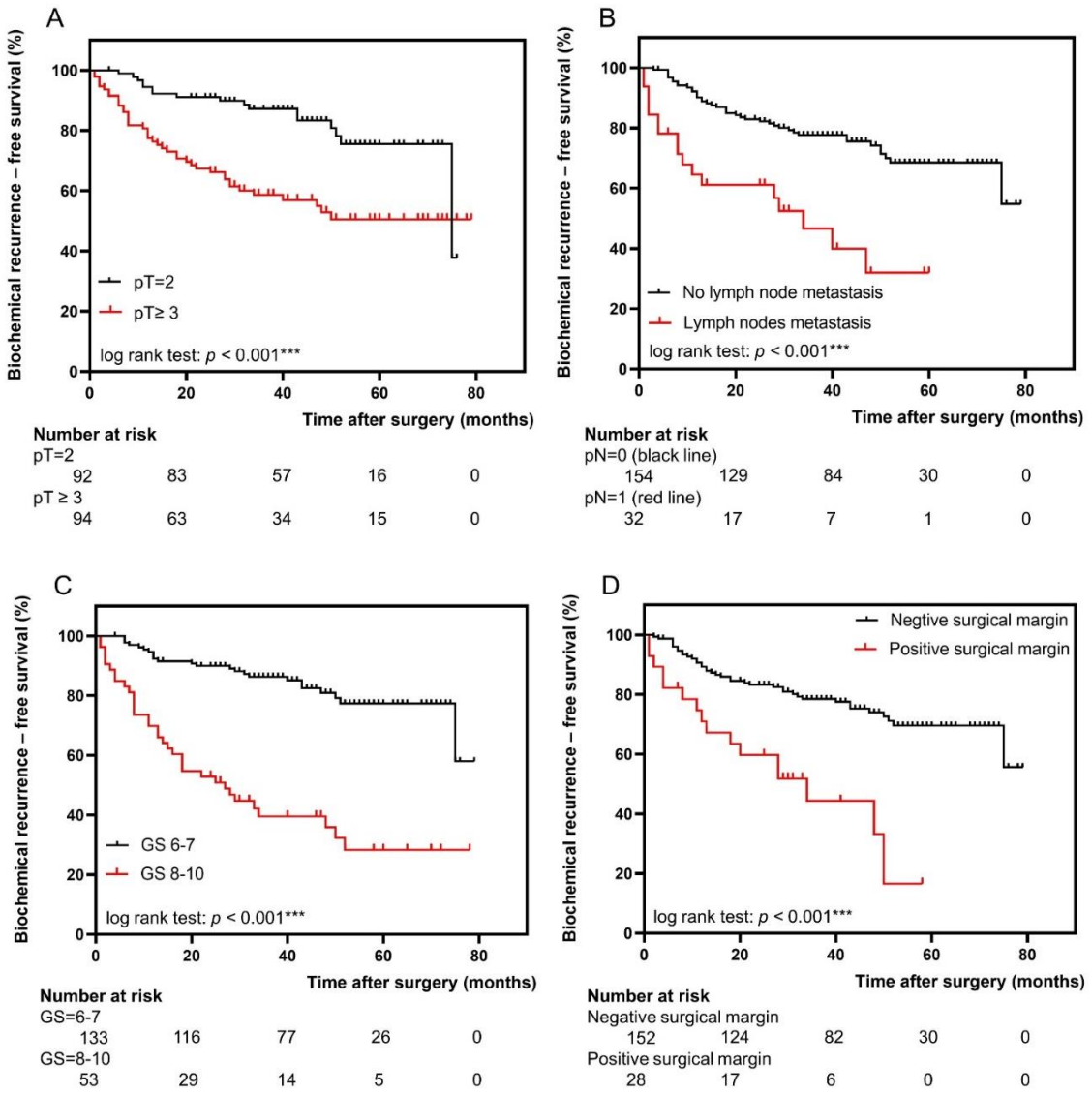

Figure 29. Longer biochemical recurrence-free survival was associated with (A) pT = 2, (B) pN = 0, (C) Gleason Score < 8 and (D) negative surgical margin.

When stratified by ^{68}Ga-PSMA-11 PET image findings (Figure 30-Figure 33), high BCR free survival rates were observed in patients with low SUV_{mean} (Figure 32) and SUV_{max} (Figure 33).

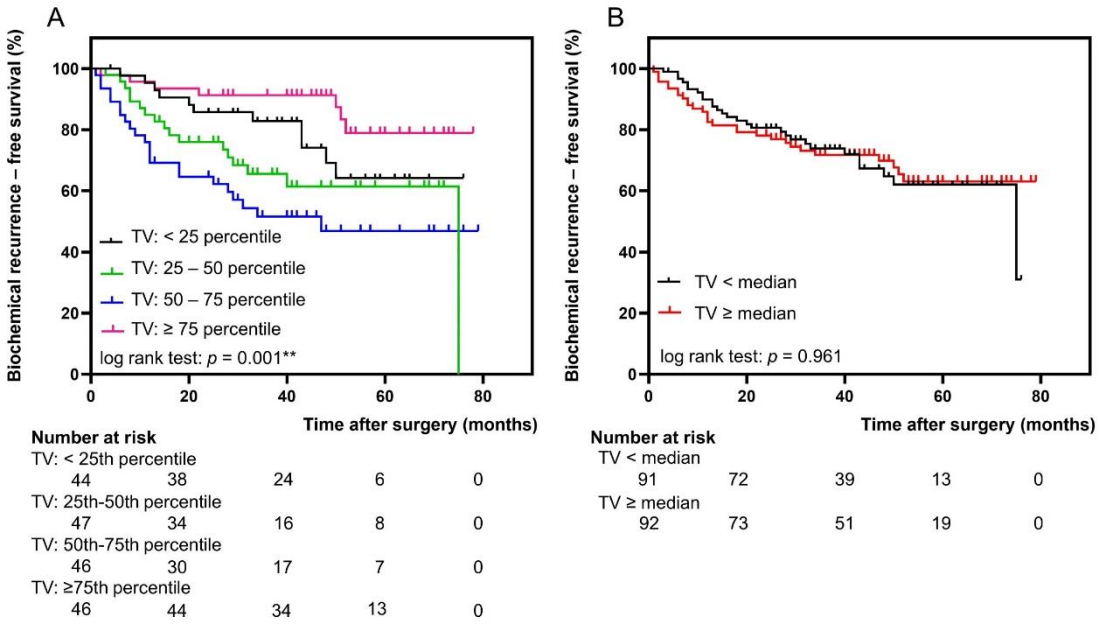

Figure 30. Biochemical recurrence-free survival according to tumor volume stratified by (A) percentiles and (B) median.

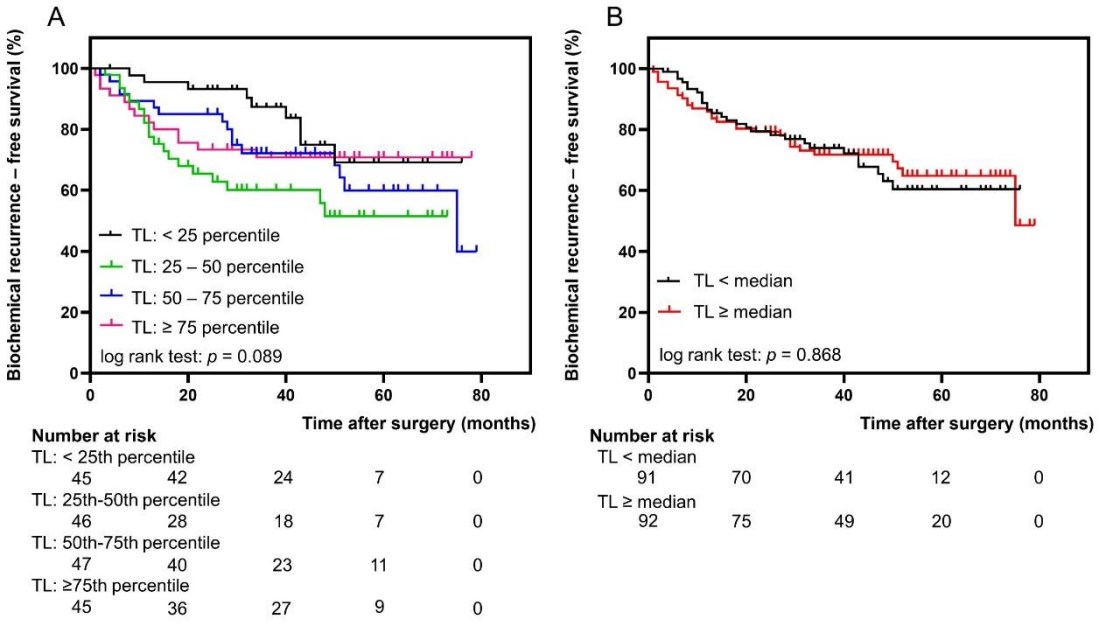

Figure 31. Biochemical recurrence-free survival according to total lesion stratified by (A) percentiles and (B) median.

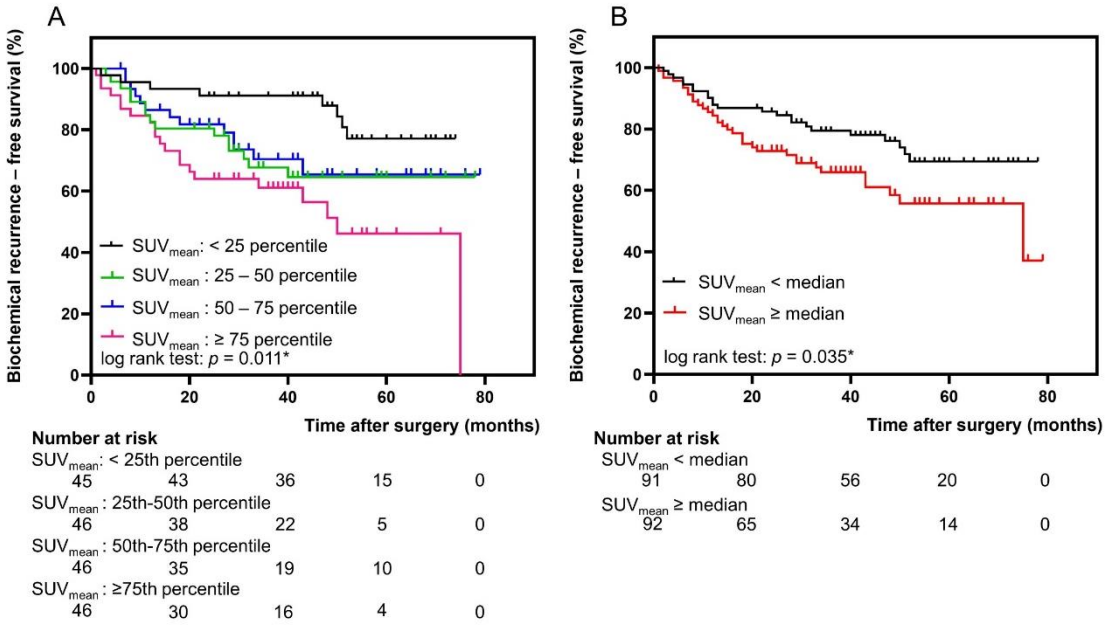

Figure 32. Biochemical recurrence-free survival according to SUV_{mean} stratified by (A) percentiles and (B) median.

Long biochemical recurrence-free survival was associated with low SUV_{mean}.

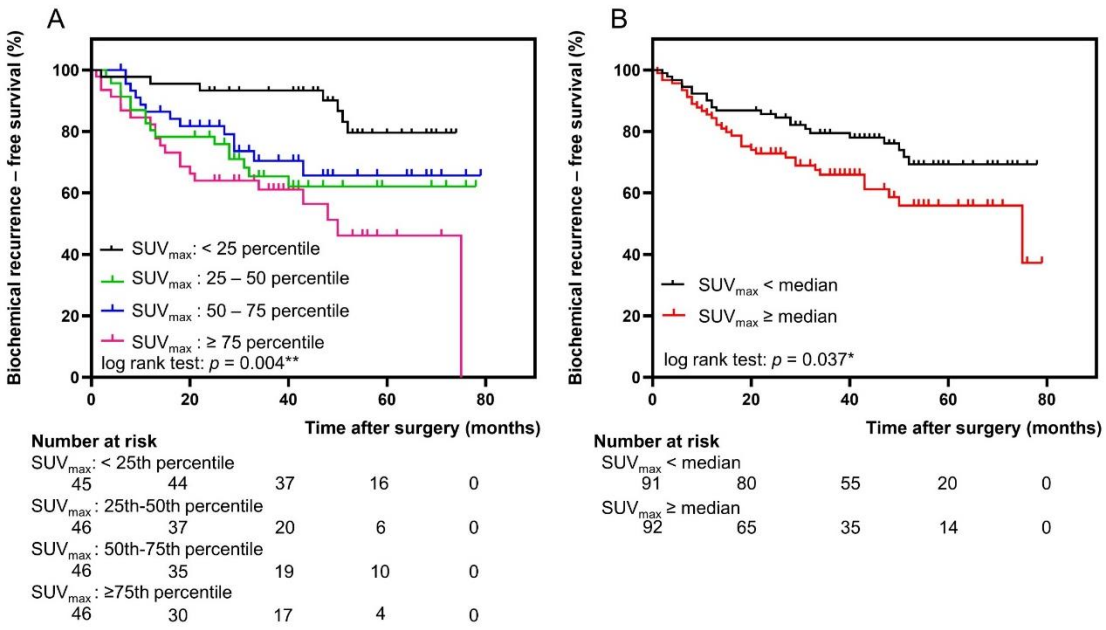

Figure 33. Biochemical recurrence-free survival according to SUV_{max} stratified by (A) percentiles and (B) median.

Long biochemical recurrence-free survival was associated with low SUV_{max}.

Moreover, we examined preoperative and postoperative risk factors for disease BCR prediction in the cohort. In the univariate Cox regression analysis (Table

28), we found that age (HR: 1.056, 95%CI: 1.018-1.096, $p = 0.004$), iPSA (HR: 1.021, 95%CI: 1.007-1.035, $p = 0.003$), Gleason Score (GS ≥ 8 vs. GS < 8, HR: 5.097, 95%CI: 3.013-8.625, $p < 0.001$), miT stage (miT ≥ 3a vs. miT < 3, HR: 2.811, 95%CI: 1.673-4.722, $p < 0.001$), miN stage (miN1 vs. miN0, HR: 2.691, 95%CI: 1.311-5.527, $p = 0.007$), SUV_{mean} of prostatic lesions (HR: 1.019, 95%CI: 1.002-1.036, $p = 0.028$), SUV_{max} of prostatic lesions (HR: 1.015, 95%CI: 1.004-1.026, $p = 0.008$), pT stage (pT ≥ 3 vs. pT < 3, HR: 2.935, 95%CI: 1.665-5.173, $p < 0.001$), pN stage (pN1 vs. pN0, HR: 3.378, 95%CI: 1.901-6, $p < 0.001$) and surgical margin (positive vs. negative, HR: 3.421, 95%CI: 1.890-6.193, $p < 0.001$) were positively associated with BCR in the patients included.

In multivariate Cox regression analysis (Table 29) revealed the independent predictors of BCR to be serum PSA level (HR: 1.024, 95% CI: 1.005-1.043, $p = 0.014$), advanced pathological Gleason Score (GS ≥ 8 vs. GS < 8, HR: 3.253, 95% CI: 1.779-5.950; $p < 0.001$) and miT stage (miT ≥ 3a vs. miT < 3, HR: 1.941, 95% CI: 1.047-3.599, $p = 0.035$).

Table 28. Univariable analysis for the association of baseline factors with BCR-free survival.

	No. of evaluable patients	Hazard ratio	95% CI	*p* value*
Age	186	1.056	1.018-1.096	**0.004**
iPSA	184	1.021	1.007-1.035	**0.003**
Gleason score in surgical specimen, no., n = 186				
6-7	133	Reference		
8-10	53	5.097	3.013-8.625	**< 0.001**
PROMISE (miTNM) classification based on PROMISE, no., n = 186				
miT status from PSMA PET				
2	125	Reference		
≥ 3a	61	2.811	1.673-4.722	**< 0.001**
miN status from PSMA PET				
No LN metastasis	168	Reference		
With LN metastasis	18	2.691	1.311-5.527	**0.007**

SUV_{mean} of prostate lesions from PSMA PET	183	1.019	1.002-1.036	**0.028**
SUV_{mean} of prostate lesions from PSMA PET, no. n = 183				
≤ 25th percentile	45	Reference		
25th-50th percentile	46	2.331	0.983-5.531	0.055
50th-75th percentile	46	2.032	0.838-4.928	0.117
> 75th percentile	46	3.675	1.619-8.343	**0.002**
SUV_{mean} of prostate lesions from PSMA PET, no. n = 183				
< median	91	Reference		
≥ median	92	1.752	1.030-2.981	**0.039**
SUV_{max} of prostate lesions from PSMA PET	183	1.015	1.004-1.026	**0.008**
SUV_{max} of prostate lesions from PSMA PET, no. n = 183				
≤ 25th percentile	45	Reference		
25th-50th percentile	46	3.030	1.238-7.416	**0.015**
50th-75th percentile	46	2.381	0.945-5.999	0.066
> 75th percentile	46	4.318	1.825-10.215	**0.001**
SUV_{max} of prostate lesions from PSMA PET, no. n = 183				
< median	91	Reference		
≥ median	92	1.744	1.025-2.968	**0.040**
TV of prostate lesions from PSMA PET	183	0.948	0.909-0.988	**0.011**
TV of prostate lesions from PSMA PET, no., n = 183				
≤ 25th percentile	45	Reference		
25th-50th percentile	46	1.664	0.779-3.556	0.188
50th-75th percentile	46	2.411	1.167-4.979	**0.017**
> 75th percentile	46	0.529	0.205-1.366	0.188
TV of prostate lesions from PSMA PET, no., n = 183				
< median	91	Reference		
≥ median	92	0.987	0.587-1.661	0.962
TL of prostate lesions from PSMA PET	183	1.003	1.000-1.006	0.072

TL of prostate lesions from PSMA PET, no., n = 183				
≤ 25th percentile	45	Reference		
25th- 50th percentile	46	2.642	1.193-5.850	**0.017**
50th-75th percentile	46	1.740	0.767-3.948	0.185
> 75th percentile	46	1.554	0.664-3.636	0.310
TL of prostate lesions from PSMA PET, no., n = 183				
< median	91	Reference		
≥ median	92	0.957	0.568-1.612	0.869
Pathological stage, no., n = 186				
pT status[b]				
2	92	Reference		
≥3	94	2.935	1.665-5.173	**< 0.001**
pN status[b]				
0	154	Reference		
1	32	3.378	1.901-6.000	**< 0.001**
Surgical margin, no., n = 180				
Negative	152	Reference		
Positive	28	3.421	1.890-6.193	**< 0.001**

BCR = biochemical recurrence; CI = confidence interval; iPSA = initial PSA; IQR = interquartile range; LN = lymph node; PET = positron emission tomography; PROMISE = prostate cancer molecular imaging standardized evaluation; PSMA = prostate-specific membrane antigen; PSA = prostate-specific antigen; SUV = standardized uptake value; TL = total lesion; TV = tumor volume.

[*]Significant associations are given in bold.

Table 29. Multivariable analysis for the association of baseline factors with BCR-free survival.

	No. of evaluable patients	Hazard ratio	95% CI	*p* value*
Age, no., n = 186				
Continuous		1.030	0.991-1.071	0.133
iPSA, no., n = 184				
Continuous		1.024	1.005-1.043	**0.014**

Gleason score in surgical specimen, no., n = 186				
6-7	133	Reference		
8-10	53	3.253	1.779-5.950	**< 0.001**
miT status from PSMA PET, no., n = 186				
2	125	Reference		
≥ 3a	61	1.941	1.047-3.599	**0.035**
miN status from PSMA PET, no., n = 186				
No LN metastasis	168	Reference		
With LN metastasis	18	1.233	0.389-3.908	0.722
SUV_{mean}, no., n = 183				
Continuous		0.743	0.491-1.123	0.159
SUV_{max}, no., n = 183				
Continuous		1.202	0.943-1.532	0.137
TV				
Continuous		0.934	0.883-0.988	**0.017**
pT status, no., n = 186				
2	92	Reference		
3	94	1.471	0.773-2.797	0.239
pN status, no., n = 186				
No LN metastasis	154	Reference		
With LN metastasis	32	1.027	0.418-2.525	0.954
Surgical margin, no., n = 180				
Negative	152	Reference		
Positive	28	1.539	0.716-3.305	0.269

BCR = biochemical recurrence; CI = confidence interval; iPSA = initial PSA; LN = lymph node; PET = positron emission tomography; PSMA = prostate-specific membrane antigen; PSA = prostate-specific antigen; SUV = standardized uptake value; TV = tumor volume.

* Significant associations are given in bold.

Moreover, we established a miTNM staging system by combining miTNM classification and SUV_{max} to predict BCR for localized prostate cancer patients. An

overview of the miTNM staging system (version 1.0) was given in Table 30. Twenty of 186 (10.8%) patients were classified into the stage group IA, 96 (51.6%) in IB, 40 (21.5%) in IIA, 7 (3.8%) in IIB, 16 (8.6%) in III, and 7 (3.8%) in IV. Due to the limited sample size in miTNM stage group ≥ IIA, the current study only proposed a cut-off of SUV_{max} in miTNM stage group I and generated 2 sub-groups. Kaplan-Meier curves on BCR free-survival with different miTNM stage groups were shown in Figure 34. The higher BCR free survival rates were observed in patients in miTNM stage group IA compared with miTNM stage group IB (log-rank, $p = 0.022$). Pair-wise comparisons between all different stages with log-rank test were conducted, and all pair-wise *p* values were significant.

Table 30. miTNM staging for ^{68}Ga-PSMA-11 PET/CT or MRI.

Stage Group	miT	miN	miM	SUV_{max}
IA	2	0	0	< 5.4
IB	2	0	0	≥ 5.4
IIA	3	0	0	Any
IIB	4	0	0	Any
III	Any	1 and 2	0	Any
IV	Any	Any	1	Any

CT = computed tomography; MRI = magnetic resonance imaging; PET = positron emission tomography; PSMA = prostate-specific membrane antigen; SUV = standardized uptake value.

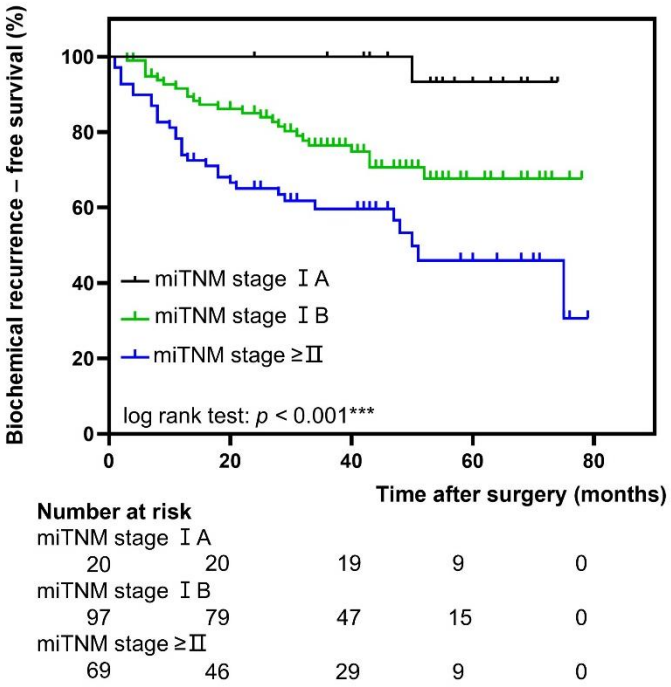

Figure 34. Biochemical recurrence-free survival according to miTNM stage.

Pairwise comparison: miTNM stageIA vs. miTNM stageIB, $p = 0.022$; miTNM stageIA vs. miTNM stage ≥ II, $p = 0.001$; miTNM stageIB vs. miTNM stage ≥ II, $p = 0.005$.

6. Discussion

6.1. Correlation of PSMA-ligand uptake and Histopathology findings

PSMA-ligands have been increasingly used for imaging and treatment of prostate cancer (T Maurer, M Eiber, et al., 2016), while PSMA expression status hold promise to serve as a risk stratification factor. PSMA-ligands are small molecules that bind to the active site in the extracellular domain of PSMA, leading to enhanced tumor uptake and high image quality (A Afshar-Oromieh et al., 2013; A Ghosh et al., 2004; SA Rajasekaran et al., 2003; SM Schwarzenboeck et al., 2017). This high and specific tumor uptake occurs because PSMA is highly expressed in primary prostate cancer and metastatic lesions (DG Bostwick et al., 1998; S Mannweiler et al., 2009; V Yao et al., 2010). Moreover, an immunohistochemical study by Ross et al. has indicated that patients with high tumor PSMA expression exhibited a significantly increased tumor grade ($p = 0.03$), pathological stage ($p = 0.029$), aneuploidy ($p = 0.01$) and rate of BCR ($p = 0.001$) as compared to tumors featuring a lower PSMA expression (JS Ross et al., 2003). However, so far non-invasive imaging techniques are lacking to determine PSMA-expression at initial diagnosis to add this information for potential therapy decisions. Since the understanding of the correlation between PSMA-ligand uptake and pathological features could close this gap, we planned to investigate the potential of PSMA-ligands to predict post-surgical pathological outcomes and most importantly, tumor aggressiveness.

This is the first preclinical study demonstrating the correlation of the uptake of ^{99m}Tc-PSMA-I&S ligand using high resolution ARG and histopathology findings. Our data demonstrate a significantly higher uptake of ^{99m}Tc-PSMA-I&S in Gleason Pattern 4 and Gleason Pattern 5 compared to Gleason Pattern 3 and non-neoplastic tissue. This result also translated into differences for Gleason Scores. Higher PSMA-ligand uptake was observed in Gleason Score ≥ 8 than Gleason Score < 8. These promising data support the potential of PSMA-ligands to non-invasively assess tumor aggressiveness.

6.1.1. Influence of non-pathological parameters on detection of intraprostatic foci by PSMA-ligands imaging

In the current study, our results show that ARG failed to detect all histopathology-confirmed prostate cancer ROIs and 65.3% of ROIs were positive in ARG. Thus, although the sensitivity and specificity of PSMA-ligand PET are promising (W Cytawa et al., 2020; TA Hope et al., 2019; S Kimura et al., 2020; M Mix et al., 2018; M Perera et al., 2016; K Sprute et al., 2020; J Zhou et al., 2019), it is essential to study the reasons for the presence of PSMA negative foci in prostate cancer in PSMA-ligand PET images. There are two explanations of non-pathological parameters:

Firstly, the lesions are PSMA positive and the ligands bind PSMA, however, the lesions are too small to be detected given the intrinsic spatial resolution of the technique used. Our results show a considerably larger area of ARG positive ROIs of intraprostatic lesions in histopathology than ARG negative ROIs (179.8 ± 195.1 vs. 7.6 ± 14.6 mm^2, $p < 0.001$). It has been reported that the minimal detection size of fluorodeoxyglucose (FDG), choline, and acetate-based clinical PET imaging was limited to 5 mm (IJ de Jong et al., 2003; JJ Fox et al., 2012; H Jadvar, 2011), and limited performance was observed for lesions smaller than 9 mm (E Mena et al., 2012). Besides, Van Leeuwen et al. reported that by ^{68}Ga-PSMA PET/CT non-detectable positive lymph nodes had an average size of 2.73 ± 1.29 mm, which was significantly smaller than true-positive lymph nodes (4.73 ± 1.45 mm, $p = 0.001$) (PJ van Leeuwen et al., 2017). Our data suggest that there is high possibility of positive signals in large tumor areas. However, because of the limited sample size and different tissue types, more studies are needed to compare the detection limitation between ARG and PSMA-ligand PET. Currently, the PET scanner is limited by detector design and photon non-collinearity (FP DiFilippo, 2015). The spatial resolution of PET cameras is between 4.9 and 5.1 mm with state-of-the-art “time of flight” technology (JA Kolthammer et al., 2014; PJ van Leeuwen et al., 2017), which is able to enhance the spatial resolution of clinical PET scanners. A high-resolution imaging method to accurately localize cancer would be highly beneficial (M Conti, 2014).

Secondly, some prostate tumor foci might have lower perfusion than other foci, and the PSMA-ligands accumulate better in the highly perfused areas. Around 70% of prostate adenocarcinoma arises from epithelial cells in the peripheral zone (YJ Choi et al., 2007). Angiogenesis is vital in prostate cancer progression and metastasis (Y Li et al., 2010). Furthermore, the tumor blood flow is usually unevenly distributed, and it can reverse its direction leaving ischemic regions (G Russo et al., 2012). The delivery of therapeutic agents is opposed by ischemic regions (RK Jain, 2001), and these regions contribute to hypoxia (H Zhong et al., 1999). In our ex vivo experiment, we evaluated the efficacy of ligand binding. Due to the limitation of cryosections, it is difficult to annotate Gleason Scores/Gleason Patterns on HE staining sections. Thus, our analysis was based on the percentage of tumor cells per 1 mm^2. Our results indicate a significantly high tracer uptake in high density tumors (> 40%, $p < 0.001$). Besides, tumor cells have significantly higher tracer uptake than normal prostate tissue ($p < 0.001$). Although high efficacy of ligand binding was observed, further studies are needed to evaluate the correlation between ligand binding and PSMA expression confirmed by IHC. Because of the clinical procedure, we cannot image tissues that were used for cryosections. We hypothesize that if negative foci in ARG but positive in ex vivo experiment is observed, there is a possibility that perfusion affects the distribution of PSMA-ligands. Thus, further studies are needed to evaluate it. Moreover, PSMA-ligands could be designed with a longer half-life to prolong their existing time in the circulation, which will be advantageous to tracer accumulation.

6.1.2. Influence of pathological parameters on detection of intraprostatic foci by PSMA-ligands imaging

It is known that the Gleason Pattern and Gleason Score are of paramount importance in the management of prostate cancer patients. In 2014, a new grading system resulting in five prognostically distinct Grade Groups for prostate carcinoma based on data from Johns Hopkins Hospital was proposed (JI Epstein, L Egevad, et al., 2016). The authors proposed the system based on the prognosis and classified it as Grade Groups (Table 2). These findings were validated by Epstein et al. (JI Epstein, MJ Zelefsky, et al., 2016). In this study, 20,845 consec-

utive patients treated by RP and 5501 men treated with radiotherapy at two academic institutions between 2005 and 2014 were included. They confirmed a significant difference in recurrence rates between Gleason 3 + 4 versus 4 + 3 and Gleason 8 versus 9. Because of the excellent correlation between the grade groups and the prognosis, it takes on even greater importance when a Gleason Score 4+3 lesion is underestimated when evaluating Gleason Score from prostate specimens' HE slides depends entirely on the expertise of pathologists. Besides, in prostate biopsy specimens, quantifying and distinguishing the proportion of Gleason Pattern 3 and 4 is also challenging (S Bravaccini et al., 2018). Thus, PSMA expression analysis and PSMA-ligand PET assessment could be valuable tools to learn the disease outcome in primary prostate cancer patients. This will be a benefit to individualized disease management. However, as stated above, the low resolution of PET imaging limited the direct comparison between PSMA-ligands PET images and histological images. Our study used ARG, which has a high resolution, was used to demonstrate the correlation of the PSMA-ligand uptake and clinicopathological findings. The intriguing aspect of this method is that it allows a 1:1 correlation between radioactivity signals and tissue, which is further processed for histopathology sections. In our study, we evaluated the association between PSMA-ligand uptake, PSMA expression and Gleason Score/Pattern, in order to provide indisputable evidence for the application of PSMA-ligands PET as a predictive tool for clinicopathological outcomes in primary prostate cancer patients. We displayed our results using four different radioactivity units (Bq, CPM, SUV_{ARG} and SUL_{ARG}) to generate data easily compared with data from other research groups. Moreover, in the clinical study, we confirmed the predictive value of ^{68}Ga-PSMA-11 PET findings for aggressive tumor types (Gleason Score ≥ 8) and positive surgical margin.

Many studies have reported the PSMA expression patterns in prostate cancer and hypothesized that different tracer uptake of PMSA-ligands might correlate with the PSMA expression status. In our ROI-based analysis, remarkably, PSMA-negative areas were observed in 49% (n = 59) ROIs measuring between 0.05 and 853.9 mm^2 with histopathology proven prostate cancer. A heterogeneous expression of PSMA was observed in 42% (n = 59) of the investigated primary prostate cancer ROIs and fully PSMA-negative areas were observed in four of

them. Our data are in line with data by Ferraro et al. reported recently (DA Ferraro et al., 2020). Their study including 74 patients indicated that 40 primary tumors (54%) fully expressed PSMA, and PSMA-negative areas were observed in 34. A homogeneous PSMA expression was observed in 25 specimens (34%), and a heterogeneous PSMA expression was observed in 49 (66%). Besides, in a study including 51 patients with primary prostate cancer and distant metastases, PSMA-negative cells were observed in highly PSMA positive cases of any Gleason Score. (S Mannweiler et al., 2009).

Moreover, our results indicate that 90% of ROIs with PSMA negative area > 50% were Gleason Score 6 and 7. However, 22.4% of ROIs with PSMA negative area < 50% were Gleason Score 6 and 7. Our data show a positive correlation between IRS and Gleason Scores ($r = 0.607$, $p < 0.001$). Our grid-based data show that Gleason Pattern 5 has a higher IRS compared with Gleason Pattern 3. (Gleason Pattern 5 vs. Gleason Pattern 4 vs. Gleason Pattern 3 vs. normal prostate tissue: 9.53 ± 3.43, 8.96 ± 3.59, 3.43 ± 3.25, 0.3 ± 0.63). In line with our results, Bravaccini et al. observed stronger PSMA staining intensity in Gleason Pattern 4 and 5 than in Gleason Pattern 3 (S Bravaccini et al., 2018).

Using ^{99m}Tc-PSMA-I&S, we could demonstrate that the uptake of intraprostatic lesions is associated with histopathology findings at microscopic level using ARG. In detail, our ROI-based data suggest that the majority of ROIs (91%) with Gleason Score ≥ 7b were positive in ARG, and in a majority (63%) of ARG negative ROIs a Gleason Score < 7b was present. Our grid-based analyses also show high tracer uptake in aggressive Gleason Scores (Gleason Score ≥ 8 vs. Gleason Score < 8, $p < 0.001$). As known from other studies, the tracer uptake from PSMA-ligands PET increases in parallel with the rising Gleason Score (C Uprimny et al., 2017).

As important findings, in our grid-based analysis, we assessed the annotation classified by benign/malignant prostate tissue and Gleason Pattern. It has been proven that tumor uptake in prostate cancer is higher than in normal prostate tissue. However, the threshold of SUV varies from studies. We summarized the cutoff of SUV_{max} from PSMA-ligands PET based on the ROC curves (Table 31). Rahbar et al. reported a significant difference ($p < 0.001$) in median SUV_{max} of

clinical PET-imaging between true-positive prostate cancer (11.0 ± 7.8) and normal prostate tissue (2.7 ± 0.9) (K Rahbar et al., 2016). Furthermore, Woythal et al. documented a significantly higher SUV_{max} of prostate cancer (14.06 ± 15.56) than that of normal prostate (2.43 ± 0.63; $p < 0.001$) (N Woythal et al., 2018). In line with these results, our results indicate a significantly higher uptake in malignant lesions than in cancer-free prostate tissues (SUV_{ARG}, 15.6 ± 11.7 vs. 5.0 ± 5.4, $p < 0.001$). However, in Rowe et al.'s study, they found a lower SUV_{max} using ^{18}F-DCFBC (median SUV_{max}, 3.5 vs. 2.2, $p = 0.004$) (SP Rowe et al., 2015).

To our knowledge, our study is the first to generate a cutoff SUV_{ARG} and SUL_{ARG} for predicting prostate cancer from non-tumor tissue using ^{99m}Tc-PSMA-I&S ARG images. The validated cutoff for SUV_{ARG} is 6.2 and 4.6 for SUL_{ARG}. Both enable prostate cancer diagnosis with high sensitivity and specificity (sensitivity and specificity of 77.7% and 76.8%, sensitivity and specificity of 78.2% and 76.6%, respectively). In a study from Prasad's group, a SUV_{max} cutoff of 3.2 from ^{68}Ga-PSMA PET/CT imaging allowed a sensitivity of 94.3% and a specificity of 100% (V Prasad et al., 2016). However, this study lacks histopathological confirmation. In one of their latest study with immunohistochemistry, a SUV_{max} cutoff of 3.15 (a sensitivity and specificity of 97% and 90%) was reported, and it was in accordance with the former result (N Woythal et al., 2018).

Our findings of SUV_{ARG} cutoff are comparable to published data. However, care has to be taken when comparing SUV_{max} and SUV_{ARG}. First of all, different PSMA-ligands are used raising issues about different pharmacokinetics in vivo; secondly, the calculation methods for SUV_{max} and SUV_{ARG} are different. Unlike PET scan, ARG sample preparation was done manually, and the tissue thickness was 4-7 mm, and it is impossible to acquire an accurate value for volume calculation using the current workflow. Although results from ARG are not robust evidence for generating cutoff for PSMA-ligands PET because of the variety of ligands and calculation procedure, it still can be an alternative reference. More studies are necessary to evaluate the comparison between SUV_{max} and SUV_{ARG}.

In the current study, we have reported the association between PSMA-ligand uptake using four radioactive units and Gleason Pattern. A slight difference is observed among the results of different units, and multiple steps of the calculations

could be one of the explanations. Our data show that prostate carcinoma with Gleason pattern 4 (Bq, CPM, SUV, SUL: estimate: 20.15, 1185.36, 0.43, 0.33) and 5 (Bq, CPM, SUV, SUL: estimate: 10.95, 419.82, 0.07, 0.07) have a significantly higher uptake compared with non-neoplastic prostate tissue ($p < 0.001$, respectively). Besides, the estimated values in Gleason Pattern 3 and normal epithelia are negative, which is highly impossible in clinical application. The estimated values are calculated based on the statistic model, and the interpretation should consider the clinical practice. Thus, we conclude that Gleason Pattern 3 and normal epithelia do not associate with the tracer uptake. PIN and stroma were both detected significantly correlated with trace uptake. However, the sample size in PIN group is small (n = 81), but a relatively large number of grids contain stroma (n = 4635), and the range of 95% CI in PIN is broad (Bq, CPM, SUV, SUL: 1.12-21.16, 41.8-1814.49, 0.02-0.47, 0.02-0.37). Thus, the results regarding these two tissue types should be interpreted carefully. Our results highlight the promising role of PSMA-ligands PET in the prediction of tumor aggressiveness.

The correlation between SUV_{max} on ^{68}Ga-PSMA-11 PET and PSMA expression in primary prostate cancer has been reported (N Woythal et al., 2018). Similar to published data, our ROI-based results show that ARG positive ROIs had higher IRS than ARG negative ROIs (10 ± 3 vs. 5 ± 4, $p < 0.001$). Besides, our grid-based data demonstrate high tracer uptake in the high PSMA expression group (IRS ≥ 2).

To the best of our knowledge, our clinical study is the first to investigate the prognostic potential of preoperational intraprostatic ^{68}Ga-PSMA-11 PET findings in relation to postoperative histopathological outcomes such as Gleason Score and surgical margin and BCR after RP. In this study, we identify that miT stage (miT ≥ 3a) of prostate lesions from ^{68}Ga-PSMA-11 PET as an independent predictor of aggressive tumor type (GS ≥ 8, OR: 2.696, $p = 0.003$), and pelvic lymph node metastasis in imaging (miN1) as an independent predictor of positive surgical margin (OR: 5.428, $p = 0.004$). In our cohort SUV showed no prognostic value. However, a prior study demonstrated that Gleason Score ≥ 8 had a significantly high ^{68}Ga-PSMA-11 uptake (SUV_{max}) in primary prostate cancer patients

(C Uprimny et al., 2017). Our results indicate that perioperative ^{68}Ga-PSMA-11 PET findings have implications for disease management. A miT ≥ 3a and a miN1 could be potential prognostic markers for aggressive tumor type and positive surgical margin. Active surveillance and local therapy after RP should be considered in these patients.

6.2. BCR prediction by ^{68}Ga-PSMA-11 PET findings

Prognostic tools of BCR are urgently required and essential for improving treatment management of prostate cancer patients and reducing prostate cancer associated mortality for patients developing BCR after primary treatment (JA Brockman et al., 2015). Previous studies have proven that clinicopathological characteristics have strong associations with BCR, such as a higher Gleason score (D Cao et al., 2010; SJ Freedland et al., 2003; M Han et al., 2003; T Inagaki et al., 2009; X Xu et al., 2020), positive nerve invasion (X Xu et al., 2020), pathological T stage (M Han et al., 2003; T Inagaki et al., 2009) and preoperative PSA (SJ Freedland et al., 2003; M Han et al., 2003). Our findings are consistent with published data. Moreover, ^{68}Ga-PSMA-11 PET detected 13/32 with histological proven pelvic lymph nodes metastases while in 5 patients false positive lymph nodes metastases were detected by ^{68}Ga-PSMA-11 PET. This finding corresponds to our earlier findings, where a ^{68}Ga-PSMA-11 PET sensitivity and specificity of 65.9% and 98.9% on a patient-based analysis has been reported (T Maurer, JE Gschwend, et al., 2016).

6.2.1. Value of quantitative parameters from ^{68}Ga-PSMA-11 PET to predict BCR-free survival

As a framework for PSMA-ligands PET reporting, we performed a prognostic validation of the miTNM system in a relatively large cohort. Preoperational ^{68}Ga-PSMA-11 PET and the miTNM classification could help evaluate the risk of BCR after RP, which is of importance in the clinical patient's management assessed.

In the current study, our data show that a miT stage ≥ 3a can serve as a predictor of worse BCR-free survival (HR: 1.941, 95% CI: 1.047-3.599, p = 0.035). In miN subgroup analysis, our results do not demonstrate different BCR-free survival

between patients with and without pelvic lymph node metastasis from ^{68}Ga-PSMA-11 PET (HR: 1.233, 95% CI: 0.389-3.908, p = 0.722). In our cohort, the detection rate of pelvic lymph node metastasis of ^{68}Ga-PSMA-11 PET is relatively low (41%, n = 32) and the sample size (miN1, n = 18) is relatively small. These could explain the observation from the miN subgroup.

Besides, our results indicate a negative association of TV with BCR free survival rate (HR: 0.934, 95%CI: 0.883-0.988, p = 0.017). However, Choi et al. have reported a significant high BCR-free survival probability when percent tumor volume ≤ 7.5% in histopathology with pT2 prostate cancer patients (p < 0.001) (SY Choi et al., 2020). This is partly related to the methods of obtaining tumor volume and further studies are necessary to clarify the most representative method of TV calculation from ^{68}Ga-PSMA-11 PET.

6.2.2. Value of molecular imaging staging to predict BCR-free survival

In order to preoperatively classify primary prostate cancer patients into risk groups based on PSMA-ligand imaging, the miTNM staging system (version 1.0) was introduced. The 8th edition of the American Joint Committee on Cancer (AJCC) cancer staging system based on clinicopathological parameters proves a fundamental tool and informs treatment decisions (MK Buyyounouski et al., 2017). Bhindi et al. has confirmed the ability of the 8th edition to predict oncologic outcomes (B Bhindi et al., 2017). However, with the increasing use of PSMA-ligand PET in the clinic, a logical next step is to use non-invasive imaging prior to definite treatment. Therefore, the proposed staging system acknowledging PSMA-ligand PET findings needed to be tested for potential prognostic implications.

We have shown that miT stage was an independent predictor of BCR, and we observed a widely varying prognosis in the miT2 stage patients. Similarly, a study has revealed that high intraprostatic ^{68}Ga-PSMA-11 uptake (SUV_{max} > 8) can predict a low progression-free survival rate among patients with Gleason Score 3+4 on biopsy (MJ Roberts et al., 2020). We reviewed relevant publications to reference a cutoff of SUV_{max}. Several studies have evaluated the cutoff of SUV_{max} in different PSMA-ligands, and Table 31 lists the current findings.

Table 31. Cutoffs of SUV_{max} with different PSMA-ligands.

Study	SUV_{max} cutoff	PSMA-ligand	Sample size	Differentiation parameter
Bergh et al (L Van den Bergh et al., 2012).	2.7	^{11}C-choline	1,176 octants	Malignant/benign
Demirci et al (E Demirci et al., 2019).	9.1	^{68}Ga-PSMA-11	141 patients	Gleason Score ≤7a/≥7b
Fendler et al (WP Fendler et al., 2016).	6.5	^{68}Ga-PSMA-11	100 segments	Malignant/benign
Hoffmann et al (MA Hoffmann et al., 2017).	5.4	^{68}Ga-PSMA-11	25 patients	Gleason Score ≤7a/≥7b
Hoffmann et al (MA Hoffmann et al., 2017).	6.5	^{18}FEC	40 patients	Gleason Score ≤7a/≥7b
Lavallée et al (E Lavallée et al., 2019).	4.6	^{18}F-FDG	148 patients	BCR
Perrot et al (T de Perrot et al., 2014).	3.044	^{18}F-fluorocholine	26 patients	Malignant/benign
Rahbar et al (K Rahbar et al., 2016).	4.0	^{68}Ga-PSMA-11	112 segments	Malignant/benign
Shiiba et al (M Shiiba et al., 2012).	3.15	^{11}C-MET	184 specimens	not malignant or HGPIN/Gleason Score ≤7

Shiiba et al (M Shiiba et al., 2012).	3.76	^{11}C-MET	184 specimens	Gleason Score ≤7/Gleason Score ≥8
Tabotta et al (F Tabotta et al., 2019).	19.5	^{99m}Tc-DPD	265 prostate cancer bone metastases	spinal and pelvic prostate cancer bone metastases
Woythal et al (N Woythal et al., 2018).	3.15	^{68}Ga-PSMA-11	62 tissue samples	Malignant/benign

BCR = biochemical recurrence; DPD = diphosphonate; FDG = fluorodeoxyglucose; FEC = fluoroethylcholine; HGPIN = high grade prostatic intraepithelial neoplasia; MET = Methionine; PSMA = prostate-specific membrane antigen; SUV = standardized uptake value.

The significant difference in BCR free survival rate has been confirmed in IA and IB stage groups. Our findings indicate that a cutoff of 5.4 of SUV_{max} (log-rank-test: $p < 0.001$) in miT2 primary prostate cancer patients could be a potential biobarker for worse prognosis, which is of vital importance in disease management. Further studies are necessary for prognostic validation of other stage groups, and further adjustments are required before the optimized applicability.

6.3. Limitations

The present study has several limitations. In the preclinical study, although we included over 4000 grids in the analysis, the sample size of each tissue type varies. Thus, further studies with more tumor samples especially for Gleason Pattern 3/5 and PIN are needed. We scanned the prostate specimens after the surgery, and the time between injection and surgery was over 18 hours. Because of the short half-life of ^{99m}Tc, tumors with low uptake might not be captured during the process. With the current workflow, it is impossible to detect the redistribution of the PSMA-ligand. Tissue configuration shrinkage happens during histological sample preparation, which might cause misalignment during imaging registration.

Although we performed ARG with a higher resolution than clinical PET, new approaches are still needed. The sample thickness for ARG was around 6 mm, however, the thickness of samples for histology was 5-10 µm.

The clinical study is a retrospective study and included patients that came from a single center, which can introduce potential bias. We included a large number of patients to evaluate the ability of miTNM classification as a predictor to BCR, but the number of patients in miM1 group was too low to draw a conclusion. The sample size in miN1 group was also relatively small. Once the metastasis of extra-pelvic lymph nodes and viscera appears, most patients do not undergo radical prostatectomy but either get systemic treatment or neo-adjuvant treatment prior to a definitive therapy. This explains the low number of patients in miTNM stage group III and IV. Patients in this study underwent ^{68}Ga-PSMA-11 PET. However, in clinical practice different ^{18}F-labelled PSMA-ligands are used. Thus, the comparison between studies applying different PSMA-ligands should be viewed with caution. Although the robustness of the miTNM classification was validated with our dataset, further research with larger sample size and other PSMA ligands are required. Further investigation is necessary for improving miTNM staging groups, and other clinical outcomes should be considered, such as overall survival.

7. Conclusion

We evaluated the intraprostatic PSMA-ligand distribution using the high-resolution ARG. A clear correlation between ARG images and histopathology images in morphology was observed. Besides, intraprostatic PSMA-ligand uptake was correlated with PSMA expression, Gleason Score and Gleason Pattern. Furthermore, high expression of PSMA was observed in aggressive tumor types. Heterogeneous expression of PSMA within the same patient was observed. Our study demonstrated the positive association between PSMA expression and PSMA-ligand uptake, and SUV_{ARG} can be used to detect and localize prostate cancer. PSMA-ligands PET yields the potential to predict tumor aggressiveness with a significantly strong signal in aggressive cancers.

The most important finding of our clinical study was that BCR free survival was independently associated with the miT stage. Primary prostate cancer patients who have high miTNM status should be administered more strictly to prevent or detect early BCR. In miT2 subgroup patients, a $SUV_{max} < 5.4$ was associated with longer BCR-free survival. In the miT2 patients with $SUV_{max} \geq 5.4$, more aggressive treatment options should be considered. We have observed that subgroups in the recently introduced miTNM staging system can serve as risk stratification for prognosis prediction of prostate cancer patients based on the results of preoperative PSMA-ligand PET. However, the endpoint of our study was BCR, which is not suitable for late-stage prostate cancer patients. To apply this risk stratification system into clinical practice, OS should be included as an endpoint in future studies.

References

Abuzallouf S, Dayes I, Lukka H. (2004). Baseline staging of newly diagnosed prostate cancer: a summary of the literature. *J Urol, 171*(6 Pt 1), 2122-2127.

Afshar-Oromieh A, Avtzi E, Giesel FL, Holland-Letz T, Linhart HG, Eder M, et al. (2015). The diagnostic value of PET/CT imaging with the 68Ga-labelled PSMA ligand HBED-CC in the diagnosis of recurrent prostate cancer. *Eur J Nucl Med Mol Imaging, 42*(2), 197-209.

Afshar-Oromieh A, Haberkorn U, Eder M, Eisenhut M, Zechmann CM. (2012). [68Ga]Gallium-labelled PSMA ligand as superior PET tracer for the diagnosis of prostate cancer: comparison with 18F-FECH. *Eur J Nucl Med Mol Imaging, 39*(6), 1085-1086.

Afshar-Oromieh A, Malcher A, Eder M, Eisenhut M, Linhart HG, Hadaschik BA, et al. (2013). PET imaging with a [68Ga]gallium-labelled PSMA ligand for the diagnosis of prostate cancer: biodistribution in humans and first evaluation of tumour lesions. *Eur J Nucl Med Mol Imaging, 40*(4), 486-495.

Alpajaro SIR, Harris JAK, Evans CP. (2019). Non-metastatic castration resistant prostate cancer: a review of current and emerging medical therapies. *Prostate Cancer Prostatic Dis, 22*(1), 16-23.

Andriole GL, Crawford ED, Grubb III RL, Buys SS, Chia D, Church TR, et al. (2012). Prostate cancer screening in the randomized Prostate, Lung, Colorectal, and Ovarian Cancer Screening Trial: mortality results after 13 years of follow-up. *J Natl Cancer Inst, 104*(2), 125-132.

Benz P, Oberhausen E, Berberich R. (1991). Monoclonal antibody BW431/26 labelled with technetium 99m and indium 111: an investigation of the biodistribution and the dosimetry in patients. *Eur J Nucl Med, 18*(10), 813-816.

Beresford MJ, Gillatt D, Benson RJ, Ajithkumar T. (2010). A systematic review of the role of imaging before salvage radiotherapy for post-prostatectomy biochemical recurrence. *Clin Oncol (R Coll Radiol), 22*(1), 46-55.

Bettendorf O, Oberpenning F, Köpke T, Heinecke A, Hertle L, Boecker W, et al. (2007). Implementation of a map in radical prostatectomy specimen allows visual estimation of tumor volume. *Eur J Surg Oncol, 33*(3), 352-357.

Bhindi B, Karnes RJ, Rangel LJ, Mason RJ, Gettman MT, Frank I, et al. (2017). Independent validation of the American Joint Committee on Cancer 8th edition prostate cancer staging classification. *J Urol, 198*(6), 1286-1294.

Bostwick DG, Pacelli A, Blute M, Roche P, Murphy GP. (1998). Prostate specific membrane antigen expression in prostatic intraepithelial neoplasia and adenocarcinoma: a study of 184 cases. *Cancer, 82*(11), 2256-2261.

Bratan F, Niaf E, Melodelima C, Chesnais AL, Souchon R, Mège-Lechevallier F, et al. (2013). Influence of imaging and histological factors on prostate cancer detection and localisation on multiparametric MRI: a prospective study. *Eur Radiol, 23*(7), 2019-2029.

Bravaccini S, Puccetti M, Bocchini M, Ravaioli S, Celli M, Scarpi E, et al. (2018). PSMA expression: a potential ally for the pathologist in prostate cancer diagnosis. *Sci Rep, 8*(1), 4254.

Brierley JD, Gospodarowicz MK, Wittekind C. (2017). *TNM classification of malignant tumours* (8th ed.). Oxford: Wiley-Blackwell.

Briganti A, Blute ML, Eastham JH, Graefen M, Heidenreich A, Karnes JR, et al. (2009). Pelvic Lymph Node Dissection in Prostate Cancer. *Eur Urol, 55*(6), 1251-1265.

Briganti A, Larcher A, Abdollah F, Capitanio U, Gallina A, Suardi N, et al. (2012). Updated nomogram predicting lymph node invasion in patients with prostate

cancer undergoing extended pelvic lymph node dissection: the essential importance of percentage of positive cores. *Eur Urol, 61*(3), 480-487.

Briganti A, Passoni N, Ferrari M, Capitanio U, Suardi N, Gallina A, et al. (2010). When to perform bone scan in patients with newly diagnosed prostate cancer: external validation of the currently available guidelines and proposal of a novel risk stratification tool. *Eur Urol, 57*(4), 551-558.

Brockman JA, Alanee S, Vickers AJ, Scardino PT, Wood DP, Kibel AS, et al. (2015). Nomogram Predicting Prostate Cancer-specific Mortality for Men with Biochemical Recurrence After Radical Prostatectomy. *Eur Urol, 67*(6), 1160-1167.

Brogsitter C, Zöphel K, Kotzerke J. (2013). 18F-Choline, 11C-choline and 11C-acetate PET/CT: comparative analysis for imaging prostate cancer patients. *Eur J Nucl Med Mol Imaging, 40 Suppl 1*, S18-27.

Bunschoten A, van den Berg NS, Olmos RAV, Blokland JA, van Leeuwen FW. (2016). *Tracers applied in radioguided surgery*. Cham: Springer.

Buyyounouski MK, Choyke PL, McKenney JK, Sartor O, Sandler HM, Amin MB, et al. (2017). Prostate cancer - major changes in the American Joint Committee on Cancer eighth edition cancer staging manual. *CA Cancer J Clin, 67*(3), 245-253.

Cao D, Kibel AS, Gao F, Tao Y, Humphrey PA. (2010). The Gleason Score of Tumor at the Margin in Radical Prostatectomy is Predictive of Biochemical Recurrence. *Am J Surg Pathol, 34*(7), 994-1001.

Castellucci P, Ceci F, Graziani T, Schiavina R, Brunocilla E, Mazzarotto R, et al. (2014). Early biochemical relapse after radical prostatectomy: which prostate cancer patients may benefit from a restaging 11C-Choline PET/CT scan before salvage radiation therapy? *J Nucl Med, 55*(9), 1424-1429.

Ceci F, Castellucci P, Nanni C, Fanti S. (2016). PET/CT imaging for evaluating response to therapy in castration-resistant prostate cancer. *Eur J Nucl Med Mol Imaging, 43*(12), 2103-2104.

Ceci F, Herrmann K, Castellucci P, Graziani T, Bluemel C, Schiavina R, et al. (2014). Impact of 11C-choline PET/CT on clinical decision making in recurrent prostate cancer: results from a retrospective two-centre trial. *Eur J Nucl Med Mol Imaging, 41*(12), 2222-2231.

Chatalic KL, Heskamp S, Konijnenberg M, Molkenboer-Kuenen JD, Franssen GM, Clahsen-van Groningen MC, et al. (2016). Towards Personalized Treatment of Prostate Cancer: PSMA I&T, a Promising Prostate-Specific Membrane Antigen-Targeted Theranostic Agent. *Theranostics, 6*(6), 849-861.

Cheung DC, Fleshner N, Sengupta S, Woon D. (2020). A narrative review of pelvic lymph node dissection in prostate cancer. *Transl Androl Urol, 9*(6), 3049-3055.

Chistiakov DA, Myasoedova VA, Grechko AV, Melnichenko AA, Orekhov AN. (2018). New biomarkers for diagnosis and prognosis of localized prostate cancer. *Semin Cancer Biol, 52*(Pt 1), 9-16.

Choi SY, Chi BH, Lim B, Kyung YS, You D, Jeong IG, et al. (2020). Percent tumor volume vs American Joint Committee on Cancer staging system subclassification for predicting biochemical recurrence in patients with pathologic T2 prostate cancer. *J Cancer Res Clin Oncol, 146*(2), 537-543.

Choi YJ, Kim JK, Kim N, Kim KW, Choi EK, Cho KS. (2007). Functional MR imaging of prostate cancer. *Radiographics, 27*(1), 63-75; discussion 75-67.

Cimadamore A, Cheng M, Santoni M, Lopez-Beltran A, Battelli N, Massari F, et al. (2018). New Prostate Cancer Targets for Diagnosis, Imaging, and Therapy: Focus on Prostate-Specific Membrane Antigen. *Front Oncol, 8*, 653.

Conti M. (2014). New prospects for PET in prostate cancer imaging: a physicist's viewpoint. *EJNMMI Phys, 1*(1), 11.

Corfield J, Perera M, Bolton D, Lawrentschuk N. (2018). 68 Ga-prostate specific membrane antigen (PSMA) positron emission tomography (PET) for primary staging of high-risk prostate cancer: a systematic review. *World J Urol, 36*(4), 519-527.

Culp MB, Soerjomataram I, Efstathiou JA, Bray F, Jemal A. (2020). Recent Global Patterns in Prostate Cancer Incidence and Mortality Rates. *Eur Urol, 77*(1), 38-52.

Cytawa W, Seitz AK, Kircher S, Fukushima K, Tran-Gia J, Schirbel A, et al. (2020). (68)Ga-PSMA I&T PET/CT for primary staging of prostate cancer. *Eur J Nucl Med Mol Imaging, 47*(1), 168-177.

D'Amico AV, Whittington R, Malkowicz SB, Schultz D, Blank K, Broderick GA, et al. (1998). Biochemical outcome after radical prostatectomy, external beam radiation therapy, or interstitial radiation therapy for clinically localized prostate cancer. *Jama, 280*(11), 969-974.

D'Amico AV, Chen MH, Renshaw AA, Loffredo M, Kantoff PW. (2008). Androgen suppression and radiation vs radiation alone for prostate cancer: a randomized trial. *Jama, 299*(3), 289-295.

Davies A, Conteduca V, Zoubeidi A, Beltran H. (2019). Biological Evolution of Castration-resistant Prostate Cancer. *Eur Urol Focus, 5*(2), 147-154.

Davis MI, Bennett MJ, Thomas LM, Bjorkman PJ. (2005). Crystal structure of prostate-specific membrane antigen, a tumor marker and peptidase. *Proc Natl Acad Sci U S A, 102*(17), 5981-5986.

De Giorgi U, Caroli P, Burgio SL, Menna C, Conteduca V, Bianchi E, et al. (2014). Early outcome prediction on 18F-fluorocholine PET/CT in metastatic castration-resistant prostate cancer patients treated with abiraterone. *Oncotarget, 5*(23), 12448-12458.

De Giorgi U, Caroli P, Scarpi E, Conteduca V, Burgio SL, Menna C, et al. (2015). (18)F-Fluorocholine PET/CT for early response assessment in patients with metastatic castration-resistant prostate cancer treated with enzalutamide. *Eur J Nucl Med Mol Imaging, 42*(8), 1276-1283.

de Jong IJ, Pruim J, Elsinga PH, Vaalburg W, Mensink HJ. (2002). Visualization of prostate cancer with 11C-choline positron emission tomography. *Eur Urol, 42*(1), 18-23.

de Jong IJ, Pruim J, Elsinga PH, Vaalburg W, Mensink HJ. (2003). Preoperative staging of pelvic lymph nodes in prostate cancer by 11C-choline PET. *J Nucl Med, 44*(3), 331-335.

de Perrot T, Rager O, Scheffler M, Lord M, Pusztaszeri M, Iselin C, et al. (2014). Potential of hybrid 18 F-fluorocholine PET/MRI for prostate cancer imaging. *Eur J Nucl Med Mol Imaging, 41*(9), 1744-1755.

Demirci E, Kabasakal L, Şahin OE, Akgün E, Gültekin MH, Doğanca T, et al. (2019). Can SUVmax values of Ga-68-PSMA PET/CT scan predict the clinically significant prostate cancer? *Nucl Med Commun, 40*(1), 86-91.

Desmond AD, Arnold AJ, Hastie KJ. (1988). Subcapsular orchiectomy under local anaesthesia. Technique, results and implications. *Br J Urol, 61*(2), 143-145.

DiFilippo FP. (2015). Enhanced PET resolution by combining pinhole collimation and coincidence detection. *Phys Med Biol, 60*(20), 7969-7984.

Eiber M, Herrmann K, Calais J, Hadaschik B, Giesel FL, Hartenbach M, et al. (2018). Prostate Cancer Molecular Imaging Standardized Evaluation (PROMISE): Proposed miTNM Classification for the Interpretation of PSMA-Ligand PET/CT. *J Nucl Med, 59*(3), 469-478.

Eiber M, Kroenke M, Wurzer A, Ulbrich L, Jooß L, Maurer T, et al. (2020). (18)F-rhPSMA-7 PET for the Detection of Biochemical Recurrence of Prostate Cancer After Radical Prostatectomy. *J Nucl Med, 61*(5), 696-701.

Eiber M, Maurer T, Souvatzoglou M, Beer AJ, Ruffani A, Haller B, et al. (2015). Evaluation of Hybrid ^{68}Ga-PSMA Ligand PET/CT in 248 Patients with Biochemical Recurrence After Radical Prostatectomy. *J Nucl Med, 56*(5), 668-674.

Eminaga O, Hinkelammert R, Semjonow A, Neumann J, Abbas M, Koepke T, et al. (2010). Clinical map document based on XML (cMDX): document architecture with mapping feature for reporting and analysing prostate cancer in radical prostatectomy specimens. *BMC Med Inform Decis Mak, 10*, 71.

Epstein JI, Allsbrook WC, Jr., Amin MB, Egevad LL. (2005). The 2005 International Society of Urological Pathology (ISUP) Consensus Conference on Gleason Grading of Prostatic Carcinoma. *Am J Surg Pathol, 29*(9), 1228-1242.

Epstein JI, Egevad L, Amin MB, Delahunt B, Srigley JR, Humphrey PA. (2016). The 2014 International Society of Urological Pathology (ISUP) Consensus Conference on Gleason Grading of Prostatic Carcinoma: Definition of Grading Patterns and Proposal for a New Grading System. *Am J Surg Pathol, 40*(2), 244-252.

Epstein JI, Zelefsky MJ, Sjoberg DD, Nelson JB, Egevad L, Magi-Galluzzi C, et al. (2016). A Contemporary Prostate Cancer Grading System: A Validated Alternative to the Gleason Score. *Eur Urol, 69*(3), 428–435.

Evans JC, Malhotra M, Cryan JF, O'Driscoll CM. (2016). The therapeutic and diagnostic potential of the prostate specific membrane antigen/glutamate carboxypeptidase II (PSMA/GCPII) in cancer and neurological disease. *Br J Pharmacol, 173*(21), 3041-3079.

Fendler WP, Schmidt DF, Wenter V, Thierfelder KM, Zach C, Stief C, et al. (2016). 68Ga-PSMA PET/CT Detects the Location and Extent of Primary Prostate Cancer. *J Nucl Med, 57*(11), 1720-1725.

Ferlay J, Laversanne M, Ervik M, Lam F, Colombet M, Mery L, et al. (2020). Global Cancer Observatory: Cancer Tomorrow. Retrieved from https://gco.iarc.fr/tomorrow.

Ferlay J, Soerjomataram I, Dikshit R, Eser S, Mathers C, Rebelo M, et al. (2015). Cancer incidence and mortality worldwide: sources, methods and major patterns in GLOBOCAN 2012. *Int J Cancer, 136*(5), E359-386.

Ferlay J, Steliarova-Foucher E, Lortet-Tieulent J, Rosso S, Coebergh JW, Comber H, et al. (2013). Cancer incidence and mortality patterns in Europe: estimates for 40 countries in 2012. *Eur J Cancer, 49*(6), 1374-1403.

Ferraro DA, Rüschoff JH, Muehlematter UJ, Kranzbühler B, Müller J, Messerli M, et al. (2020). Immunohistochemical PSMA expression patterns of primary prostate cancer tissue are associated with the detection rate of biochemical recurrence with (68)Ga-PSMA-11-PET. *Theranostics, 10*(14), 6082-6094.

Fossati N, Suardi N, Gandaglia G, Bravi CA, Soligo M, Karnes RJ, et al. (2019). Identifying the Optimal Candidate for Salvage Lymph Node Dissection for Nodal Recurrence of Prostate Cancer: Results from a Large, Multi-institutional Analysis. *Eur Urol, 75*(1), 176-183.

Fossati N, Willemse PM, Van den Broeck T, van den Bergh RCN, Yuan CY, Briers E, et al. (2017). The Benefits and Harms of Different Extents of Lymph Node Dissection During Radical Prostatectomy for Prostate Cancer: A Systematic Review. *Eur Urol, 72*(1), 84-109.

Fox JJ, Schöder H, Larson SM. (2012). Molecular imaging of prostate cancer. *Curr Opin Urol, 22*(4), 320-327.

Freedland SJ, Presti JC, Amling CL, Kane CJ, Aronson WJ, Dorey F, et al. (2003). Time trends in biochemical recurrence after radical prostatectomy: results of the SEARCH database. *Urology, 61*(4), 736-741.

Ghosh A, Heston WD. (2004). Tumor target prostate specific membrane antigen (PSMA) and its regulation in prostate cancer. *J Cell Biochem, 91*(3), 528-539.

Gleason DF. (1966). Classification of prostatic carcinomas. *Cancer Chemother Rep, 50*(3), 125-128.

Gleason DF, Mellinger GT. (1974). Prediction of prognosis for prostatic adenocarcinoma by combined histological grading and clinical staging. *J Urol, 111*(1), 58-64.

Hamdy FC, Donovan JL, Lane JA, Mason M, Metcalfe C, Holding P, et al. (2016). 10-Year Outcomes after Monitoring, Surgery, or Radiotherapy for Localized Prostate Cancer. *N Engl J Med, 375*(15), 1415-1424.

Han M, Partin AW, Zahurak M, Piantadosi S, Epstein J, Walsh P. (2003). Biochemical (Prostate Specific Antigen) Recurrence Probability Following Radical Prostatectomy for Clinically Localized Prostate Cancer. *J Urol, 169*(2), 517-523.

Heidegger I. (2019). PSA screening-a matter of debate? *Memo 12*, 244-248.

Hemminki K. (2012). Familial risk and familial survival in prostate cancer. *World J Urol, 30*(2), 143-148.

Hijazi S, Meller B, Leitsmann C, Strauss A, Meller J, Ritter CO, et al. (2015). Pelvic lymph node dissection for nodal oligometastatic prostate cancer detected by 68Ga-PSMA-positron emission tomography/computerized tomography. *Prostate, 75*(16), 1934-1940.

Hoffmann MA, Miederer M, Wieler HJ, Ruf C, Jakobs FM, Schreckenberger M. (2017). Diagnostic performance of 68Gallium-PSMA-11 PET/CT to detect significant prostate cancer and comparison with 18FEC PET/CT. *Oncotarget, 8*(67), 111073-111083. doi:10.18632/oncotarget.22441.

Hofman MS, Hicks RJ, Maurer T, Eiber M. (2018). Prostate-specific Membrane Antigen PET: Clinical Utility in Prostate Cancer, Normal Patterns, Pearls, and Pitfalls. *Radiographics, 38*(1), 200-217.

Hofman MS, Lawrentschuk N, Francis RJ, Tang C, Vela I, Thomas P, et al. (2020). Prostate-specific membrane antigen PET-CT in patients with high-risk prostate cancer before curative-intent surgery or radiotherapy (proPSMA): a prospective, randomised, multicentre study. *Lancet, 395*(10231), 1208-1216.

Hofman MS, Violet J, Hicks RJ, Ferdinandus J, Thang SP, Akhurst T, et al. (2018). [177Lu]-PSMA-617 radionuclide treatment in patients with metastatic castration-resistant prostate cancer (LuPSMA trial): a single-centre, single-arm, phase 2 study. *Lancet Oncol, 19*(6), 825-833.

Hope TA, Goodman JZ, Allen IE, Calais J, Fendler WP, Carroll PR. (2019). Metaanalysis of (68)Ga-PSMA-11 PET Accuracy for the Detection of Prostate Cancer Validated by Histopathology. *J Nucl Med, 60*(6), 786-793.

Horn T, Krönke M, Rauscher I, Haller B, Robu S, Wester HJ, et al. (2019). Single Lesion on Prostate-specific Membrane Antigen-ligand Positron Emission Tomography and Low Prostate-specific Antigen Are Prognostic Factors for a Favorable Biochemical Response to Prostate-specific Membrane Antigen-targeted Radioguided Surgery in Recurrent Prostate Cancer. *Eur Urol, 76*(4), 517-523.

Hövels AM, Heesakkers RA, Adang EM, Jager GJ, Strum S, Hoogeveen YL, et al. (2008). The diagnostic accuracy of CT and MRI in the staging of pelvic lymph nodes in patients with prostate cancer: a meta-analysis. *Clin Radiol, 63*(4), 387-395.

Hricak H, Choyke PL, Eberhardt SC, Leibel SA, Scardino PT. (2007). Imaging prostate cancer: a multidisciplinary perspective. *Radiology, 243*(1), 28-53.

Hruby G, Eade T, Emmett L, Ho B, Hsiao E, Schembri G, et al. (2018). (68) Ga-PSMA-PET/CT staging prior to definitive radiation treatment for prostate cancer. *Asia Pac J Clin Oncol, 14*(4), 343-346.

Hupe MC, Philippi C, Roth D, Kümpers C, Ribbat-Idel J, Becker F, et al. (2018). Expression of Prostate-Specific Membrane Antigen (PSMA) on Biopsies Is an

Independent Risk Stratifier of Prostate Cancer Patients at Time of Initial Diagnosis. *Front Oncol, 8*, 623.
Inagaki T, Kohjimoto Y, Nishizawa S, Kuramoto T, Nanpo Y, Fujii R, et al. (2009). PSA at postoperative three months can predict biochemical recurrence in patients with pathological T3 prostate cancer following radical prostatectomy. *Int J Urol, 16*(12), 941-946.
Israeli RS, Powell CT, Corr JG, Fair WR, Heston WD. (1994). Expression of the prostate-specific membrane antigen. *Cancer Res, 54*(7), 1807-1811.
Jadvar H. (2011). Prostate cancer: PET with 18F-FDG, 18F- or 11C-acetate, and 18F- or 11C-choline. *J Nucl Med, 52*(1), 81-89.
Jain RK. (2001). Delivery of molecular medicine to solid tumors: lessons from in vivo imaging of gene expression and function. *J Control Release, 74*(1-3), 7-25.
Janmahasatian S, Duffull SB, Ash S, Ward LC, Byrne NM, Green B. (2005). Quantification of lean bodyweight. *Clin Pharmacokinet, 44*(10), 1051-1065.
Janssen JC, Meißner S, Woythal N, Prasad V, Brenner W, Diederichs G, et al. (2018). Comparison of hybrid (68)Ga-PSMA-PET/CT and (99m)Tc-DPD-SPECT/CT for the detection of bone metastases in prostate cancer patients: Additional value of morphologic information from low dose CT. *Eur Radiol, 28*(2), 610-619.
Kawakami M, Nakayama J. (1997). Enhanced expression of prostate-specific membrane antigen gene in prostate cancer as revealed by in situ hybridization. *Cancer Res, 57*(12), 2321-2324.
Key TJ. (2014). Nutrition, hormones and prostate cancer risk: results from the European prospective investigation into cancer and nutrition. *Recent Results Cancer Res, 202*, 39-46.
Kimura S, Abufaraj M, Janisch F, Iwata T, Parizi MK, Foerster B, et al. (2020). Performance of [(68)Ga] Ga-PSMA 11 PET for detecting prostate cancer in the lymph nodes before salvage lymph node dissection: a systematic review and meta-analysis. *Prostate Cancer Prostatic Dis, 23*(1), 1-10.
King CR. (2012). The timing of salvage radiotherapy after radical prostatectomy: a systematic review. *Int J Radiat Oncol Biol Phys, 84*(1), 104-111.
Klotz L, Boccon-Gibod L, Shore ND, Andreou C, Persson BE, Cantor P, et al. (2008). The efficacy and safety of degarelix: a 12-month, comparative, randomized, open-label, parallel-group phase III study in patients with prostate cancer. *BJU Int, 102*(11), 1531-1538.
Kolthammer JA, Su KH, Grover A, Narayanan M, Jordan DW, Muzic RF. (2014). Performance evaluation of the Ingenuity TF PET/CT scanner with a focus on high count-rate conditions. *Phys Med Biol, 59*(14), 3843-3859.
Kyriakopoulos CE, Chen YH, Carducci MA, Liu G, Jarrard DF, Hahn NM, et al. (2018). Chemohormonal Therapy in Metastatic Hormone-Sensitive Prostate Cancer: Long-Term Survival Analysis of the Randomized Phase III E3805 CHAARTED Trial. *J Clin Oncol, 36*(11), 1080-1087.
Lam TBL, MacLennan S, Willemse PM, Mason MD, Plass K, Shepherd R, et al. (2019). EAU-EANM-ESTRO-ESUR-SIOG Prostate Cancer Guideline Panel Consensus Statements for Deferred Treatment with Curative Intent for Localised Prostate Cancer from an International Collaborative Study (DETECTIVE Study). *Eur Urol, 76*(6), 790-813.
Lavallée E, Bergeron M, Buteau F-A, Blouin A-C, Duchesnay N, Dujardin T, et al. (2019). Increased Prostate Cancer Glucose Metabolism Detected by 18F-fluorodeoxyglucose Positron Emission Tomography/Computed Tomography in Localised Gleason 8–10 Prostate Cancers Identifies Very High–risk Patients for Early Recurrence and Resistance to Castration. *Eur Urol Focus, 5*(6), 998-1006.

Le JD, Tan N, Shkolyar E, Lu DY, Kwan L, Marks LS, et al. (2015). Multifocality and prostate cancer detection by multiparametric magnetic resonance imaging: correlation with whole-mount histopathology. *Eur Urol, 67*(3), 569-576.

Leitzmann MF, Rohrmann S. (2012). Risk factors for the onset of prostatic cancer: age, location, and behavioral correlates. *Clin Epidemiol, 4*, 1-11.

Li Y, Cozzi PJ. (2010). Angiogenesis as a strategic target for prostate cancer therapy. *Med Res Rev, 30*(1), 23-66.

Lippi G, Mattiuzzi C. (2015). Fried food and prostate cancer risk: systematic review and meta-analysis. *Int J Food Sci Nutr, 66*(5), 587-589.

Litwin MS, Tan HJ. (2017). The Diagnosis and Treatment of Prostate Cancer: A Review. *Jama, 317*(24), 2532-2542.

Loeb S, Bruinsma SM, Nicholson J, Briganti A, Pickles T, Kakehi Y, et al. (2015). Active surveillance for prostate cancer: a systematic review of clinicopathologic variables and biomarkers for risk stratification. *Eur Urol, 67*(4), 619-626.

Mannweiler S, Amersdorfer P, Trajanoski S, Terrett JA, King D, Mehes G. (2009). Heterogeneity of prostate-specific membrane antigen (PSMA) expression in prostate carcinoma with distant metastasis. *Pathol Oncol Res, 15*(2), 167-172.

Marchal C, Redondo M, Padilla M, Caballero J, Rodrigo I, García J, et al. (2004). Expression of prostate specific membrane antigen (PSMA) in prostatic adenocarcinoma and prostatic intraepithelial neoplasia. *Histol Histopathol, 19*(3), 715-718.

Martin R, Jüttler S, Müller M, Wester H-J. (2014). Cationic eluate pretreatment for automated synthesis of [68Ga]CPCR4.2. *Nuclear Medicine and Biology, 41*(1), 84-89.

Maurer T, Eiber M, Schwaiger M, Gschwend JE. (2016). Current use of PSMA-PET in prostate cancer management. *Nat Rev Urol, 13*(4), 226-235.

Maurer T, Gschwend JE, Rauscher I, Souvatzoglou M, Haller B, Weirich G, et al. (2016). Diagnostic Efficacy of (68)Gallium-PSMA Positron Emission Tomography Compared to Conventional Imaging for Lymph Node Staging of 130 Consecutive Patients with Intermediate to High Risk Prostate Cancer. *J Urol, 195*(5), 1436-1443.

Maurer T, Robu S, Schottelius M, Schwamborn K, Rauscher I, Van Den Berg N, et al. (2018). 99mTechnetium-based Prostate-specific Membrane Antigen-radioguided Surgery in Recurrent Prostate Cancer. *Eur Urol, 75*(4), 659-666.

Maurer T, Weirich G, Schottelius M, Weineisen M, Frisch B, Okur A, et al. (2015). Prostate-specific membrane antigen-radioguided surgery for metastatic lymph nodes in prostate cancer. *Eur Urol, 68*(3), 530-534.

McCarty KS, Jr., Miller LS, Cox EB, Konrath J, McCarty KS, Sr. (1985). Estrogen receptor analyses. Correlation of biochemical and immunohistochemical methods using monoclonal antireceptor antibodies. *Arch Pathol Lab Med, 109*(8), 716-721.

Mena E, Lindenberg ML, Shih JH, Adler S, Harmon S, Bergvall E, et al. (2018). Clinical impact of PSMA-based (18)F-DCFBC PET/CT imaging in patients with biochemically recurrent prostate cancer after primary local therapy. *Eur J Nucl Med Mol Imaging, 45*(1), 4-11.

Mena E, Turkbey B, Mani H, Adler S, Valera VA, Bernardo M, et al. (2012). 11C-Acetate PET/CT in localized prostate cancer: a study with MRI and histopathologic correlation. *J Nucl Med, 53*(4), 538-545.

Mesters JR, Barinka C, Li W, Tsukamoto T, Majer P, Slusher BS, et al. (2006). Structure of glutamate carboxypeptidase II, a drug target in neuronal damage and prostate cancer. *EMBO J, 25*(6), 1375-1384.

Mhawech-Fauceglia P, Zhang S, Terracciano L, Sauter G, Chadhuri A, Herrmann FR, et al. (2007). Prostate-specific membrane antigen (PSMA) protein expression in normal and neoplastic tissues and its sensitivity and specificity in prostate

adenocarcinoma: an immunohistochemical study using mutiple tumour tissue microarray technique. *Histopathology, 50*(4), 472-483.
Minner S, Wittmer C, Graefen M, Salomon G, Steuber T, Haese A, et al. (2011). High level PSMA expression is associated with early PSA recurrence in surgically treated prostate cancer. *Prostate, 71*(3), 281-288.
Mitchell CR, Lowe VJ, Rangel LJ, Hung JC, Kwon ED, Karnes RJ. (2013). Operational characteristics of (11)c-choline positron emission tomography/computerized tomography for prostate cancer with biochemical recurrence after initial treatment. *J Urol, 189*(4), 1308-1313.
Mix M, Reichel K, Stoykow C, Bartholomä M, Drendel V, Gourni E, et al. (2018). Performance of (111)In-labelled PSMA ligand in patients with nodal metastatic prostate cancer: correlation between tracer uptake and histopathology from lymphadenectomy. *Eur J Nucl Med Mol Imaging, 45*(12), 2062-2070.
Mottet N, van den Bergh RCN, Briers E, Cornford P, De Santis M, Fanti S, et al. (2020). *EAU - ESTRO - ESUR - SIOG Guidelines on Prostate Cancer 2020. In European Association of Urology Guidelines. 2020 Edition.* (Vol. presented at the EAU Annual Congress Amsterdam 2020). Arnhem, The Netherlands: European Association of Urology Guidelines Office.
Oefelein MG, Feng A, Scolieri MJ, Ricchiutti D, Resnick MI. (2000). Reassessment of the definition of castrate levels of testosterone: implications for clinical decision making. *Urology, 56*(6), 1021-1024.
Østergren PB, Kistorp C, Fode M, Henderson J, Bennedbæk FN, Faber J, et al. (2017). Luteinizing Hormone-Releasing Hormone Agonists are Superior to Subcapsular Orchiectomy in Lowering Testosterone Levels of Men with Prostate Cancer: Results from a Randomized Clinical Trial. *J Urol, 197*(6), 1441-1447.
Parker C, Nilsson S, Heinrich D, Helle SI, O'sullivan J, Fosså SD, et al. (2013). Alpha emitter radium-223 and survival in metastatic prostate cancer. *N Engl J Med, 369*(3), 213-223.
Paschalis A, Sheehan B, Riisnaes R, Rodrigues DN, Gurel B, Bertan C, et al. (2019). Prostate-specific Membrane Antigen Heterogeneity and DNA Repair Defects in Prostate Cancer. *Eur Urol, 76*(4), 469-478.
Payne H, Cornford P. (2011). Prostate-specific antigen: an evolving role in diagnosis, monitoring, and treatment evaluation in prostate cancer. *Urol Oncol, 29*(6), 593-601.
Perera M, Papa N, Christidis D, Wetherell D, Hofman MS, Murphy DG, et al. (2016). Sensitivity, Specificity, and Predictors of Positive (68)Ga-Prostate-specific Membrane Antigen Positron Emission Tomography in Advanced Prostate Cancer: A Systematic Review and Meta-analysis. *Eur Urol, 70*(6), 926-937.
Perner S, Hofer MD, Kim R, Shah RB, Li H, Möller P, et al. (2007). Prostate-specific membrane antigen expression as a predictor of prostate cancer progression *Hum Pathol, 38*(5), 696-701.
Petrylak DP, Tangen CM, Hussain MH, Lara PN, Jr., Jones JA, Taplin ME, et al. (2004). Docetaxel and estramustine compared with mitoxantrone and prednisone for advanced refractory prostate cancer. *N Engl J Med, 351*(15), 1513-1520.
Pezaro C, Omlin A, Lorente D, Rodrigues DN, Ferraldeschi R, Bianchini D, et al. (2014). Visceral disease in castration-resistant prostate cancer. *Eur Urol, 65*(2), 270-273.
Pfister D, Bolla M, Briganti A, Carroll P, Cozzarini C, Joniau S, et al. (2014). Early salvage radiotherapy following radical prostatectomy. *Eur Urol, 65*(6), 1034-1043.
Plouznikoff N, Artigas C, Sideris S, Martinez Chanza N, Gil T, Peltier A, et al. (2019). Evaluation of PSMA expression changes on PET/CT before and after initiation

of novel antiandrogen drugs (enzalutamide or abiraterone) in metastatic castration-resistant prostate cancer patients. *Ann Nucl Med, 33*(12), 945-954.

Prasad V, Steffen IG, Diederichs G, Makowski MR, Wust P, Brenner W. (2016). Biodistribution of [(68)Ga]PSMA-HBED-CC in Patients with Prostate Cancer: Characterization of Uptake in Normal Organs and Tumour Lesions. *Mol Imaging Biol, 18*(3), 428-436.

Pyka T, Okamoto S, Dahlbender M, Tauber R, Retz M, Heck M, et al. (2016). Comparison of bone scintigraphy and (68)Ga-PSMA PET for skeletal staging in prostate cancer. *Eur J Nucl Med Mol Imaging, 43*(12), 2114-2121.

Rahbar K, Weckesser M, Huss S, Semjonow A, Breyholz HJ, Schrader AJ, et al. (2016). Correlation of Intraprostatic Tumor Extent with ^{68}Ga-PSMA Distribution in Patients with Prostate Cancer. *J Nucl Med, 57*(4), 563-567.

Rajasekaran SA, Anilkumar G, Oshima E, Bowie JU, Liu H, Heston W, et al. (2003). A novel cytoplasmic tail MXXXL motif mediates the internalization of prostate-specific membrane antigen. *Mol Biol Cell, 14*(12), 4835-4845.

Rauscher I, Düwel C, Haller B, Rischpler C, Heck MM, Gschwend JE, et al. (2018). Efficacy, Predictive Factors, and Prediction Nomograms for (68)Ga-labeled Prostate-specific Membrane Antigen-ligand Positron-emission Tomography/Computed Tomography in Early Biochemical Recurrent Prostate Cancer After Radical Prostatectomy. *Eur Urol, 73*(5), 656-661.

Roberts MJ, Morton A, Donato P, Kyle S, Pattison DA, Thomas P, et al. (2020). (68)Ga-PSMA PET/CT tumour intensity pre-operatively predicts adverse pathological outcomes and progression-free survival in localised prostate cancer. *Eur J Nucl Med Mol Imaging*.

Robu S, Schottelius M, Eiber M, Maurer T, Gschwend J, Schwaiger M, et al. (2017). Preclinical evaluation and first patient application of 99mTc-PSMA-I&S for SPECT imaging and radioguided surgery in prostate cancer. *J Nucl Med, 58*(2), 235-242.

Ross JS, Sheehan CE, Fisher HA, Kaufman RP, Jr., Kaur P, Gray K, et al. (2003). Correlation of primary tumor prostate-specific membrane antigen expression with disease recurrence in prostate cancer. *Clin Cancer Res, 9*(17), 6357-6362.

Rowe SP, Gage KL, Faraj SF, Macura KJ, Cornish TC, Gonzalez-Roibon N, et al. (2015). ^{18}F-DCFBC PET/CT for PSMA-Based Detection and Characterization of Primary Prostate Cancer. *J Nucl Med, 56*(7), 1003-1010.

Russo G, Mischi M, Scheepens W, De la Rosette JJ, Wijkstra H. (2012). Angiogenesis in prostate cancer: onset, progression and imaging. *BJU int, 110*(11c), E794-E808.

Schoots IG, Petrides N, Giganti F, Bokhorst LP, Rannikko A, Klotz L, et al. (2015). Magnetic resonance imaging in active surveillance of prostate cancer: a systematic review. *Eur Urol, 67*(4), 627-636.

Schröder FH, Hugosson J, Roobol MJ, Tammela TL, Ciatto S, Nelen V, et al. (2012). Prostate-cancer mortality at 11 years of follow-up. *N Engl J Med, 366*(11), 981-990.

Schwarzenböck SM, Eiber M, Kundt G, Retz M, Sakretz M, Kurth J, et al. (2016). Prospective evaluation of [11C]Choline PET/CT in therapy response assessment of standardized docetaxel first-line chemotherapy in patients with advanced castration refractory prostate cancer. *Eur J Nucl Med Mol Imaging, 43*(12), 2105-2113.

Schwarzenboeck SM, Rauscher I, Bluemel C, Fendler WP, Rowe SP, Pomper MG, et al. (2017). PSMA Ligands for PET Imaging of Prostate Cancer. *J Nucl Med, 58*(10), 1545-1552.

Sciarra A, Fasulo A, Ciardi A, Petrangeli E, Gentilucci A, Maggi M, et al. (2016). A meta-analysis and systematic review of randomized controlled trials with

degarelix versus gonadotropin-releasing hormone agonists for advanced prostate cancer. *Medicine (Baltimore), 95*(27), e3845.
Shariat SF, Roehrborn CG. (2008). Using biopsy to detect prostate cancer. *Rev Urol, 10*(4), 262-280.
Shen G, Deng H, Hu S, Jia Z. (2014). Comparison of choline-PET/CT, MRI, SPECT, and bone scintigraphy in the diagnosis of bone metastases in patients with prostate cancer: a meta-analysis. *Skeletal Radiol, 43*(11), 1503-1513.
Shiiba M, Ishihara K, Kimura G, Kuwako T, Yoshihara N, Sato H, et al. (2012). Evaluation of primary prostate cancer using 11 C-methionine-PET/CT and 18 F-FDG-PET/CT. *Ann Nucl Med, 26*(2), 138-145.
Silver DA, Pellicer I, Fair WR, Heston WD, Cordon-Cardo C. (1997). Prostate-specific membrane antigen expression in normal and malignant human tissues. *Clin Cancer Res, 3*(1), 81-85.
Smith-Jones PM, Vallabahajosula S, Goldsmith SJ, Navarro V, Hunter CJ, Bastidas D, et al. (2000). In vitro characterization of radiolabeled monoclonal antibodies specific for the extracellular domain of prostate-specific membrane antigen. *Cancer Res, 60*(18), 5237-5243.
Souvatzoglou M, Eiber M, Martinez-Moeller A, Fürst S, Holzapfel K, Maurer T, et al. (2013). PET/MR in prostate cancer: technical aspects and potential diagnostic value. *Eur J Nucl Med Mol Imaging, 40 Suppl 1*, S79-88.
Soyka JD, Muster MA, Schmid DT, Seifert B, Schick U, Miralbell R, et al. (2012). Clinical impact of 18F-choline PET/CT in patients with recurrent prostate cancer. *Eur J Nucl Med Mol Imaging, 39*(6), 936-943.
Sprute K, Kramer V, Koerber S, Meneses M, Fernandez R, Soza-Ried C, et al. (2020). Diagnostic accuracy of (18)F-PSMA-1007-PET/CT imaging for lymph node staging of prostate carcinoma in primary and biochemical recurrence. *J Nucl Med*.
Suardi N, Gandaglia G, Gallina A, Di Trapani E, Scattoni V, Vizziello D, et al. (2015). Long-term Outcomes of Salvage Lymph Node Dissection for Clinically Recurrent Prostate Cancer: Results of a Single-institution Series with a Minimum Follow-up of 5 Years. *Eur Urol, 67*(2), 299-309.
Sweat SD, Pacelli A, Murphy GP, Bostwick DG. (1998). Prostate-specific membrane antigen expression is greatest in prostate adenocarcinoma and lymph node metastases. *Urology, 52*(4), 637-640.
Tabotta F, Jreige M, Schaefer N, Becce F, Prior JO, Lalonde MN. (2019). Quantitative bone SPECT/CT: high specificity for identification of prostate cancer bone metastases. *BMC musculoskeletal disorders, 20*(1), 619.
Tannock IF, de Wit R, Berry WR, Horti J, Pluzanska A, Chi KN, et al. (2004). Docetaxel plus prednisone or mitoxantrone plus prednisone for advanced prostate cancer. *N Engl J Med, 351*(15), 1502-1512.
Thomsen FB, Brasso K, Klotz LH, Røder MA, Berg KD, Iversen P. (2014). Active surveillance for clinically localized prostate cancer--a systematic review. *J Surg Oncol, 109*(8), 830-835.
Torlakovic G, Grover VK, Torlakovic E. (2005). Easy method of assessing volume of prostate adenocarcinoma from estimated tumor area: using prostate tissue density to bridge gap between percentage involvement and tumor volume. *Croat Med J, 46*(3), 423-428.
Treglia G, Ceriani L, Sadeghi R, Giovacchini G, Giovanella L. (2014). Relationship between prostate-specific antigen kinetics and detection rate of radiolabelled choline PET/CT in restaging prostate cancer patients: a meta-analysis. *Clin Chem Lab Med, 52*(5), 725-733.
Uprimny C, Kroiss AS, Decristoforo C, Fritz J, von Guggenberg E, Kendler D, et al. (2017). 68Ga-PSMA-11 PET/CT in primary staging of prostate cancer: PSA and

Gleason score predict the intensity of tracer accumulation in the primary tumour. *Eur J Nucl Med Mol Imaging, 44*(6), 941-949.

Van den Bergh L, Koole M, Isebaert S, Joniau S, Deroose CM, Oyen R, et al. (2012). Is there an additional value of 11C-choline PET-CT to T2-weighted MRI images in the localization of intraprostatic tumor nodules? *Int J Radiat Oncol Biol Phys, 83*(5), 1486-1492.

Van den Bergh L, Lerut E, Haustermans K, Deroose CM, Oyen R, Isebaert S, et al. (2015). Final analysis of a prospective trial on functional imaging for nodal staging in patients with prostate cancer at high risk for lymph node involvement. *Urol Oncol, 33*(3), 109 e23-109 e31.

van der Poel HG, van den Bergh RCN, Briers E, Cornford P, Govorov A, Henry AM, et al. (2018). Focal Therapy in Primary Localised Prostate Cancer: The European Association of Urology Position in 2018. *Eur Urol, 74*(1), 84-91.

van Leeuwen PJ, Emmett L, Ho B, Delprado W, Ting F, Nguyen Q, et al. (2017). Prospective evaluation of 68Gallium-prostate-specific membrane antigen positron emission tomography/computed tomography for preoperative lymph node staging in prostate cancer. *BJU Int, 119*(2), 209-215.

Violet J, Sandhu S, Iravani A, Ferdinandus J, Thang SP, Kong G, et al. (2020). Long-Term Follow-up and Outcomes of Retreatment in an Expanded 50-Patient Single-Center Phase II Prospective Trial of (177)Lu-PSMA-617 Theranostics in Metastatic Castration-Resistant Prostate Cancer. *J Nucl Med, 61*(6), 857-865.

Warde P, Mason M, Ding K, Kirkbride P, Brundage M, Cowan R, et al. (2011). Combined androgen deprivation therapy and radiation therapy for locally advanced prostate cancer: a randomised, phase 3 trial. *Lancet, 378*(9809), 2104-2111.

Weineisen M, Schottelius M, Simecek J, Baum RP, Yildiz A, Beykan S, et al. (2015). 68Ga- and 177Lu-Labeled PSMA I&T: Optimization of a PSMA-Targeted Theranostic Concept and First Proof-of-Concept Human Studies. *J Nucl Med, 56*(8), 1169-1176.

Wondergem M, Jansen BHE, van der Zant FM, van der Sluis TM, Knol RJJ, van Kalmthout LWM, et al. (2019). Early lesion detection with (18)F-DCFPyL PET/CT in 248 patients with biochemically recurrent prostate cancer. *Eur J Nucl Med Mol Imaging, 46*(9), 1911-1918.

Woythal N, Arsenic R, Kempkensteffen C, Miller K, Janssen JC, Huang K, et al. (2018). Immunohistochemical Validation of PSMA Expression Measured by (68)Ga-PSMA PET/CT in Primary Prostate Cancer. *J Nucl Med, 59*(2), 238-243.

Xu X, Li Q, Chang C, Wang X, Xie L. (2020). Metabolic Syndrome Is Not Associated With Prostate Cancer Recurrence: A Retrospective Analysis of a Chinese Cohort. *Front Oncol, 10*, 63.

Xue J, Qin Z, Cai H, Zhang C, Li X, Xu W, et al. (2017). Comparison between transrectal and transperineal prostate biopsy for detection of prostate cancer: a meta-analysis and trial sequential analysis. *Oncotarget, 8*(14), 23322-23336.

Yao V, Berkman CE, Choi JK, O'Keefe DS, Bacich DJ. (2010). Expression of prostate-specific membrane antigen (PSMA), increases cell folate uptake and proliferation and suggests a novel role for PSMA in the uptake of the non-polyglutamated folate, folic acid. *Prostate, 70*(3), 305-316.

Yaxley JW, Raveenthiran S, Nouhaud FX, Samaratunga H, Yaxley WJ, Coughlin G, et al. (2019). Risk of metastatic disease on (68) gallium-prostate-specific membrane antigen positron emission tomography/computed tomography scan for primary staging of 1253 men at the diagnosis of prostate cancer. *BJU Int, 124*(3), 401-407.

Zamboglou C, Drendel V, Jilg CA, Rischke HC, Beck TI, Schultze-Seemann W, et al. (2017). Comparison of (68)Ga-HBED-CC PSMA-PET/CT and multiparametric MRI for gross tumour volume detection in patients with primary prostate cancer

based on slice by slice comparison with histopathology. *Theranostics, 7*(1), 228-237.

Zamboglou C, Schiller F, Fechter T, Wieser G, Jilg CA, Chirindel A, et al. (2016). (68)Ga-HBED-CC-PSMA PET/CT Versus Histopathology in Primary Localized Prostate Cancer: A Voxel-Wise Comparison. *Theranostics, 6*(10), 1619-1628.

Zhao J, Stockwell T, Roemer A, Chikritzhs T. (2016). Is alcohol consumption a risk factor for prostate cancer? A systematic review and meta-analysis. *BMC Cancer, 16*(1), 845.

Zhong H, De Marzo AM, Laughner E, Lim M, Hilton DA, Zagzag D, et al. (1999). Overexpression of hypoxia-inducible factor 1alpha in common human cancers and their metastases. *Cancer Res, 59*(22), 5830-5835.

Zhou J, Gou Z, Wu R, Yuan Y, Yu G, Zhao Y. (2019). Comparison of PSMA-PET/CT, choline-PET/CT, NaF-PET/CT, MRI, and bone scintigraphy in the diagnosis of bone metastases in patients with prostate cancer: a systematic review and meta-analysis. *Skeletal Radiol, 48*(12), 1915-1924.

List of Figures

Figure 1. Schematic representation of PSMA/GCPII transmembrane protein (homodimer) (JC Evans et al., 2016). 11

Figure 2. ^{18}F-rhPSMA7–PET/MRI of a 66-year-old patient with primary prostate cancer (serum initial PSA (iPSA): 8.74 ng/ml and Gleason Score 8 at radical prostatectomy).16

Figure 3. Comparison of detection rates of ^{68}Ga and ^{18}F labeled PSMA-ligands. 17

Figure 4. miTNM classification for reporting by PSMA-ligand PET/CT/MRI. 21

Figure 5. PSMA positive prostate cancer cells can be targeted using radiotracers..... 22

Figure 6. Kaplan-Meier curves of PSMA expression in prostate cancer patients. 25

Figure 7. PSMA expression and recurrence (postoperative PSA of 0.1 ng/ml and rising) free survival in prostate cancer patients. 25

Figure 8. An example map of reangulated slices from one patient. 27

Figure 9. Schematic diagram of ARG for ex vivo analysis. 34

Figure 10. The workflow of preclinical study. 36

Figure 11. Sample preparation of in vivo PSMA-ligand uptake analysis. 37

Figure 12. Schematic diagram of ARG for in vivo PSMA-ligand uptake analysis. 38

Figure 13. Flowchart of inclusion and exclusion steps, narrowing down initially 253 patients to the final 186 eligible patients. 42

Figure 14. Representative images from eight specimens. 47

Figure 15. Scatter plot of QLs in eight sections. 47

Figure 16. Relative activities in different tumor density groups. 48

Figure 17. Absolute activities in different tumor density groups. 49

Figure 18. Representative sections of image registration. 53

Figure 19. Overview of the different PSMA staining patterns. 54

Figure 20. Overview of the different PSMA heterogeneity patterns. 55

Figure 21. Correlation of histology and IHC. 57

Figure 22. Comparison between ARG positive and negative ROIs. 59

Figure 23. Distribution of the percentage of different cell types with the normal curves. 60

Figure 24. PSMA-ligand uptake in tumor and non-tumor grids. 62

Figure 25. Bar charts of IRS-related parameters in normal prostate tissue and Gleason Patterns. 63

Figure 26. PSMA-ligand uptake in different Gleason Scores and groups. 65

Figure 27. Bar charts of PSMA-ligand uptake in different groups. 67

Figure 28. Longer biochemical recurrence-free survival was associated with (A) miT = 2 and (B) miN = 0. 74

Figure 29. Longer biochemical recurrence-free survival was associated with (A) pT = 2, (B) pN = 0, (C) Gleason Score < 8 and (D) negative surgical margin. 75

Figure 30. Biochemical recurrence-free survival according to tumor volume stratified by (A) percentiles and (B) median. 76

Figure 31. Biochemical recurrence-free survival according to total lesion stratified by (A) percentiles and (B) median. 76

Figure 32. Biochemical recurrence-free survival according to SUV_{mean} stratified by (A) percentiles and (B) median. 77

Figure 33. Biochemical recurrence-free survival according to SUV_{max} stratified by (A) percentiles and (B) median. 77

Figure 34. Biochemical recurrence-free survival according to miTNM stage. 83

List of Tables

Table 1. Clinical TNM classification of prostate cancer (JD Brierley et al., 2017) 2

Table 2. Grades of ISUP 2014 (JI Epstein, L Egevad, et al., 2016) 3

Table 3. EAU risk groups (N Mottet et al., 2020) 3

Table 4. miTNM Classification for PSMA-ligand PET/CT or PET/MRI (M Eiber et al., 2018). 18

Table 5. Sextant Segmentation of Prostate Gland (M Eiber et al., 2018). 19

Table 6. Lymph Node Regions (M Eiber et al., 2018). 19

Table 7. Description of anatomical delineation of pelvic lymph node territories (M Eiber et al., 2018) 20

Table 8. Pattern of Bone Involvement (M Eiber et al., 2018). 20

Table 9. Technical equipment 30

Table 10. Consumable supplies 30

Table 11. Reagents and chemicals 31

Table 12. Buffers and solutions 31

Table 13. Antibodies used for IHC 32

Table 14. Kits 32

Table 15. Software 32

Table 16. Four-point IRS Classification (KS McCarty, Jr. et al., 1985; N Woythal et al., 2018) 41

Table 17. Relative and absolute activities in tumor density groups. 47

Table 18. Patient Characteristics 50

Table 19. Sample characteristics 60

Table 20. Respective activities using four units in different Gleason Scores. 63

List of Tables

Table 21. The correlation of PSMA ligand uptake and Gleason Pattern. 66

Table 22. PSMA expression vs. PSMA ligand uptake. 68

Table 23. Patient characteristics. 69

Table 24. ^{68}Ga-PSMA-11 PET findings. 70

Table 25. Univariate analysis for the association of ^{68}Ga-PSMA-11 PET findings with surgical margin status. 71

Table 26. Multivariate analysis for the association of ^{68}Ga-PSMA-11 PET findings with surgical margin status. 72

Table 27. Univariate analysis for the association of ^{68}Ga-PSMA-11 PET findings with Gleason Score. 73

Table 28. Univariable analysis for the association of baseline factors with BCR-free survival. 78

Table 29. Multivariable analysis for the association of baseline factors with BCR-free survival. 80

Table 30. miTNM staging for ^{68}Ga-PSMA-11 PET/CT or MRI. 82

Table 31. Cutoffs of SUV_{max} with different PSMA-ligands. 93

Publications

1. Amiel T, Würnschimmel C, Heck M, Horn T, Nguyen N, Budäus L, Knipper S, Wenzel M, Rauscher I, Eiber M, **Wang H**, Maurer T. Regional Lymph Node Metastasis on Prostate Specific Membrane Antigen Positron Emission Tomography Correlates with Decreased Biochemical Recurrence-Free and Therapy-Free Survival after Radical Prostatectomy: A Retrospective Single-Center Single-Arm Observational Study. J Urol. 2021 Feb 4: 101097JU0000000000001596. doi: 10.1097/JU.0000000000001596.

2. **Wang H**, Eiber M, Langbein T. A rare case of polyostotic fibrous dysplasia detected on ^{18}F-rhPSMA-7 PET/CT. Eur J Nucl Med Mol Imaging. 2020 Nov; 47(12): 2927-2929. doi: 10.1007/s00259-020-04751-9.

3. Gafita A, Fendler WP, **Hui W**, Sandhu S, Weber M, Esfandiari R, Calais J, Rauscher I, Rathke H, Tauber R, Delpassand ES, Weber WA, Herrmann K, Czernin J, Eiber M, Hofman MS. Efficacy and Safety of ^{177}Lu-labeled Prostate-specific Membrane Antigen Radionuclide Treatment in Patients with Diffuse Bone Marrow Involvement: A Multicenter Retrospective Study. Eur Urol. 2020 Aug; 78(2): 148-154. doi: 10.1016/j.eururo.2020.05.004.

4. Gafita A, **Wang H**, Tauber R, D'Alessandria C, Weber WA, Eiber M. Exceptional 4-year response to ^{177}Lu-PSMA radioligand therapy in metastatic castration-resistant prostate cancer. Eur J Nucl Med Mol Imaging. 2019 Sep; 46(10): 2212-2213. doi: 10.1007/s00259-019-04410-8.

5. Gafita A, Calais J, Franz C, Rauscher I, **Wang H**, Roberstson A, Czernin J, Weber WA, Eiber M. Evaluation of SUV normalized by lean body mass (SUL) in ^{68}Ga-PSMA11 PET/CT: a bi-centric analysis. EJNMMI Res. 2019 Dec; 9(1): 103. doi: 10.1186/s13550-019-0572-z.

6. Gafita A, Bieth M, Krönke M, Tetteh G, Navarro F, **Wang H**, Günther E, Menze B, Weber WA, Eiber M. qPSMA: Semiautomatic Software for Whole-Body Tumor Burden Assessment in Prostate Cancer Using ^{68}Ga-PSMA11 PET/CT. J Nucl Med. 2019 Sep; 60(9): 1277-1283. doi: 10.2967/jnumed.118.224055.

Acknowledgements

I sincerely want to thank Prof. Dr. Matthias Eiber for accepting me as a doctoral student in the Nuclear medicine department and supporting my study and research. His valuable guidance helped me to choose the right direction and successfully complete my dissertation.

I would like to thank my two mentors Prof. Dr. Wolfgang Weber and PD. Dr. med Thomas Horn. Their insightful feedback pushed me to think out of the box and brought my work to a higher level.

I would also like to thank my colleague Nahid Yusufi for showing me almost every measurement technique available in our laboratories and basics in animal experiments. I thank here for always being open to my questions and patient support.

I would also like to thank all my cooperation partners for their enthusiasm, trustworthiness, and collaborative effort during data collection and sample preparation.

I would like to thank my parents Haiming Wang and Jingyuan Gao, who supported me throughout my whole life with love and advice. Moreover, I want to thank everyone at Nuclear medicine for creating such a warm, friendly, and helpful, but professional working atmosphere. Finally, I would like to thank my boyfriend, Simon Qian, who has supported me and had to put up with my stresses and moans for the past three years of study!